MODELING AND DESIGN OF A HELIX-CABLE ACTUATED STEERABLE INSTRUMENT FOR MINIMALLY INVASIVE SURGERY

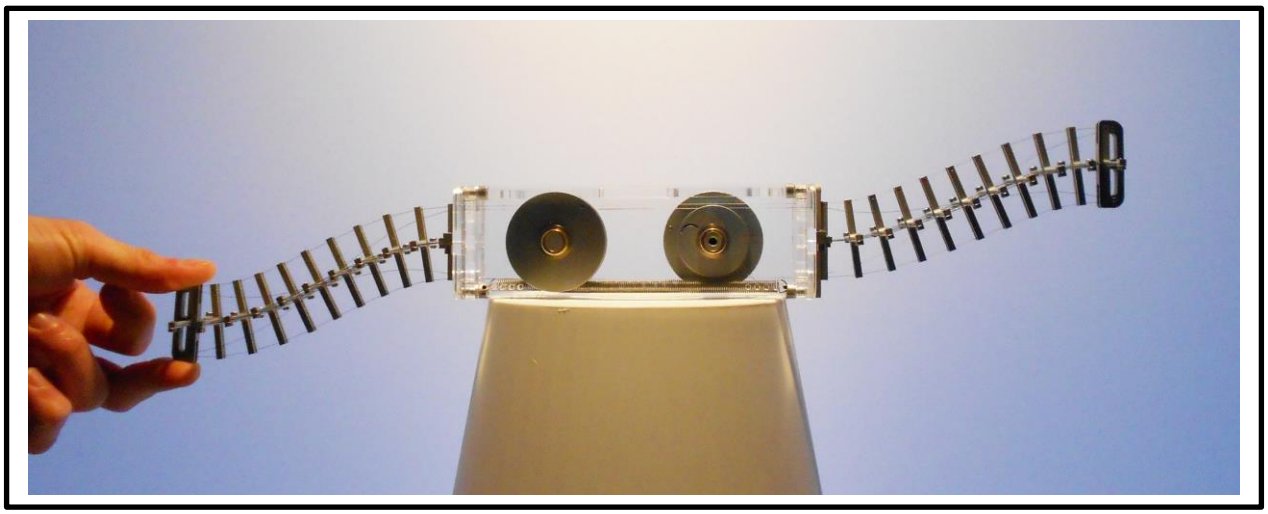

PAUL HENSELMANS

MSC THESIS

-2013-

SUPERVISION BY:

PROF. DR. IR. J. DANKELMAN

PROF. DR. IR. P. BREEDVELD

IR. E. ARKENBOUT

TU DELFT, THE NETHERLANDS

FACULTY MECHANICAL, MARITIME & MATERIALS ENGINEERING

DEPARTMENT BIO-MECHANICAL ENGINEERING

Abstract

Minimally Invasive Surgery or MIS is a branch of surgery focused on reducing the invasiveness of surgical procedures, accomplished by minimizing the size and number of incisions. The approach inevitable leads to confinement of the operational space and restricts the movement of the used instrumentation. In this thesis, a MIS procedure called Endonasal Skull Base Surgery (ESBS) is presented to illustrate the need for maneuverable instruments.

The maneuverability of an instrument can be enhanced by adding one or multiple cable-actuated steerable elements to the tip of the instrument. Currently the cables in these (multi-)steerable instruments are placed parallel to the longitudinal axis of the steerable element. This thesis proposes the use of helix cables as means of multi-steerable actuating, wherein the cables are rotated along the longitudinal axis of the steerable element.

A force driven two dimensional simulation model was developed and validated in order to analyze the actuation behavior of helix cables in a steerable element. The results enabled the creation of a mechanical control method, which is integrated in a demonstrational prototype. The prototype reveals three additional functionalities to a steerable element: 1) The expansion of the shape domain of a steerable element, resulting a higher diversity of possible direction and position combinations of the tip. 2) The incorporation of a local positional stiffness of the tip. 3) The incorporation of a sampling behavior between the control handle and tip, meaning that only the lowest frequencies of the shape in the handle is passed on to the tip.

Acknowledgments

The creation of this thesis was not possible without the help and support of the people involved with me and/or this project. I would therefore like to start by thanking my parents for their support and patience throughout my education.

I would also like to thank Ewout Arkenbout for his input and feedback during all the facets of this project. Especially the time he managed to make free for me even though my visits where often unannounced is very much appreciated.

Furthermore I owe thanks to David Jager en Menno Lageweg for their professional and helpful attitude towards the fabrication of the validation model and the prototype.

Finally I would like to thank Paul Breedveld for his close interests in the project, whilst still allowing me the freedom of making my own decisions and occasional mistakes. He thereby managed to give me the needed motivation and inspiration for successfully finishing the project, which is very much appreciated.

Table of contents

1 Introduction

1.1 Background

Minimally Invasive Surgery or MIS, is a quickly evolving branch of medical interventions. It attempts to minimize the invasiveness of open surgery procedures by reducing the volume of incisions to the bare minimum.

Natural Orifice Translumenal Endoscopic Surgery (NOTES) is a specific branch of MIS that uses the natural orifices of the patient as an entrance point, completely eliminating the need for skin incisions. An example of a NOTES procedure is Endonasal Skull Base Surgery, (ESBS). The goal of ESBS is to reach a tumor growing on or next to the pituitary gland by entering through one or both nostrils of the patient (Figure 1).

During ESBS, the path to reach the tumor can become rather complex including multiple bends, since it is initially bound by the patients uniquely curved anatomy of the nasal cavity. At the back of the nasal cavity, the surgeon needs to drill through the bony walls of the sphenoid sinus, which is an empty cavity in front of the pituitary gland, as illustrated in Figure 1. The resulting holes restrict the range of motion of the instrumentation. The surgeon, however, would like to have the ability of altering the position and direction of the tools after passing the sphenoid sinus cavity.

ESBS therefore imposes a certain level of adaptability of the instrumentation. A potential solution can be found in the development of steerable equipment, as is illustrated in Figure 1.

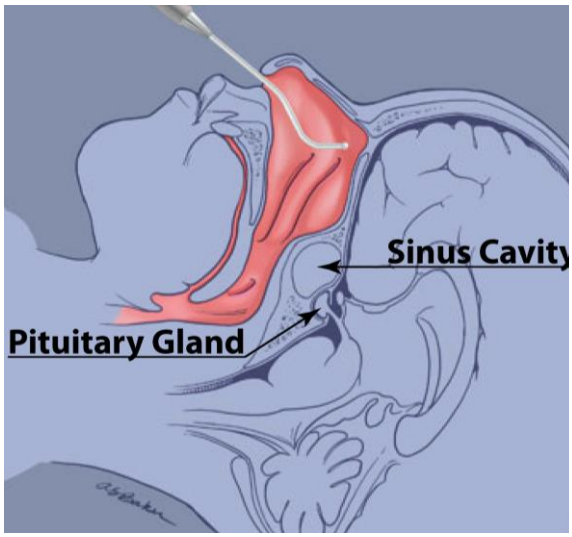

Figure 1: Endonasal Skull Base Surgery. In order to reach the pituitary gland while entering through a nostril of the patient, one must first drill through the walls of the sinus cavity. Figure is copied from [11].

1.2 Instrumentation

MIS-instrumentation must fit through small incisions and allow the surgeon to manipulate tissue with sufficient force. Current MIS-instrumentation is therefore slender and rigid. Figure 2 depicts a typical example of such an instrument consisting of a handle, shaft and tip onto which a tool is installed. Insertion of such instruments through an incision in the skin or natural orifice (as in ESBS) reduces the freedom of movement of the instrument to the four degrees of freedom (DOF) illustrated in Figure 2.

The surgeon's ability of positioning and directing the instrument is thereby drastically reduced. Additionally, DOF 1 and 2 of Figure 2 include a coupling between the position and the direction of the instrument. This makes it impossible to reposition the tool sideways without changing the direction of the tool as well.

Steerable instrumentation enhances the freedom of movement by adding a steerable element at the tip. A steerable element contains additional DOF that enable the decoupling between the tools position and direction.

T. Nai [1] presents multiple manners in which

Figure 2: Left: The four remaining DOF of an inserted instrument [7]. Right: A typical MIS slender and rigid instrument, consisting of a handle, shaft and tip onto which a tool is installed.

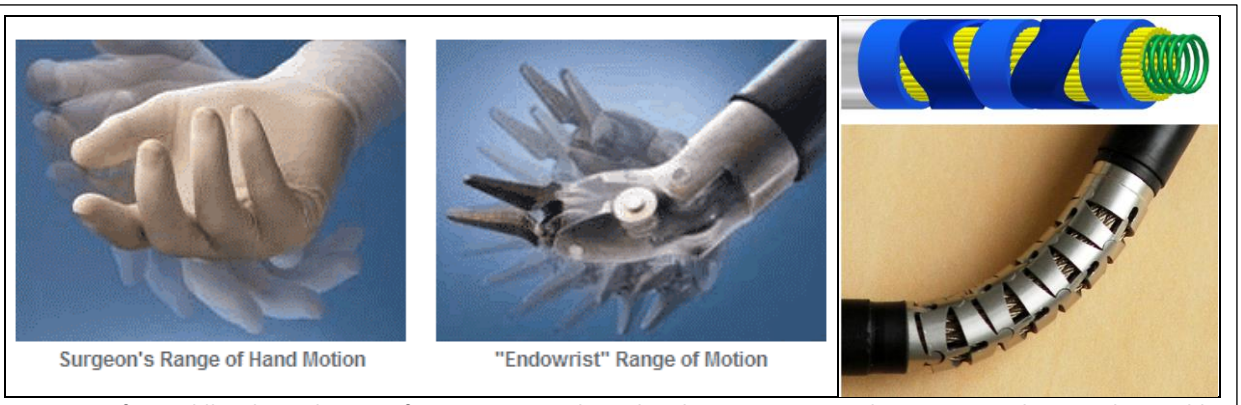

Figure 3: Left& middle: The Endowrist of Intuitive Surgical, used in the Da Vinci surgical system, a single-jointed steerable element constructed with pulleys [4]. Right: The cable ring forceps structure by P. Breedveld et al. [7], a multi-jointed steerable element constructed out of a ring of cables enclosed by a spring and rings.

steerable elements can be actuated: e.g. gears, rods, heat actuation etc. Cable actuation is however the most used type of actuation [1] & [2], due to its flexible nature it allows for simple and easy to miniaturization of structures. Furthermore it reduces operational risks due to failure, by the exclusion of high pressures, high temperatures or electric energy inside the body of the patient.

All known cable-actuated instruments work by the same principle [2]. A pulling force is exerted on a cable thereby creating a moment around a single joint or multiple joints. The result is a deflection of the steerable element. A single-jointed segment with two steerable DOF is fully actuated and therefore stiff. A multi-jointed segment with two steerable DOF is, however, under actuated and subsequently less stiff [2].

A popular example of a single-jointed cable actuated instrument is the Endowrist of Intuitive Surgical, as shown in Figure 3 [3]. The instrument has a diameter of 5 mm and allows the surgeon to redirect the tip of the instrument with an additional 2 DOF [4]. Its construction does, however, include pulleys which impose rather small bending radii on the cables, resulting in cable fatigue and eventual failure. The purchasing and maintenance of the Endowrist is therefore quite expensive [5].

The Endowrist shows that the minimal bending radii of the cables pose a serious minimization problem. A solution is found in the enlargement of the length of a steerable element by creating a multi-jointed structure. The cable ring forceps construction of Figure 3 incorporates this idea. Just like the Endo Wrist the segment is steerable in 2 DOF, but now the cables are enclosed by a spring and multiple ring shaped joints. The addition of these extra joints does, however, make the instrument under actuated and therefore less stiff.

The instrument presented in Figure 4 includes a solution to the stiffness problem by enclosing the cables by a braided structure [6]. A braided structure is a woven structure of clockwise and counter-clockwise spiraling wires, which will be referred to as helix wires. After one full spiral the helix wires are fixated on both ends of the cylinder, thereby conserving their lengths. The result is a torsion stiff structure that can only bend to a shape with a constant radius.

Incorporating this structure into a steerable element will enhance its stiffness, since it resists deformation to non-constant radius shapes due to external forces. This behavior can be explained by studying the change in length of a helix wire during a bending motion of the structure.

The right part of Figure 4 illustrates a deformed steerable element with a constant bending radius. One can see that the path lengths of the parallel blue wires with the minimal and maximal bending radii are respectively shortened and elongated. The path length of the central placed parallel wire does, however, not change. The figure also shows that while the bending radius of a parallel wire is constant, the bending radius of a helix wire continually changes along the cylinder. If the cylinder is deformed with a constant bending radius, the average bending radius of a helix wire will be equal to the central bending radius. Therefore the path length of the helix wire will not change. If however the cylinder should bend with a non-constant bending radius, the path lengths of the

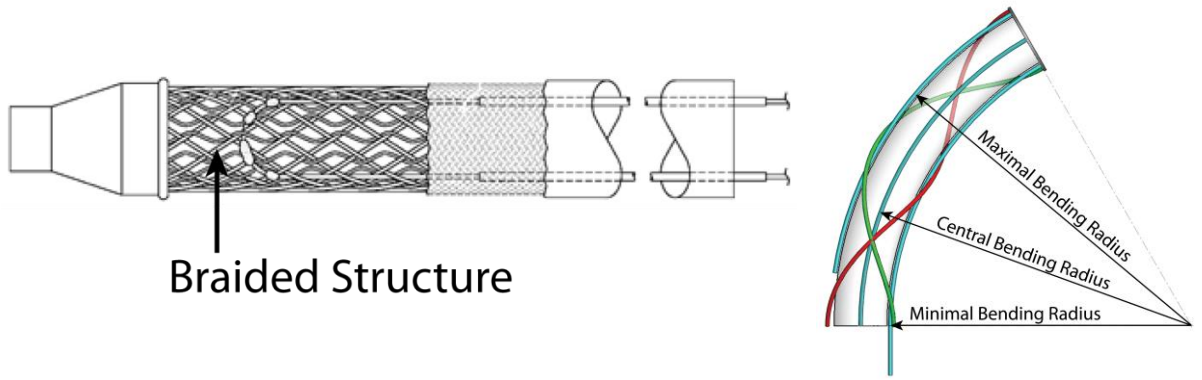

Figure 4: Left: The braided structure used in a steerable element by D. Stefanchik et al. [6]. It ensures that the steerable element can only bend with a constant bending radius. Right: The parallel wires (blue) of the braided structure have a constant bending radius while the bending radii of the helix wires (red and green) continually change. When the lengths of the helix wires are conserved by fixating both ends, the structure is only able to bend with a constant radius.

helix wires will be shortened or elongated, depending on the position of the cable.

In a braided structure the helix wires are woven into each other and their lengths are conserved by the fixation on both ends. Through these conditions, the structure cannot bend with a non-constant bending radius, thus making the steerable element of Figure 4 stiff.

By the same principle, the braided structure is also torsion stiff. A clockwise rotation along the longitudinal axis would namely induce a reduction of the path lengths of the clockwise wires, while increasing the path lengths of the counter-clockwise wires.

The so far presented steerable instruments are all equipped with a single steerable element at the tip, restricting the shape domain of the instrument to a single bend with a constant radius. Instrumentation suitable for ESBS must however be capable of complex shapes consisting of multiple bends and therefore a non-constant bending radius. The Multiflex presented in Figure 5 is capable of creating these complex shapes [7]. It consists of five steerable elements placed in series. Each segment is actuated by its own set of actuation cables, making it possible to steer each segment independently and thereby creating more complex shapes. The addition of steerable elements and extra actuation cables does, however, limit the possibility of minimizing the diameter of the instrument.

This limitation creates the need for a steerable element that is not only able to create a constant radius bend, but also capable of forming complex shapes with a non-constant bending radius. This thesis proposes the idea of using the helix wires of a braided structure as actuation cables, expecting them to be able to induce a non-constant bending radius of a steerable element while preserving the stiffness qualities of a braided structure.

1.3 Problem definition

Cable actuated steerable elements used in current (multi-)steerable instrumentation are limited to constant bending radii, have low stiffness and/or suffer from cable fatigue.

1.4 Goal

- To investigate the behavior of a steerable element actuated by helix cables, while focusing on the creation of complex shapes and stiffness of the steerable element.

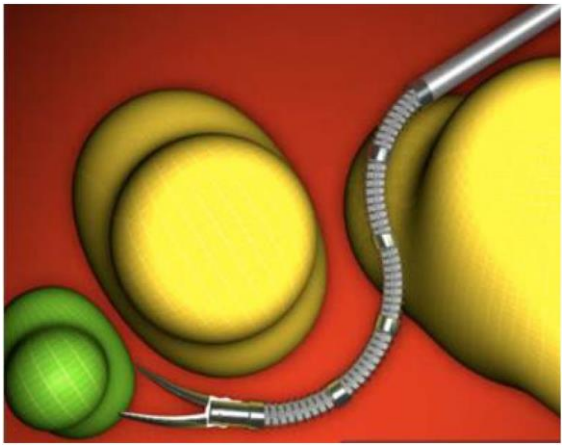

Figure 5: A drawing of the Multiflex created by P. Breedveld et al. [11]. A single-jointed multi-steerable instrument consisting of five serial placed steerable elements, capable of creating complex shapes.

- Creating and validating a simulation model based on the mechanical analysis of a cable actuated segment.
- Creating a steering mechanism, able to create complex non-constant radius shapes.

1.5 Contents

The thesis consists of two main parts i.e. the simulation model and the demonstration prototype, each described in a separate chapter.

Chapter 2 is dedicated to the simulation model. In Section 2.1 the basic configuration and the corresponding assumptions and simplifications of the simulation model are presented. Section 2.2 is dedicated to the actual workings of the model and its implementation into the used software package Matlab. The results of the simulation model are presented and analyzed in Section 2.3. These results suggest a possible inversion of the model which is briefly presented in Section 2.4. The results of the simulation model are validated based on a physical model. Section 2.5 discusses the validation process and the design of the physical model. Section 2.6 reveals the results of the validation process. The final section of Chapter 2, Section 2.7, discusses the simulation model itself, its validation and introduces possible enhancements.

Chapter 3 is dedicated to the demonstration prototype, starting in Section 3.1 with an introduction of its use and functionality. Section 3.2 discusses currently used methods of control and defines the control problem that is addressed by the prototype. A solution to this control problem is presented in Section 3.3. Next, Section 3.4 describes the incorporation of this newly found solution into a working prototype. The finished prototype is then presented and its behavior is analyzed in Section 3.5. Finally in Section 3.6 the demonstration prototype is discussed base on its behavior, implications and possible improvements.

The last chapter of this thesis presents the overall conclusions based on the previous determined goals.

2 Simulation model

2.1 Mechanics

The developed simulation model is a computer tool for investigating the behavior of a steerable element actuated by helix cables. The choice to make a computer model rather than a physical model is based on the following reasons.

First of all, in contrast to a physical model, the dimensions and characteristics of a steerable element in a computer model can easily be altered. This allows for a more thorough investigation of the structure. Furthermore a computer model allows the investigation of extreme positions which would otherwise cause permanent damage to a physical model.

The computer model is based on a segmented approach similar to the finite element method for structural analysis. Matlab is used to perform a static analysis of the segments. The choice for Matlab is due to the transparent and highly adaptable nature of this software package.

2.1.1 Configuration

To reduce the complexity of this first simulation model of a helix system, it was chosen to begin the study with a two dimensional representation of a single steerable element. This segment should be capable of forming complex shapes and therefore must contain multiple joints.

These joints are created by dividing a flexible core into *n* segments with the use of ribs. This approach is similar to the cable ring forceps construction of Figure 3, where the flexible core is a spring and the structure is segmented with the use of rings. The construction of the model is illustrated in Figure 6.

The actuation cables are fixated at the top rib and pass through fixed holes in the remaining ribs through which they can slide. A cable can lie parallel to the flexible axis or skewed, thereby forming a helix cable. A helix cable has a direction change when the end of a rib is reached. The bottom rib of the model is fixed to the ground.

2.1.2 Assumptions & Simplifications

In a (multi-)steerable instrument, the length change of a steerable element due to longitudinal forces can generally be neglected. The flexible axis of the model is therefore considered incompressible.

Each segment must represent the characteristics of a single bending 1-DOF joint, which can only deform with a constant radius.

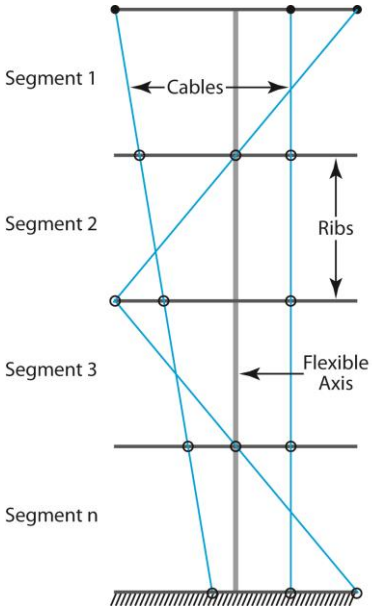

Figure 6: The model is built up out of a flexible central axis which is divided by ribs into n segments. The actuation cables are fixated at the top rib and pass through holes in the other ribs.

The function of the ribs is to fixate the position between a cable and the flexible axis. To ensure no unwanted alterations in this position, the ribs are modeled as being infinitively stiff.

All elements in the model are modeled with just one dimension, which is their length. Their thickness is neglected.

A simulation model will always be a simplification of reality and in this model a number of simplifications have been made to reduce the mathematical complexity. Next to the two-dimensional simplification, the model is also a kinematic static representation. This means that the model can be used to find the static equilibrium of an actuated segment while no dynamic effects are included. Other simplifications are; the neglection of friction, mass and the bending stiffness of cables.

Friction and the bending stiffness of cables probably do play a major role when a steerable element is minimized but are neglected for the purpose of this very first model of a helix system. In the miniature construction of surgical instruments, the actuation forces are much higher than the forces associated with the inertia. Hence dynamic effects and mass are neglected.

2.2 Mechanical model

The working principle of the simulation model is similar to the conjugate beam method for calculating the deformation of a loaded beam [8]. In this method the beam is divided into segments of length ℓ and the deformation angle $d\theta$ of a segment can be calculated by:

$$d\theta = \frac{M \cdot \ell}{E \cdot I} \qquad \text{Eq. 2-1}$$

where M is the total moment, E the modulus of elasticity and I the moment of inertia. By combining all segment deformations through integration, the elastic curve function $\theta(x)$ describing the deformation of the beam is realized.

The simulation model calculates the deformation of a segment in an equal manner. There is however one major difference in that the conjugate beam method works only for small deformations. Therefore it can neglect the direction change of the shear force in a deformed segment. Furthermore it also neglects the contribution of the normal force to the moment balance of that segment. The simulation model works with large deformations and these effects can therefore not be neglected.

2.2.1 Variables

The stiffness of the flexible axis denoted by c with unit [Nmm/rad] is based on Eq. 2-1:

$$c = \frac{E \cdot I}{\ell} \qquad \text{Eq. 2-2}$$

The dimension notations of the model of which the bottom three are illustrated in Figure 7 are:

n	segment number	
m	cable number	
r	radius of the steerable element	[mm]
ℓ	length of a segment	[mm]
β	angle of a cable	[rad]

A parallel cable lies (as the name implies) parallel to the flexible axis and has a $\angle\beta$-value of ½ π. A helix cable has a positive direction to the right for $\angle\beta$-value above ½ π and conversely a $\angle\beta$-value below ½ π will give the helix cable a negative direction to the left.

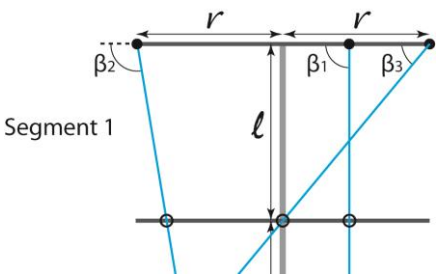

Figure 7: Segment 1 with dimensions.

2.2.2 Construction

The segments of the model are distinguished by two different types, namely segment 1 and segments 2 to n. Segment 1 has the cables fixated to the rib, while in segment 2 to n the cables pass through the ribs.

The calculation process starts by singling out segment 1 and grounding its bottom rib, thereby creating its own local coordination system. A deformation is induced by the actuation of one or multiple cables. After the deformation of the segment is derived, segment 1 is released. This derivation process is repeated for each segment in sequence until from top to bottom all segment deflections have been derived.

The following description of the model focuses on a single helix cable, starting at the right side of the top rib. Forces directed up and to the right are considered positive. Sine, cosine and tangent terms are written as s(…), c(…) and t(…). Equations marked with * are derived in more detail in Appendix A.1.

Segment 1

The model is fitted with a single helix cable fixated at point C_1 and passing through point C_2, as illustrated in Figure 8. The distances of these points compared to the flexible axis are noted by r_{C1} and r_{C2}. These variables have positive values when located at the right side of the flexible axis and negative values when located at the left.

The pulling force F_{C1} creates a moment around point A_2, thereby deforming the flexible axis with a constant bending radius $|A_1O_1|$. The deformation is described by $\angle\alpha_1$, which is the variable of interest. Its value can be derived by solving the moment balance around point A_2. From Figure 8 can be derived that the moment balance is equal to:

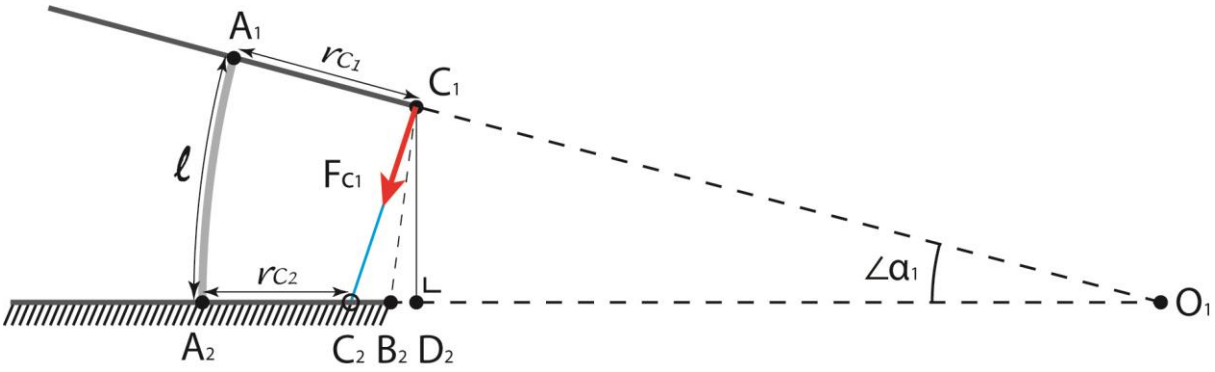

Figure 8: Deformed segment 1. The segment bends with a constant radius $|A_1O_1|$ and is value by angle $\angle\alpha_1$.

$$\sum M_{A_2} = 0 : \; M_{r_1} - F_{C_1x} \cdot d_{C_1y} + F_{C_1y} \cdot d_{C_1x} = 0 \qquad \textbf{Eq. 2-3}$$

In this notation a counter-clockwise moment is considered positive. A positive F_{C1x} thereby creates a negative moment, while a positive F_{C1y} results in a positive moment. In Figure 8 both components of F_{c1} are negative. Now each component of the moment balance must be expressed as functions of $\angle\alpha_1$, which will now be described separately.

M_{r1}

The value of the reaction moment M_{r1} is equal to the bending moment of the flexible axis and can be described by:

$$M_{r_1} = c \cdot \alpha_1 \qquad \textbf{Eq. 2-4}$$

F_{C1}

The positive force F_{C1} is decomposed into F_{C1x} and F_{C1y} by:

$$F_{C_1x} = -F_{C_1} \cdot s(\delta_1)$$
$$F_{C_1y} = -F_{C_1} \cdot c(\delta_1) \qquad \textbf{Eq. 2-5}$$

$\angle\delta_1$ is equal to the arctangent of $|C_2D_2|$ divided by $|C_1D_2|$. These distances are written into functions of $\angle\alpha_1$ and $\angle\delta_1$ can thereby be expressed by:

$$\angle\delta = t^{-1}\left(t\left(\frac{\alpha_1}{2}\right) + \frac{dr}{\left(\frac{\ell}{\alpha_1} - r_{C_1}\right) \cdot s(\alpha_1)} \right) \qquad \textbf{*Eq.2-6}$$

where dr is equal to the difference between r_{n-1} and r_n, (Figure 10) which is constant since in initial position a cable is straight. The value of dr is determined by:

$$dr = \ell \cdot t\left(\frac{\pi}{2} - \beta\right) \qquad \textbf{Eq. 2-7}$$

For a parallel cable dr is zero since $\angle\beta$ will be equal to half π.

d_{C1x} & d_{C1y}

The moment arms d_{C1x} and d_{C1y} are equal to respectively $|A_2D_2|$ and $|C_1D_2|$ and can be stated as:

$$d_{C_1x} = \frac{\ell}{\alpha_1} - \left(\frac{\ell}{\alpha_1} - r_{C_1}\right) \cdot c(\alpha_1)$$
$$d_{C_1y} = \left(\frac{\ell}{\alpha_1} - r_{C_1}\right) \cdot s(\alpha_1) \qquad \textbf{*Eq. 2-8}$$

The fully symbolically constructed moment balance

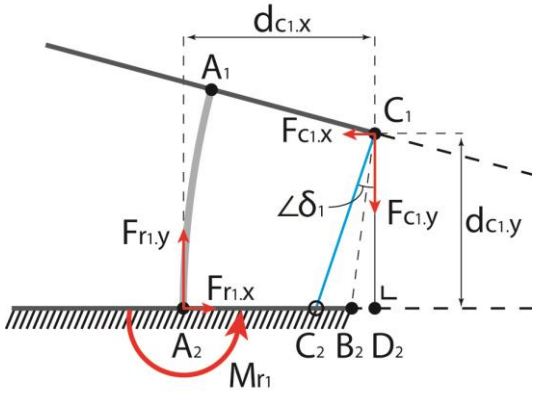

Figure 9: Decomposition of F_{r1} and F_{c1} and visualization of their moment arms for deriving the moment balance of Eq. 2-3.

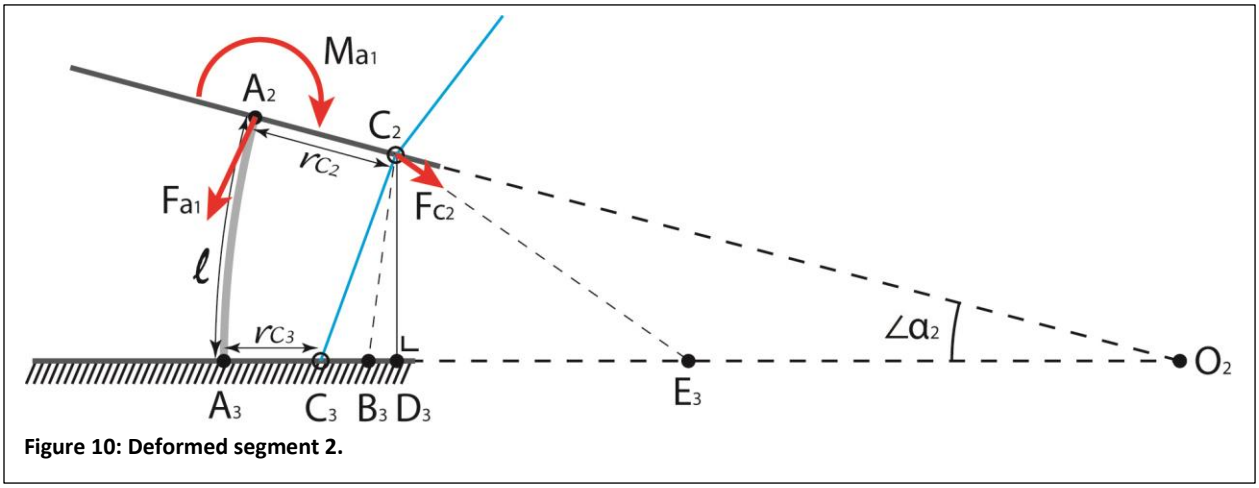

Figure 10: Deformed segment 2.

of Eq. 2-3 is presented in Appendix A.1.
The addition of multiple cables would result in the addition of force and moment arm couples while the M_{r1} term remains unchanged. The bare moment balance would therefore be equal to:

$$\sum M_{A_2} = 0 : M_{r_1} - F_{C_1x} \cdot d_{C_1y} + F_{C_1y} \cdot d_{C_1x} - F_{C_2x} \cdot d_{C_2y} + F_{C_2y} \cdot d_{C_2x} = 0 \quad \textbf{Eq. 2-9}$$

For a single cable, the moment balance can be solved symbolically with the use of Maple. However, when more cables are added the moment balance becomes symbolically unsolvable and the solution for $\angle\alpha_1$ is derived numerically.

When the value of $\angle\alpha_1$ is determined, the reaction forces F_{r1x} and F_{r1y}, needed for calculations on segment 2, can be derived from the force balances:

$$\sum F_x = F_{r_1x} + F_{C_1x}$$
$$\sum F_y = F_{r_1y} + F_{C_1y} \quad \textbf{Eq. 2-10}$$

Now the deformation of segment 1 is determined, the calculation process continues to segment 2.

Segments 2 to *n*

Figure 10 illustrates the deformed state of the second segment. The bottom rib of the segment is grounded again, creating the local coordination system of segment 2. There are two forces and one moment working on the segment, namely the action force F_{a1} which is equal but opposite from force F_{r1}, cable force F_{C2} and action moment M_{a1} which is equal but opposite from reaction moment M_{r1}.

Again the deformation $\angle\alpha_2$ is the variable of interest and can be derived from the moment balance around point A_3. _ 11 illustrates moment, the decomposed forces and related moment arms used to configure the moment balance around point A_3.

$$\sum M_{A_3} = 0 : M_{r_2} + M_{a_1} - F_{a_1x} \cdot d_{a_1y} + F_{a_1y} \cdot d_{a_1x} - F_{C_2x} \cdot d_{C_2y} + F_{C_2y} \cdot d_{C_2x} = 0 \quad \textbf{Eq. 2-11}$$

The moments, forces and moment arms of this moment balance will now be discussed separately.

M_{r2} & M_{a1}

Just as in the first segment, the reaction moment M_{r2} is equal to the bending moment of the flexible axis. Moment M_{a1} results from releasing the bottom rib of segment 1, meaning that the reaction moment M_{r1} must be compensated for. M_{a1} is therefore equal but opposite to M_{r1}.

$$M_{r_2} = c \cdot \alpha_2$$
$$M_{a_1} = -c \cdot \alpha_1 \quad \textbf{Eq. 2-12}$$

F_{a1}

Force F_{a1} results from releasing segment 1 and its magnitude is therefore equal to F_{r1}. However, due to the change in local coordination systems and the deformation of segment 2, the direction of force F_{r1} is altered. The decomposition of F_{a1} must therefore be expressed as:

$$F_{a_1x} = -F_{r_1x} \cdot c(\alpha_2) - F_{r_1y} \cdot s(\alpha_2)$$
$$F_{a_1y} = -F_{r_1y} \cdot c(\alpha_2) + F_{r_1x} \cdot s(\alpha_2) \quad \textbf{*Eq. 2-13}$$

F_{C2}

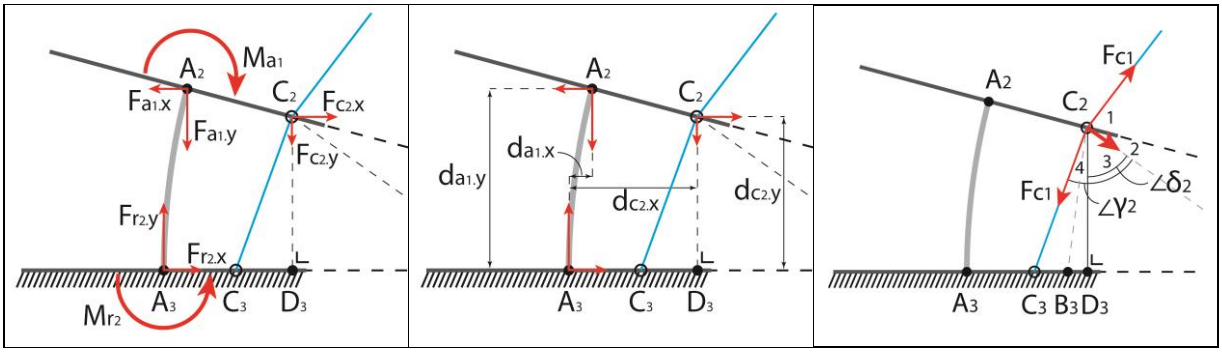

Figure 11: Left: Moment and decomposed forces. Middle: Moment arms. Right: Composition of cable force F_{C2}

Cable force F_{C2} is the result of the tension in the cable caused by force F_{C1} and the direction change of the cable at point C_2. This situation is illustrated by Figure 11. If the tension forces F_{C1} are decomposed, the longitudinal components will cancel each other out, while the components directed more perpendicular to the cable form F_{C2}. The magnitude of F_{C2} can therefore be calculated by:

$$F_{C_2} = 2 \cdot F_{C_1} \cdot c(\gamma_2) \qquad \textbf{Eq. 2-14}$$

$\angle\gamma_2$ Needs to be written as a function of $\angle\alpha_2$. Since F_{C2} is directed at the middle of the direction change of the cable one can state:

$$\begin{aligned} \angle\gamma_2 &= \angle C_{2.3} + \angle C_{2.4} \\ &= \angle C_{2.1} + \angle C_{2.2} \\ &= \frac{\angle C_{2.1} + \angle C_{2.2} + \angle C_{2.3} + \angle C_{2.4}}{2} \end{aligned} \qquad \textbf{*Eq. 2-15}$$

A description of $\angle\delta_2$ is needed for the decomposition of F_{C2}. From Figure 11 can be deducted that $\angle\delta_2$ is equal to:

$$\angle\delta_2 = \angle\gamma_2 - \angle C_{2.4} \qquad \textbf{*Eq. 2-16}$$

Force F_{C2} can now be decomposed into:

$$\begin{aligned} F_{C_{2x}} &= F_{C_2} \cdot s(\angle\delta_2) \\ F_{C_{2y}} &= -F_{C_2} \cdot c(\angle\delta_2) \end{aligned} \qquad \textbf{*Eq. 2-17}$$

Moment arms

Moment arms d_{C2x} and d_{C2y} around point A_3, as illustrated in Figure 11 can be derived in the same manner as the moment arms of segment 1. The descriptions of d_{C2x} and d_{C2y} are therefore alterations of the moment arms d_{C1x} and d_{C1y} and can be expressed as:

$$\begin{aligned} d_{C_{2x}} &= \frac{\ell}{\alpha_2} - \left(\frac{\ell}{\alpha_2} - r_{C_2}\right) \cdot c(\alpha_2) \\ d_{C_{2y}} &= \left(\frac{\ell}{\alpha_2} - r_{C_2}\right) \cdot s(\alpha_2) \end{aligned} \qquad \textbf{Eq. 2-18}$$

Since F_{a1} and F_{C2} are positioned on the same rib, the moment arms d_{a1x} and d_{a1y} can be derived in the same manner with an alteration of the multiplied length. They can therefore be written as:

$$\begin{aligned} d_{a_{1x}} &= \frac{\ell}{\alpha_2} - \frac{\ell}{\alpha_2} \cdot c(\alpha_2) \\ d_{a_{1y}} &= \frac{\ell}{\alpha_2} \cdot s(\alpha_2) \end{aligned} \qquad \textbf{Eq. 2-19}$$

The moment balance has become rather complex and its complexity grows with the addition of multiple cables. A symbolic solution can thereby not be contained and the value of $\angle\alpha_2$ is numerically calculated with the use of Matlab.

F_{r2}

When the value of α_2 is determined, the reaction force F_{r2} can be derived from the force balances of segment 2.

$$\begin{aligned} \sum F_x &= 0 : F_{r_{2x}} + F_{a_{1x}} + F_{C_{2x}} \\ \sum F_y &= 0 : F_{r_{2y}} + F_{a_{1y}} + F_{C_{1y}} \end{aligned} \qquad \textbf{Eq. 2-20}$$

Now the calculation of segment 2 is finished, the model continues to segments 3 to n, each of which

can be calculated with the same equations as segment 2.

All equations of segment 1 and 2 are suitable for negative values of $\angle\alpha$ and all possible cable combinations. This is explained in Appendix A.1.

2.2.3 Implementation

The basic build-up of the Matlab code is also divided into a section for segment 1 and a section for segments 2 to *n*. First the deformation of segment 1 is calculated. Since no symbolic solution for the moment balance can be found that includes multiple cables, the value of α_n is derived numerically. This is done by the Matlab function *fzero*, which searches for a local zero-point of the moment balance based on its direction of absolute decrease.

The algorithm uses a combination of the bisection, secant and inverse quadratic interpolation methods in order to find this direction [9]. These methods do not use derivative information from the function itself, but acquire this information from interval calculations.

The *fzero* function can be used because the moment balance within a preset domain of α is a convex function and therefore crosses the zero-line only once. A function is called convex if and only if the derivative of the function is either completely positive and/or zero or negative and/or zero. The derivatives of the moment balances (Eq. 2-3 & Eq. 2-11) are mainly influenced by the bending moment of the flexible axis, which derivative is equal to bending stiffness *c*. The derivatives of the moments created by the components of F_a and F_C are much smaller then *c*. Therefore the overall derivative of the moment balance will be constant and thus the moment balance is convex. A more detailed explanation is presented in Appendix A.4.

A symbolic solution is found for a single cable and matches the results of the numerical solution.

The full Matlab code is presented in Appendix B.1.

2.3 Simulation results

Before continuing with the explanation of the simulation model's result, a cable notation is proposed to identify the position of a cable more clearly. Figure 12 illustrates the manner of the notation. A cable notation starts with a capital letter L, M or R to identify the starting position of the cable. An extra lower-case notation for helix cables is added or subtracted, identifying the horizontal distance and direction in which the cable travels till it reaches segment n. A helix cable that starts at the left side and finishes at the right will therefore be notated by L+2r (Figure 12).

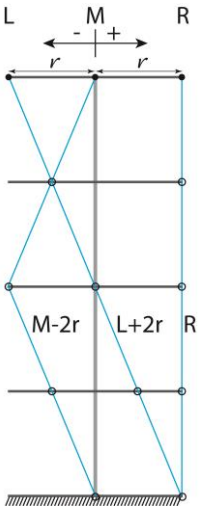

Figure 12: The notation of cables: A capital L, M or R stands for the staring position. A lowercase addition or subtraction indicates a helix cable, its direction and the horizontal distance it travels from segment 1 to *n*.

As one can expect, the model is symmetrical, meaning that mirrored cables like L+2r and R-2r will produce equal but opposite results. First the results of individual cables will be discussed, after which the results of combination of multiple cables are given.

Individual cable

Figure 13 illustrates the deformed shapes, α-graphs, forces and moments of five different cable positions. The α-graphs start at segment 1, which represents the top segment of the steerable element. From the moment balances of section 2.2.2 one knows that M_r represents the bending moment of the flexible axis and is equal to the product of stiffness *c* and $\angle\alpha$. Line M_r is therefore uniform to the α-graph.

M_r is altered by moments $M_{Fa.x}$, $M_{Fa.y}$, $M_{Fc.x}$ and $M_{Fc.y}$ resulting from the components of F_a and F_C. These moments will be referred to as force moments. In the moment-graphs the force moments are striped lines and represent the negative summation of the moment along the segments. This representation supplies a more intuitive view on their contribution to M_r, which is passed on from segment to segment. Do note that in this notation a moment in a segment will skew the moment line and for a horizontal moment line the responsible moment will be zero at those segments.

This page is not in use in order to present the following figure and description of the validation together.

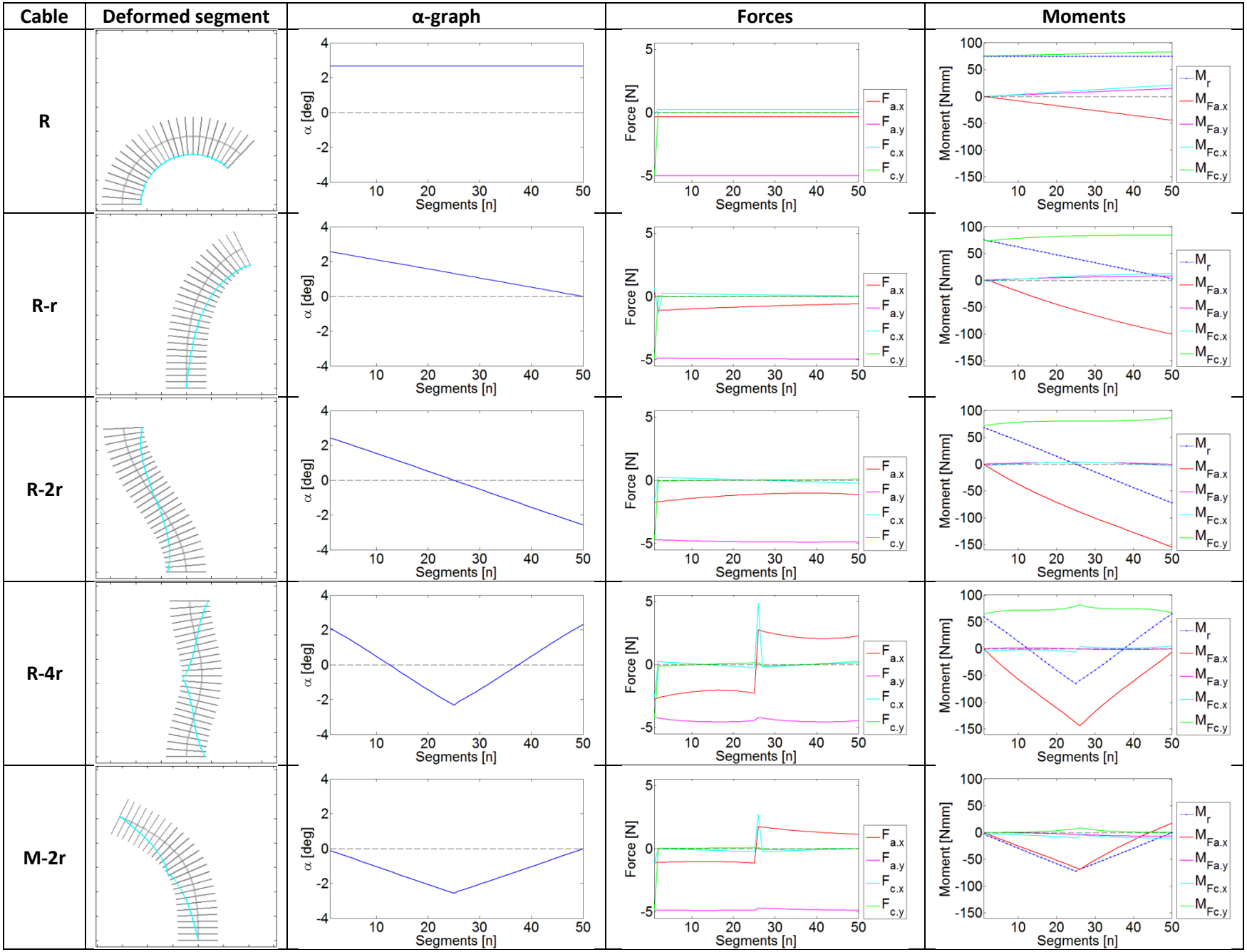

Figure 13: The deformed shape, α-graph, forces and moments of five cable positions

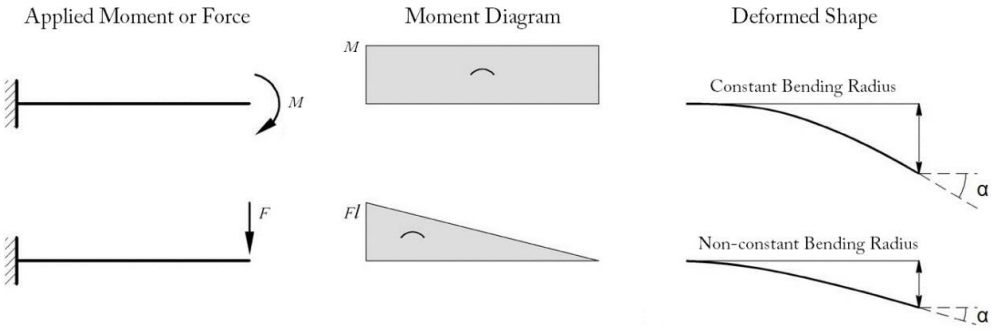

Figure 14: The deformation of a fixed beam due to a pure bending moment M or a perpendicular placed force F.

The first cable of Figure 13 is a parallel placed cable. One can see that the steerable element deforms with a constant radius, resulting in a horizontal line for ∠α. This result is identical to the behavior of parallel cable actuated instrumentation discussed in the introduction. The moment-graph shows that M_r is initially caused by $M_{Fc.y}$ of segment 1. Notice that its moment line is almost constant, meaning that the $M_{Fc.y}$ in segments 2 to *n* is close to zero. $M_{Fa.x}$ is represented by a decreasing moment line due to the addition of the moment created by F_{ax} in each segment. It is however compensated for by the other force moments.

The second cable is R-r and one can immediately see the difference with the parallel cable. Now the bending radius is no longer constant but increases constantly along the steerable element, resulting in a constantly decreasing α-value. This phenomenon is explained when realizing that contrary to the parallel cable, the helix cable includes the force F_{C1x} in segment 1. This force increases F_{a1x} and now $M_{Fa.x}$ is no longer fully compensated by the other force moments. The increase of F_{a1x} is directed to the left and can be interpreted as gradually pushing the steerable element straight.

The third cable is R-2r and one can see that the deformed shape resembles a symmetrical S-curve. The top half of the deformed shape is identical to the deformed shape of R-r, which could be expected since there they have a similar cable position. From the α-graph it is also clear to see that the shape is symmetrical, since it's a straight line which passes the zero line at half the segment domain. F_{ax} is again greater resulting in a higher value for $M_{Fa.x}$. F_{ax} can be interpreted as pushing the deformed shape even further to the left.

The fourth cable position is R-4r and it includes a direction change of the cable halfway the steerable element. In the force-graph one can see that this direction change induces a positive peak of force F_{Cx}, which results in a direction change of F_{ax}, and therefore $M_{Fa.x}$. This peak is explained by the increase of the cable bend angle at its direction change. The peak force can be interpreted as pushing the structure to the right again. The α-graph has a pyramid shape, indicating the change of direction.

The fifth cable is M-2r, which starts at the middle where the moment arm d_{Cx} is zero and therefore $M_{Fc.y}$ at segment 1 is zero. The α-graph therefore also starts at zero and the deformation in the following segments is mainly caused by $M_{Fa.x}$. The α-graph again has a pyramid shape due to the direction change of the cable.

By reviewing these results one can conclude on the following. The deformed shape of a segment is mainly caused by F_{c1y} and F_{c1x}. F_{c1y} is mainly responsible for M_{r1} that passes through the whole steerable element and induces a constant radius bend. F_{c1x} is highest for helix cables and introduces F_{a1x} that passes through every segment and deforms the steerable element with a non-constant bending radius.

The simulation model thereby show great similarities with the results of the conjugate beam method for a fixed beam loaded with a pure bending moment or a perpendicular force as illustrated in Figure 14. The moment diagrams of *M* and *F* are uniform to those of $M_{Fc.y}$ and $M_{Fa.x}$ of cable R-2r in Figure 14. This seems peculiar since the simulation model also includes extra cable forces throughout segments 2 till *n*, while the conjugate beam method only includes the shear force which does not change direction.

An explanation can be found if one looks at the force graph and the moment graph of cable R in Figure 13. F_{ax} is initiated by F_{c1x} in segment 1 and influenced throughout the remaining segments by F_{cx} and

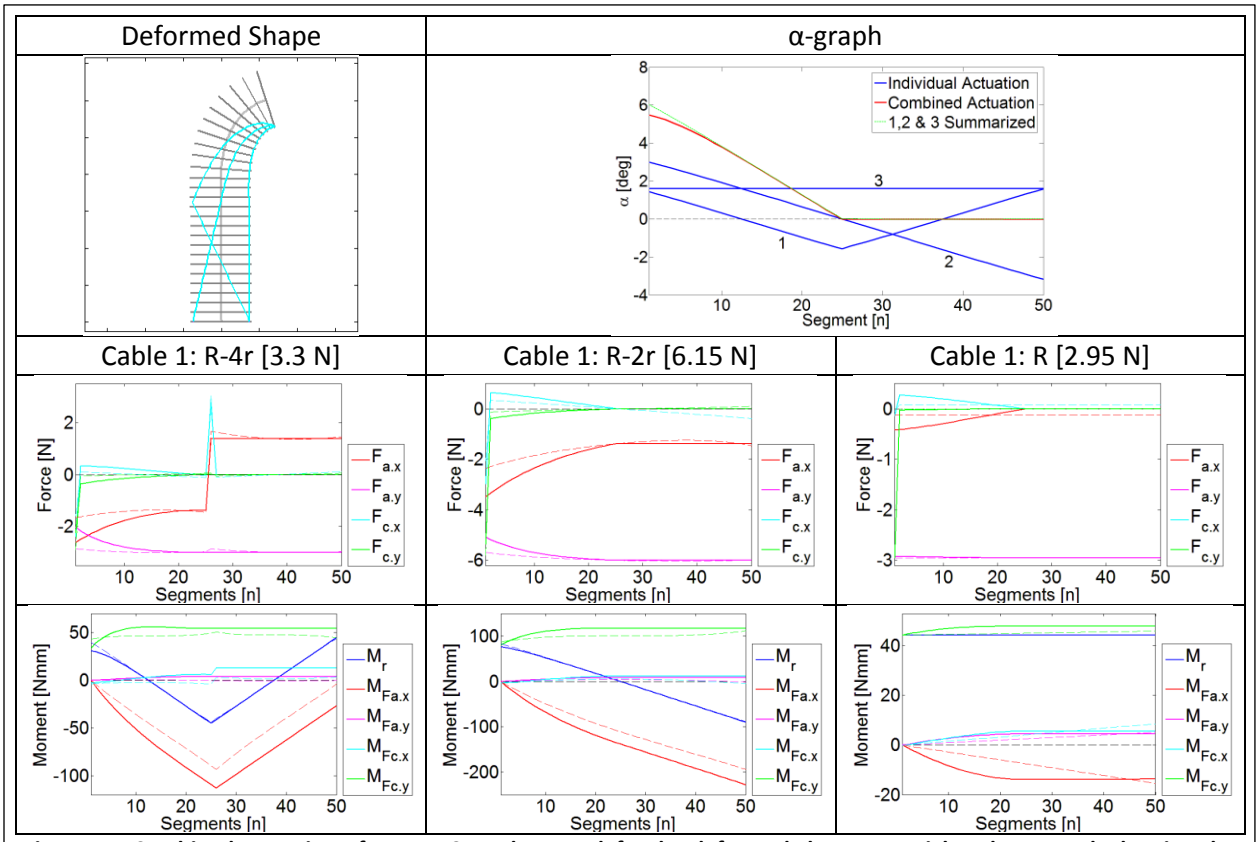

Figure 15: Combined actuation of R-4r, R-2r and R. Top left: The deformed shape. Top right: The α-graph showing the combined output, the output of the individual cables and the summarized outputs of the individual cables. Bottom: The forces and moment graphs of the individual cables. The full lines represent the forces and moments in combined actuation, the stripped lines represent the resulting forces and moments when the cables are actuating the steerable element individually.

indirectly by F_{ay} and F_{Cy} through the direction changes of local coordination systems (*Eq. 2-13). F_{ax} creates the moment $M_{Fa.x}$ which would distort the constant behavior of M_{r1}, but is however compensated for by the moments created by the same forces that influence $F_{ax,}$ namely F_{cx1}, F_{cy1} and F_{ay}. It therefore seems that the cable in the model acts as a compensation mechanism to keep the initial moments and forces set in segment 1 intact.

The same influence of the force moments $M_{Fa.y}$, $M_{Fc.x}$ and $M_{Fc1.y}$ on $M_{Fa.x}$ can be seen for helix cables, for example cable R-r of Figure 13. In this configuration $M_{Fa.x}$ dictates the behavior of M_r, which is a straight line from the initial value of $M_{Fc.y1}$ in segment 1 to zero at segment 50. $M_{Fa.x}$ does, however, deviate from a perfectly straight line and is slightly more skewed than M_r. This is however again compensated for by the M_{Fay}, $M_{Fc.x}$ and $M_{Fc.y}$.

Combined actuation

The situation wherein multiple cables are actuated simultaneously will be referred to as combined actuation. An interesting phenomenon reveals itself during combined actuation. The deformation can namely be approximated by summarizing the deformation of the individual cables. This effect is analyzed for the combined actuation of cables R-4r, R-2r and R, illustrated in Figure 15.

The α-graph of Figure 15 includes five lines. The red line represents the output of combined actuation. The three blue lines are the outputs when each cable is actuated individually. The dotted green line represents the summarized outputs of the individual cables. One can see that the green dotted line and red line almost perfectly match each other.

This indicates that in each segment, each individual cable contributes the same overall moment during combined actuation as it does when the cable is actuated individually. This seems odd, because the forces generated by a cable will differ

due to the shape change of the steerable element. These differences are illustrated by the force graphs of Figure 15, in where equal colored full and dotted lines represent a force during combined and individual actuation respectively. The force moments will inevitably change as well, as is illustrated by the deviation between the full and dotted lines of the force moment graphs of Figure 15.

The summation of the force moments into M_r however result in an almost equal value for combined and individual actuation, as is illustrated in the moment graphs. It inevitably means that the changes of the force moments compensate each other. This compensation behavior was already discovered in the analysis of the individual cables and is apparently also applicable if the shape of the steerable element is changed.

The M_r lines do however deviate at the first segments. This can be explained by the fact that M_{Fcx} and M_{Fcy} of segment 1 change due to the direction change of F_{c1} caused by the $\alpha\text{-change}_1$. The deviation is however compensated for by the force moments of the sequential segments.

The preservation of M_r reveals that one can approximate the outcome of combined actuation by summurizing the outputs of the individual cables.

2.4 Inversion of the model

The simulation model is based on an actuation-to-shape approach. The inputs of the model are the amount of cables, their positions and the actuation forces. The output of the model is the deformed shape of the steerable element. The question arises if this process can be reversed, enabling one to determine the needed cable configuration in order to reach a desired shape.

Kinematic inversion of the mechanical model is not possible. This is due to the fact that the mechanical model handles the segments individually and the deformation of a segment can be caused by numerous cable configurations. The phenomenon revealed during the combined actuation can however provide a solution. The idea is that a desired shape can be approximated by combining the outputs of individual cables.

The output of the individual cables should therefore first be expressed as an equation, referred to as the cable equation. From Figure 13 it can be seen that the output of individual cable approximate linearity. The general cable equation can therefore be written as:

$$\alpha_n = \begin{cases} n \leq n_{dc} & C_1 \cdot F_{C_1} \cdot \beta \cdot r_{C_1} - d \cdot C_2 \cdot F_{C_1} \cdot \left(\frac{\pi}{2} - \beta\right) \cdot (n-1) \\ n > n_{dc} & \alpha_{n_{dc}} + d \cdot C_3 \cdot F_{C_1} \cdot \left(\frac{\pi}{2} - \beta\right) \cdot (n - n_{dc}) \end{cases}$$

where d is the direction of the cable, n_{dc} represents the segment at which a direction change of a cable can occur and α_{ndc} is the α-value at this direction change. If the cable does not include a direction change, the value of n_{dc} will be equal to n. C_1, C_2 and C_3 are constants and are based on the dimensions and characteristics of the instrument. Deriving the cable configuration contains the following steps.

The green dotted line in the α-graph of Figure 15 serves as the desired deformed shape. First one indicates the position of the bend in the α-line. This inevitably requires a cable with a direction change in the desired direction at that position. Cable R-4r is chosen and introduced as cable 1 in the α-graph. A helix cable without a direction change is needed to skew the output of cable 1. Cable R-2r is chosen and introduced as cable 2. The combined output of cable 1 and 2 is now uniform to, but lies beneath the desired α-line. A constant α-line is needed and therefore cable R is introduced as the final cable 3.

Now that the position of the cables is known, one can determine and combine the related cable equations, whilst keeping the actuation forces variable. The resulting equation should be set equal to several α-values of the desired shape to form a system of equations. This system of equations should then be solved for the actuation forces.

2.5 Validation

A physical validation model is created in order to validate the behavior of the mechanical model. It is crucial that the simplifications made for the mechanical model are properly represented in the validation model.

2.5.1 Experimental setup

Before designing the validation model one must decide on which cable positions need to be evaluated. In Figure 16 two physical phenomena are marked with the letters a & b which indicate the crossing of the flexible axis and the direction change of a cable. Both these phenomena will be studied during the validation process and the following four cable positions are chosen for evaluation:

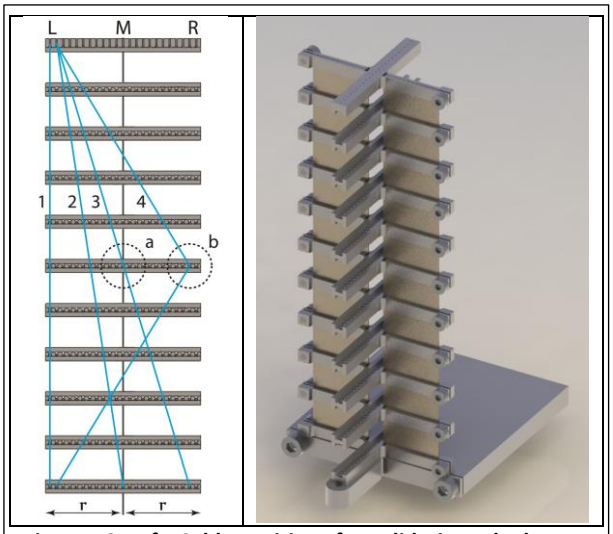

Figure 16: Left: Cable positions for validation. The letters a & b mark the crossing of the flexible axis and a direction change of a cable respectively. Right: Solidworks model of the validation model.

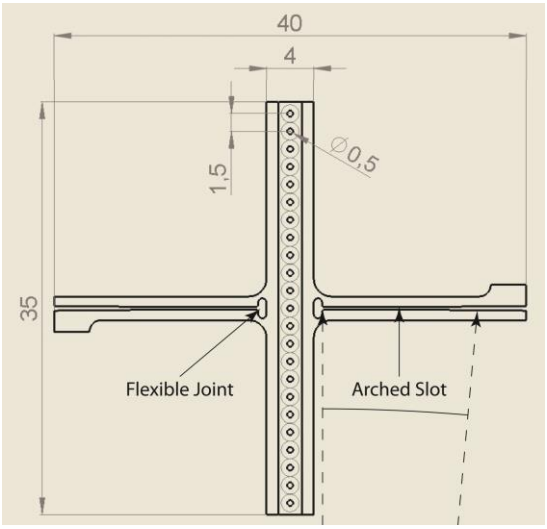

Figure 17: Drawing of a rib. The flexible joint and the arched slot ensure an evenly distributed clamping force on the leaf springs.

L : Benchmark parallel cable
L+r : Benchmark helix cable
L+2r : Crossing the flexible axis
L+4r : Direction change of the cable

The validation model should be able to evaluate combined actuation. This can however result in multiple cables passing though the same cable hole, which would lead to undesired friction and interference between the cables. To avoid the interference of cables, each rib is fitted with an extra cable hole at each end of the rib. These holes will allow a parallel cable to be placed without interfering with other helix cables.

The next step in the design process is to decide how many segments the validation model should contain. To enable the L+4r cable position, the amount of segment should be an even number. More segments will result in a higher accuracy of the measurements on the validation model. However the addition of extra segments inevitably results in higher friction and a heavier model. This tradeoff has resulted in the choice of a ten segmented validation model. Twenty-one cable holes are needed to enable the placement of cable L+r, adding the two extra holes to enable combined actuation and each rib will therefore be fitted with 23 cables holes.

Table 1: The weights of the loads used for actuation.

Load	1	2	3	4	5
Weight [gr]	100	200	298	396	493

The validation model will be actuated with the use of five loads. There weights are listed in Table 1. These loads are chosen based on the results of the simulation model.

2.5.2 Design

The design of the validation model is shown in Figure 16. In order to represent the two dimensional characteristic of the mechanical model, the cables and their resulting forces and moments should lie in the same plane. Since they must be able to cross the flexible axis, this axis should lie outside this plane, but its moments should work inside the plane. Therefore both sides of the plane should be symmetrical. This is achieved by fabricating the flexible axis out of two leaf springs, see Figure 16. The leaf springs are fabricated out of C75 spring steel due to the high maximum tensile strength.

In order to preserve the structural characteristics of the leaf springs, the ribs are fixated on the leaf springs with a slotted clamping construction, shown in Figure 17. At the beginning of the slots there is a flexible joint and the slots are slightly arched allowing an equal clamping force along the leaf spring. The clamping force is created by a screw at each end of the rib. The cable holes have a diameter of 0.5 mm and the edges are rounded in order to reduce friction between the rib and the cable. The ribs should mimic infinite rigidity and no mass and are therefore fabricated out of the high strength low

weight material aluminum.

The bending stiffness of the cables should be as low as possible. However, since a certain roughness and sharp edges around the cable holes are inevitable, Nylon or Dyneema cable are too vulnerable. Therefore woven steel cables have been chosen with a small diameter of 0.15 mm to reduce the bending stiffness.

The dimensions of the validation model are presented in Appendix D.1

2.5.3 Validation procedure

The comparison between the mechanical model and the validation model is based on their segment angles α_n. The simulation model is therefore also fitted with ten segments. In order to retrieve α_n of the validation model, the ribs are marked with red and green markers. With the use of an image processing algorithm created in Matlab and described in Appendix B.2, the positions of the ribs can now be retrieved as illustrated in Figure 18.

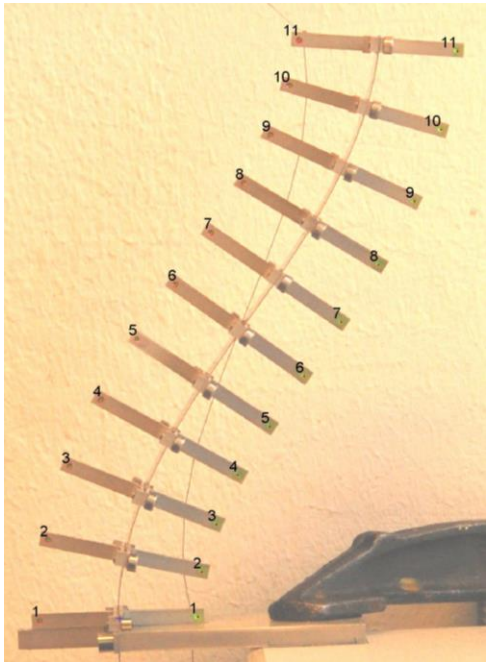

Figure 18: Result of the image processing algorithm identifying the positions of the ribs.

Unloaded position

During the validation process, the validation model without cables was regularly photographed in its unloaded position. The results of these unloaded positions are plotted together in Figure 19.

The blue lines indicate 23 unloaded positions and the red line is the average unloaded position. The deviation from this average unloaded position is plotted in a distribution plot. The shape of the distribution resembles a normal distribution around zero with a standard deviation equal to 0.35. This means that one can expect an initial error of 0.35 degrees.

The red line represents the mean of the non-actuated positions and will be used as the initial zero point reference for all measurements.

The deviation from the mean initial position can be caused by hysteresis characteristic of the leaf springs and/or the accuracy of the image processing.

Hysteresis

The validation model is loaded in two different manners: underloading and overloading. In the underloading procedure the initial load on the cable will be zero after which the cable is gently loaded. The overloading procedure load starts with an initial overload which is gently released.

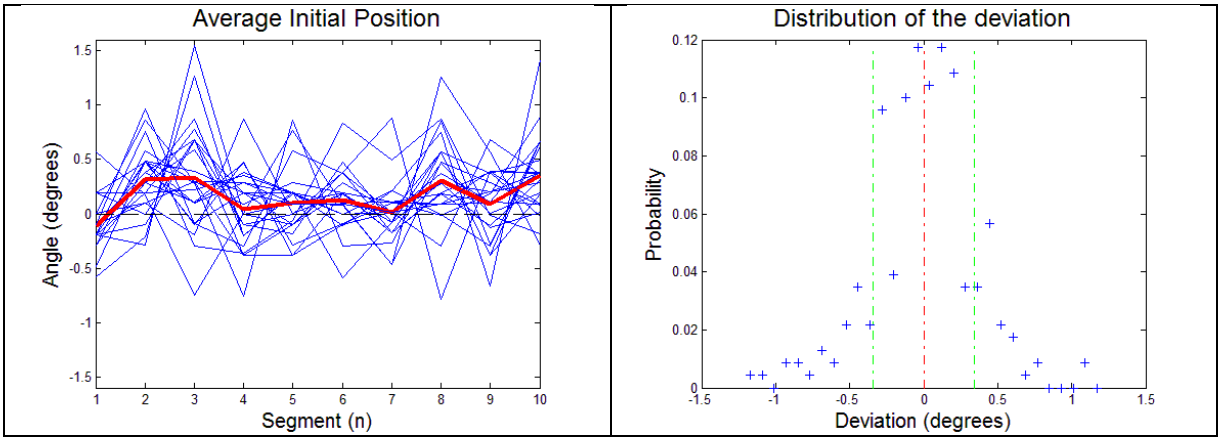

Figure 19: Left: 23 results in unloaded position. Right: Distribution of the deviation from the average unloaded position.

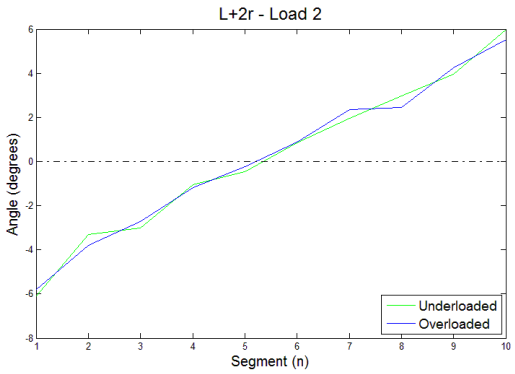

Figure 21: Results of a single underloading and overloading procedure for cable L+2r with load 2.

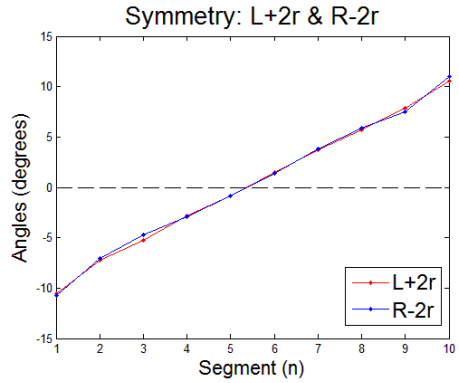

Figure 20: The results of the mirrored cables L+2r and R-2r. The sign of the output of R-2r is turned.

The different loading procedures will lead to slightly different end positions of the model. This effect is called hysteresis and is caused by a phenomenon which will be referred to as stick-slip.

Stick-slip happens when the static friction between cable and rib overcomes the dynamic friction and the cable comes to a hold prior to the static equilibrium without friction. One can reduce the magnitude of this stick-slip by sending a vibration through the model. This allows the cable to come momentarily less pressed against the ribs, which reduces the static friction and should allow the model to move closer to its friction free static equilibrium. Therefore during the validation procedure, the base of the model was tapped several times.

Even though the tapping of the model reduces the effects of stick-slip, a single measurement will not suffice as a proper indicator of a stick-slip-free static equilibrium of the validation model. With the use of a pilot study discussed in Appendix C it was determined that 10 underloading and 10 overloading procedures should be sufficient for an accurate measurement. The resulting measurement of one underloaded and one overloaded position of the cable position L+2r actuated with load 2 (200 gr) are illustrated in Figure 21.

In the plot one can detect the effect of stick-slip by the repeated crossing of the two lines. The explanation lays in the fact that the deformation of a segment *n* is effected by $M_{a.n-1}$ passed on by the previous segment *n-1*. If the deformation of segment *n-1* is smaller due to stick-slip, $M_{a.n-1}$ will be lower as well. This decrease will result in less resistance to deformation in segment *n*. This is the reason why the underloaded and overloaded positions cross each other.

The average output of all twenty measurements will be used as the values of $\angle\alpha_{validation}$.

2.6 Validation results

The results of the measurements will be presented by two numbers, namely the mean error (ME) and the standard deviation (StD).

$$\mathrm{ME} = \frac{\sum_1^p \frac{\sum_1^n \alpha_{\mathrm{model.n}} - \alpha_{\mathrm{validation.n}}}{n}}{p}$$

$$\mathrm{StD} = \frac{\sum_1^p \sqrt{\frac{\sum_1^n (\mathrm{ME} - (\alpha_{\mathrm{model.n}} - \alpha_{\mathrm{validation.n}}))^2}{n}}}{p}$$

where p is the amount of measurements. ME represents the error between the simulation model and the validation model. StD represents the standard deviation of ME.

Symmetry

The symmetry of the validation model is tested by comparing the result of the two mirrored cables L+2r and R-2r. The results of these cables are plotted in Figure 20, where the measurements of cable R-2r are multiplied by -1 in order to match the direction of mirrored cable L+2r.

One can see that the lines match up rather well. This is expressed by a low value for the mean error between both lines of -0.084 degrees with a standard deviation of 0.24 degrees.

Behavior

The behavior validation of the simulation model is based on the cables presented in the graphs of

This page is not used in order to present the following figure and description next to each other.

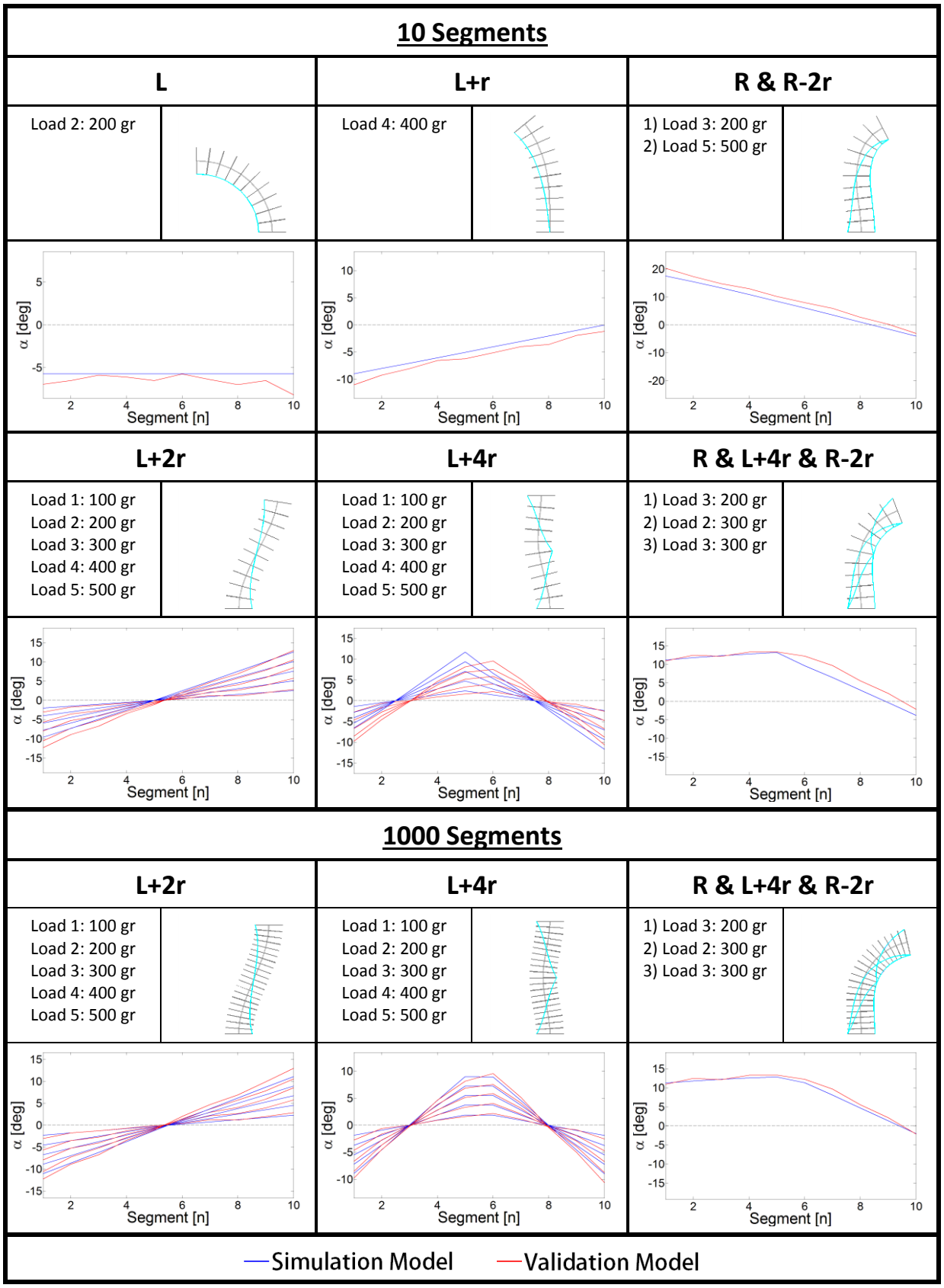

Figure 22: Top: The deformed shapes and α-graphs of the six validated cable positions based on 10 segments. Bottom: The alpha graphs of the three validated cable positions based on 1000 segments.

Figure 22**.** The figure includes α-graphs of the validation model and simulation model, which is based on 10 segments and on 1000 segments

The first impression based on the top six α-graphs of Figure 22 is that the behavior of the validation model is similar to the simulation model. There are however two phenomena that introduce a mismatch between the validation and simulation model. The first mismatch is the overall lower α-value of the simulation model. The second mismatch occurs at cables that include a direction change, which is best illustrated by the α-graph of cable L+4r. While the α-graph of the simulation model forms a pointed pyramided, the top of the α-graph of the validation model is flattened.

Both these phenomena can be explained by realizing that at these points a high sideway force F_{cx} is introduced. In the simulation model the deformation of the segment due to F_{cx} is modeled as having a constant radius. In the validation model however the resulting deformation due to F_{cx} will have a non-constant radius. This effect is equal to deflection of a fixed beam loaded with a perpendicular force (Figure 14).

In the simulation model, the moment created by F_{Cx1} therefore has a greater value. Because the moment is directed opposite from the overall moment M_{r1}, the result is a lower value for M_{r1} and therefore $\angle\alpha_1$. Since M_{r1} is passed on through following segments, the simulation model shows an overall lower α-graph.

The effect of the non-constant bending radius due to F_{cx} in the simulation model can however be reduced by increasing the amount of segments. The working principle behind this approach is the fact that the bending behavior of a smaller slice of the flexible axis will approximate a constant bending radius with higher accuracy. In order to still match the 10 segmented validation model, the outputs of each 100 sequential segments are summarized to represent one segment.

In the bottom three α-graphs of Figure 22, the validation model is compared to the simulation model based on 1000 segments One can immediately see that especially for cable L+4r the outcomes of the two models match each other with higher accuracy.

For cable L+2r the angle of the α-lines of the simulation model due to the increase of segments decreases. This phenomenon is illustrated by Figure

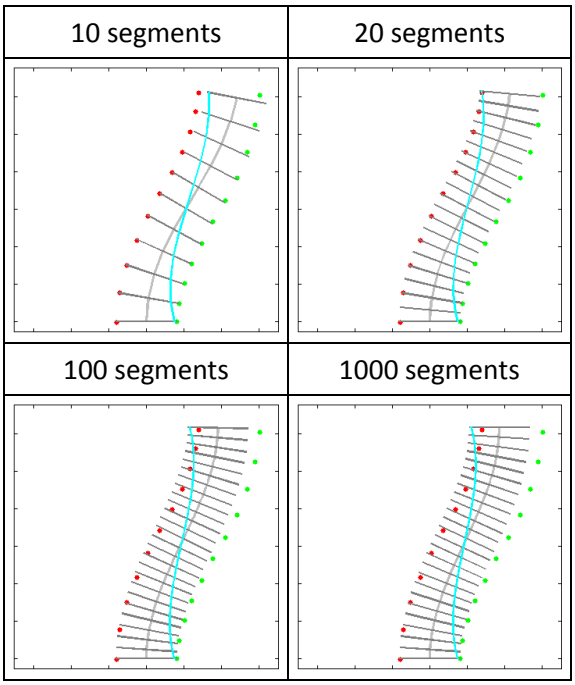

Figure 23: The red and green markers of the validation model compared to the simulation model for different amount of segments.

23. It shows the validation markers compared to the deformed shape of the simulation model. One can see that for a higher amount of segments, the overall deformation decreases. This can be explained when one realizes that the increase of segments influences the path of the cable. For the validation model, the path between sequential segments is straight. Due to the increase of segments this path is however modeled as a curve. This phenomenon decreases $\angle\delta_1$ and thereby decreases F_{C1x} and increases F_{C1y}. The sideway pushing effect of F_{C1x} therefore decreases, resulting in an overall decrease of the deformation.

Mean Error

The ME and StD values are presented in Table 2. The columns %ME and %StD represent the percentages of ME and StD of the maximal α-value of the simulation model for that cable.

The effect on the ME by the division of the simulation model into more segments varies for the different cables configurations.

For the parallel cable, one can see no significant change between 10 segments for 1000 segments. This is to be expected since a single parallel cable does not induced high values for $F_{cx.}$

For all helix cables (single or combined) except

Table 2: Table of the ME and StD values based on 10 segments and 1000 segments. The %ME and %StD values represent the percentage of ME and StD compared to the maximal deformation of the simulation model in the represented position.

10 Segments

Cable	Load	ME	% ME	StD	% StD
L	2	0,86	15,03	0,66	11,52
L+r	4	1,17	13,02	0,39	4,33
L+2r	1	0,18	7,06	0,34	13,55
	2	0,35	6,92	0,56	10,99
	3	0,51	6,75	0,72	9,48
	4	0,81	8,00	0,83	8,26
	5	0,94	7,47	0,86	6,80
L+4r	1	0,13	5,32	0,64	26,95
	2	0,20	4,19	1,10	23,16
	3	0,26	3,66	1,58	22,42
	4	0,31	3,29	2,05	21,85
	5	0,31	2,64	2,55	21,82
R **R-2r**	3 5	-1,87	-10,70	0,46	2,65
R **L+4r** **R-2r**	3 2 3	-1,34	-10,17	1,24	9,41

1000 Segments

Cable	Load	ME	% ME	Std	% Std
L	2	0,85	14,89	0,66	11,50
L+r	4	0,63	6,54	0,37	3,88
L+2r	1	-0,08	-3,32	0,34	15,12
	2	-0,16	-3,63	0,56	12,37
	3	-0,27	-4,00	0,73	10,79
	4	-0,25	-2,76	0,84	9,39
	5	-0,39	-3,54	0,87	7,85
L+4r	1	0,13	6,69	0,37	19,79
	2	0,20	5,32	0,44	11,83
	3	0,26	4,68	0,54	9,78
	4	0,31	4,25	0,62	8,46
	5	0,31	3,44	0,65	7,23
R **R-2r**	3 5	-0,50	-2,61	0,42	2,17
R **L+4r** **R-2r**	3 2 3	-0,55	-4,28	0,56	4,35

for cable L+4r, the absolute ME values decrease indicating a better overall match between both models.

For cable L+4r however the values for ME stay equal for both 10 and 1000 segments. This can be explained when one looks at the α-graphs of 10 segments of cable L+4r. It shows that the mismatch between validation and simulation model is for certain segments positive while being negative for the other segments. These deviations seem to compensate each other. The effect can be expressed by the mean absolute error (MAE) which for load 4 decreases from 1.97 to 0.48.

Standard Deviation

For the parallel cable the amount of segments has also no effect on the StD value.

For all helix cables (single or combined) except for cable L+4r, the StD values do not show a significant change between 10 or 1000 segments. The %StD value however do contain a shift. This can be explained by the increase of the maximal α-value of the simulation model, due to the fact that the moment of F_{Cx1} has less effect on M_{r1}.

The StD values for cable L+4r do show a fundamental decrease. This illustrates the positive effect of the addition of segments.

Force

The effect of different loads is evaluated for cables L+2r and L+4r. One can see in the tables of Figure 22 that the values of ME and StD go up for higher loads. While the values of %ME and %StD stay constant and decrease respectively. This shows that the error increases with heavier loads, while the variance of the error decreases. The measurements from validation model therefore seem to gain accuracy for higher loads. An explanation might be that the effect of stick-slip will be relatively lower.

2.7 Discussion

2.7.1 Shape interpretation

The shapes produced by the individual helix cables as presented in Figure 13 can be interpreted as part of a sine function. This is explained by the fact that their α-lines are linear and therefore the deviation of $\angle\alpha$ is constant. A sine function represents a line with a constant varying angle which in the deformed shape is presented by $\angle\alpha$.

The shape of cable R-2r is equal to half a period of sine, while cable R-4r results is a full period of sine. Therefore one can state that the frequency of the sine-shape is represented by $\angle\beta$, its amplitude is based on F_{C1} and the starting position r_{c1} determines the phase change.

2.7.2 Simplifying the model

The ideal design of the simulation model would be based on a symbolic solution for both moment balances of segment 1 and segments 2 to *n*. The addition of multiple cables does, however, result in a rapidly expansion of the symbolic notation of the moment balances. A symbolic solution can therefore not be obtained. The question is whether it is possible to simplify the description of the model without losing accuracy.

The mathematical description of the model could be simplified by approximating the sins, cosine and arctangent terms of the moment balances. This will however still not lead to a symbolic solution of the moment balances thus the solution would still be determined numerically. In the current process there is no need for simplification of the sine, cosine and arctangent terms.

A simplification of the simulation model based on the dismissal of the small moments of forces would distort the compensation behavior of the model and is therefore not advised.

Simplification by neglecting the change of the moment arms could however prove fruitful. The idea is that for small segments, the effect of $\angle\alpha$ on the moment arms can be neglected. The forces would however still be based on $\angle\alpha$. The resulting model would be a step closer to the conjugate beam method, with the direction change of forces as the only difference.

The high amount of segments does, however, not simulate the structure of the cable ring forceps correctly. A solution could be found by letting r_{cn} of a helix cables change per *x* amount of segments to simulate a more crudely segmented structure.

2.7.3 From 2D to 3D

Expanding the simulation model to the third dimensional realm will expand the range of motion of a segment with two additional DOF. One will be an additional bending DOF directed perpendicular to the current bending plane. The other DOF will describe a torsional deformation of the segment.

The description of the model should therefore be expanded with one additional bending plane and one torsion plane. This invokes the need for two additional moment balances. The two moment balances that describe a bending motion will be coupled together by the moment balance of the torsion motion. This can be explained by imagining a segment bend in only one bending plane. An additional torsion will redirect this bend, which would now partially lie in the second bending plane as well.

A manner in which the three dimensional deformation of a segment could be derived starts by solving the torsional moment balance. Then a temporal bending plane and moment balance is introduced which direction is determined by the torsional deformation of the segment. The calculated bending motion in this plane can finally be projected on the two permanent bending planes.

The inclusion of torsional motion could however result in undesired alterations to the shape of the steerable element and the rotational direction of the tip itself. By replacing the flexible axis by a torsion stiff deformable structure, the torsion motion can be largely excluded. This makes the torsional moment balance redundant. It would also mean that the coupled behavior between the bending moment balances disappears.

Implementation of a torsion stiff axis into a miniaturized instrument can however prove difficult. A possible solution is presented by the braided structure of section 1.2 of which the torsion stiffness was high due to the inclusion of fixated counter-clockwise and clockwise rotating helix cables. This implies that the torsion stiffness of a steerable element can be improved by including clockwise and counter clockwise cables and fixating their lengths after a desirable shape is reached.

2.7.4 Friction

Friction is totally neglected in the simulation model and sufficiently reduced in the validation model. Suppose one wants to incorporate helix cables into a construction like the cable ring forceps of Figure 3. The cables would be fully enclosed and the resulting friction could no longer be neglected.

For this reason one can state that for accurate modeling of minimized instruments, the neglection of friction will no longer suffice.

Friction can be incorporated into the model by including F_{fr} positioned at the cable points C_n. F_{fr} is

the product of F_{cn} times a friction coefficient and its direction will be normal to F_{cn} and opposite to the motion of the cable. The moment caused by F_{fr} could be incorporated into the moment balance of segments 2 to *n* by using the same moment arms as F_{cn}. The moment balance of segment 1 would not contain a friction component, since the cables are fixated at the top rib.

The two dimensional configuration of the model includes high cable forces during a direction change of a cable. This inevitable will induces high friction forces as well. One should however keep in mind that in a three dimensional configuration, the direction of a helix cable is gradually altered at every segment. The friction of helix cables in a three dimensional configuration will therefore not be focused in a specific point. Due to this gradual friction behavior, one can expect that in comparison with a parallel cable, the friction forces of a helix cable will generally be higher.

2.7.5 Mass

The model is not capable of coping with the gravitational pull of mass. This is due to the changes of local coordination systems and the fact that the model starts calculating the deformation from the top. If one would incorporate a gravitational force in segment 1, its direction would change due to the deformation of segment 2. The calculated deformation of segment 1 would therefore not be correct.

Unlike friction, the effects of mass will reduce during the minimization of the steerable element.

2.7.6 Combination of multiple cables

The compensation behavior a cable described in section 2.3 can best be viewed by comparing the path of the cable during individual actuation and combined actuation. The path of cable 1 during individual actuation can be viewed as the path of least resistance. The addition of cables during combined actuation will deform the original path of cable 1. If the bending radius of the path is increased, cable 1 reacts by increasing the appropriate cable forces. If the bending radius is decreased, cable 1 reacts by decreasing the appropriate cable forces.

2.7.7 Shape domain

The fact that the combined actuation output can be approximated by the summarized individual outputs gives insight into the possible shape domain of the steerable element. This domain can best be viewed as all the possible α-graphs one is able to produce through the combination of the linearized equations describing the outputs of individual actuation.

Because these equations are linear, one can conclude that the α-change is always constant. Its direction can however be changed by a direction change of a cable. This direction change can be seen as the beginning of a new section with its own linear behavior of $\angle\alpha$. The starting point of this section is determined by the last α-value of its predecessor. The shape domain consists of numerous combinations of these types of sections.

The linearly deviating behavior of α and the preset starting point of a new section form the two main limitations of the shape domain. Another limitation is the minimum bending radius of a segment, which is equal to r. If the bending radius becomes smaller, the ribs of the segment will hit and thereby restrict each other.

A final limitation of the shape domain restricts the amount of cables and especially the amount of direction changes in the two dimension realm. It is not a hard limit, but one should keep in mind that the addition of cables and direction changes will increase the total friction in the structure. In combined actuation, the alteration of one cable will invoke a shape change that affects all cables. Therefore all frictional forces must be overcome, even the ones not directly connected to the altered cable.

2.7.8 Extension to extreme positions

It is interesting to see to which length the simulation model would produce plausible results. A cable R-2r is therefore actuated with a rather large force. The resulting deformed shape and alpha graph is shown in Figure 24.

One can see that for 15 N the middle of the axis has become horizontal. The corresponding α-line is close to linear, which is a good indication of the plausibility of the deformation.

For 30 N the α-graph is no longer linear and seems to form a sine. It is checked if the bending radii of the deformed shape become less that the radius of the steerable element, which would result in a collision between ribs. This is not the case. The symmetric shape is however an indication that at least the calculation procedure is correct. The

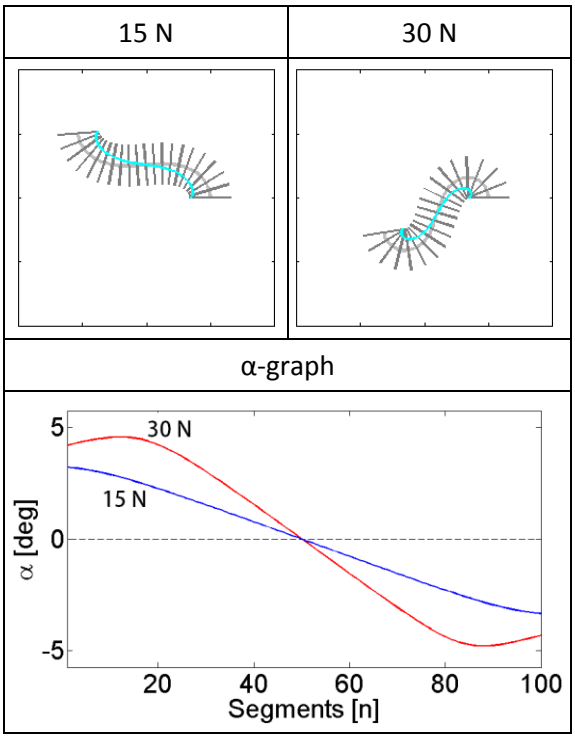

Figure 24: Extreme positions for cable R-2r.

plausibility of the shape is however disputable.

2.7.9 Validation

The error between the validation model and the mechanical model is induced by multiple factors. The first and most important reason can be described to the mechanical model's inability to cope with the non-constant bending behavior due to sideway forces combined with large segments.

A second reason of error can be indicated by the hysteresis of the validation model due to stick-slip. This is addressed by the under and overloading of the model and the overlap between the two is a good indicator for the reduction of the hysteresis error.

A third reason of error will lay in the neglection of friction in the simulation model. Friction on a cable in the validation model will lead to tension loss in the cable, thereby reducing the actuation force the cable is able to exert on the model. This error is not addressed by the hysteresis of the model.

A fourth reason for error can be pinpointed to the neglection of mass in the mechanical model. The validation model obviously has mass. In un-deformed position the weight will only affect F_{ay} due to the symmetry of the model. If the validation model is deformed, the direction of the weight in contrast to the deformed flexible axis will change. This means that the weight will now also affect F_{ax}. The effect of mass is however minimized by minimizing the mass of the validation model and the use of much heavier loads. The working principle is that the mass of the validation model itself has less effect if the actuation forces are higher.

A fifth reason of error lays in the difference in rib thickness between the mechanical and validation model. While in the mechanical model, the ribs do not possess thickness, the ribs in the validation model obviously do. Since these ribs are clamped on the leaf springs, they restrict the leaf springs from bending at those areas and thereby reducing the effective bending length of the flexible axis of the validation model.

It has become apparent that the validation model is not the perfect tool for the validation of the simulation model. The simulation model's ability to explain the change of behavior due to the increase of segments does, however, improve its validity. One could therefore confidently state that the validation process has succeeded in validating the fundamental behavior of the model.

3 Demonstration prototype

3.1 Background

From the mechanical model it has become apparent that by combining parallel and helix cable actuation an instrument is able to create complex non-constant radius shapes. The following question however remains: How can such an steerable element be controlled?

Previous work from T. Nai [1] and P. Henselmans [2] reveals that there are two prominent actuation strategies for cable actuated instruments, i.e. electrical and mechanical actuation. Which of these two strategies is the most suitable for the helix actuated instrument?

The basic principle of electric control relies on electric motors to actuate each cable individually. This type of control is therefore suitable for all types of cable actuated steering. The Endowrist, introduced in section 1.2, uses this type of control in the da Vinci robotic system. The result is a rather bulky, complex and expensive master-slave system, as seen in Figure 25 [5]. Note that the Endowrist has one steerable element based on parallel placed cables, this solution seems a bit complicated.

A more elegant solution is used by the Multiflex introduced in Section 1.2 and illustrated in Figure 26. It is based on a clever mechanical control strategy where the tip mimics the shape of the handle. Even though the Multiflex is fitted with five steerable elements, the control system can be fitted in a handheld model.

This thesis aims to explore the possibility of using a mechanical control strategy and constructing a fully functioning prototype of a single multi-steerable element.

Figure 25: The da Vinci robotic system, a master-slave control system that is capable of controlling multiple operation arms installed with the Endowrist. Figure is obtained from [12].

Figure 26: The Multiflex using mechanical control in where the tip mimics the shape of the handle [7].

The purpose of the demonstration prototype is to reveal the basic working principle of a mechanically actuated system with both parallel and helix cables. For a first demonstration model using helix cables, a simple combination of four cables - two parallel and helical - should be sufficient. From the mechanical model is learned that the combination of L and L+2r cables can lead to interesting and useful complex shapes. The demonstration model will therefore be based on these two cable positions and their mirrored cable positions R and R-2r.

3.2 Control

The validation model has proven to be a suitable structure for creating complex shapes and its dimensions are deemed reasonable for use in a demonstration prototype. The design of the demonstration model will therefore incorporate the validation model as presented in section 2.5.2.

Parallel Steering

For parallel-based cable-actuated instruments one can use the linear change in cable lengths of mirrored cables. The linearity can be explained when one studies two parallel mirrored cables in a segment, as is illustrated in Figure 27. The triangles

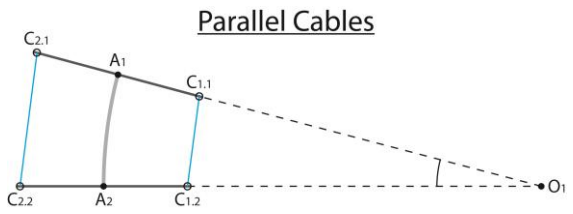

Figure 27: Segment 1 with parallel cables. Triangles $\Delta C_{1.1}O_2C_{1.2}$ and $\Delta C_{2.1}O_2C_{2.2}$ are isomorphic and length $|A_1A_2|$ is fixed. Therefore the absolute length changes of $|C_{1.1}C_{1.2}|$ and $|C_{2.1}C_{2.2}|$ are equal.

Figure 28: A schematic drawing or direct mirrored control by linked cable actuation. The motion of the tip is in the same plane and mirrored to that of the handle. The handle and tip are directly linked to each other.

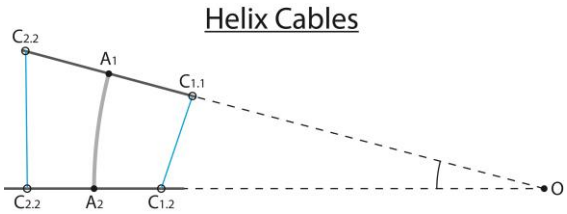

Figure 29: Segment 1 with helix cables. Figure 29: Segment 1 with parallel cables. In contrast to parallel cables, triangles $\Delta C_{1.1}O_2C_{1.2}$ and $\Delta C_{2.1}O_2C_{2.2}$ are no longer isomorphic, thus the absolute length changes of $|C_{1.1}C_{1.2}|$ and $|C_{2.1}C_{2.2}|$ are not equal.

$\Delta C_{1.1}O_2C_{1.2}$ and $\Delta C_{2.1}O_2C_{2.2}$ are isomorphic, meaning that the length of cable 1 is linearly related to the length of cable 2.

Distance $|A_1A_2|$ forms the neutral line, meaning that a cable positioned to the left will elongate and a cable at the right will shorten. Since cables 1 and 2 are mirrored copies, their absolute positions to neutral line $|A_1A_2|$are equal. One can therefore state that the absolute length changes of the cables are equal.

This linearity can be used in a control system constructed out of a handle that is identical to the design of the tip. The schematic drawing of Figure 28 illustrates this construction. Notice the mirrored behavior between the handle and the tip: if the handle moves up the tip moves down. This is due to the fact that if a cable elongates in the handle it will shorten in the tip.

The motion of the tip is in the same plane and mirrored direction to the motion in the handle. In Chuman F. et al. [10] this manner of control is called direct mirrored control. While the handle is directly linked to the tip, this actuation method is referred to as linked cable actuation.

For the creation of more complex shapes, one could place multiple segments in series and actuate each segment with its own set of cables. In [10] this type of control is called direct serial single-segment control and is used in the Mutliflex of Figure 26. A schematic drawing of its cable configuration is illustrated in Figure 30.

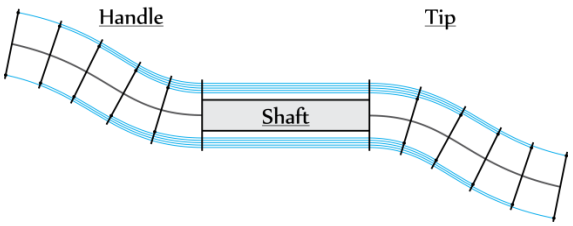

Figure 30: Schematic drawing of the cable configuration of the Multiflex which uses direct mirrored serial single-segment opposite control by linked cable actuation.

One can now ask the following question; can direct opposite control be used for helix actuated instruments? The answer (unfortunately) is no, and the reason can be found in the fact that the change in cable length of mirrored helix cables is non-linear.

This non-linearity is explained by studying two helix cables in a segment, illustrated in Figure 29. The triangles $|C_{1.1}O_2C_{1.2}|$ and $|C_{2.1}O_2C_{2.2}|$ are now not isomorphic and therefore the relation between the change in cable lengths of cables 1 and 2 is not linear.

However, a solution to this non-linear behavior can be obtained and will be explained in the following section.

3.3 From validation model to prototype

3.3.1 Working principle

The non-linear behavior between mirrored helix cables excludes the use of directly linked cable actuation. The length behavior of identical cables in the handle and tip do however show a linear relation, since they are placed in identical positions in an identical deforming shape. An elongation of a cable in the handle should therefore be mimicked by an equal elongation of its identical cable in the tip. This leads to the conclusion that the cables in the tip should be coupled to the identical cables in the handle.

Cable pairs should now either elongate or both shorten, which excludes the use of a direct cable connection. Furthermore, the pulling forces generated in the handle can no longer be directly connected to the actuation forces needed in the tip. This is explained when one realizes that a pulling force on a cable in the handle is generated by

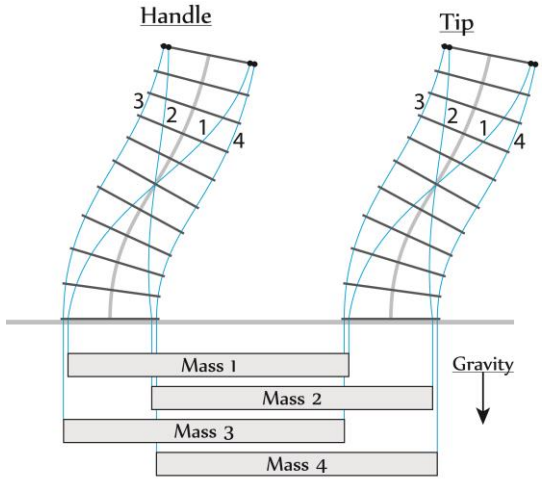

Figure 31: The working principle of direct mirrored control by unlinked pre-loaded cable actuation, using an indirect coupling between identical cable pairs of handle and tip.

resisting the elongation of that cable. The identical cable in the tip should however not resist this movement, but instead should be released to allow an equal deformation of the tip. Therefore an indirect coupling method between identical cables is proposed, as illustrated in Figure 31.

In this configuration, identical cables are indirectly connected by fixating them to the same mass. This mass has one DOF, only allowing an up or down translation. The function of this mass is to generate an equal initial load on identical cables. With initial is meant that the cables are tensioned even if the steerable element is in its non-actuated straight position. Notice that the shapes of the handle and tip are no longer mirrored.

While the handle is now indirectly linked to the tip with the intervention of a load, this manner of control will therefore be referred to as direct control by unlinked pre-loaded cable actuation.

The need for this initial load is explained by studying the behavior of cable pairs 1 and 2 of Figure 31. The cables in the handle and tip will be respectively referred to as H1, H2, T1 and T2. When H1 is elongated, it will lift up mass 1 thereby decreasing the initially set load on T1. H2 is shortened, thereby dropping mass 2 and increasing the load on T2. The difference between the decrease and increase of loads on T1 and T2 will result in a deformation of the tip.

If the shape of the handle belongs to the shape domain of the cable configuration, one can conclude that the deformation of the handle and tip will be identical. This statement is based on the following reasoning.

From the simulation model is learned that a shape is directly related to the dictated actuation profile. During validation this actuation profile was created by masses. The movements of these masses dictate the lengths of the cables. So equal to the shape, the lengthening of the cables are also directly related to the dictated actuation profile. The lengths of the cables are thereby directly related to the shape. Since the masses of Figure 31 can only move up and down, the lengths of T1 and T2 are equal to H1 and H2 respectively. The shape of the tip must therefore be equal to the shape of the handle, provided that the shape fits in the shape domain of the cable configuration.

It should be noted that the initial load on the cables should be higher than the decrease of cable load during actuation. Otherwise, one or more cables will not be loaded anymore and their lengths are no longer related to the actuation profile.

Next to proving the described working principle, the demonstration prototype should intuitively show that the principle can be incorporated into a steerable instrument. Therefore one wants the handle and tip to be place inline and opposite to each other. Furthermore one wants to exclude the use of masses because it restricts the movability of the system. The mechanical solutions to these problems will now be discussed.

3.3.2 Mechanical solutions

First the working principle is simplified by realizing cables 3 and 4 are mirrored parallel cables. These cables can therefore be controlled using the direct mirrored control by linked cable actuation method of Figure 28. This means that H3 and H4 will be directly connected to T4 and T3 respectively. Masses 3 and 4 have now become redundant and can be excluded.

The handle and tip are placed inline and opposite to each other in a mirrored configuration, allowing cables 3 and 4 to run parallel to the longitudinal axis of the shaft. This configuration is illustrated in Figure 32. Helix cables 1 and 2 are now indirectly connected to each other by pulleys. The initial load on the cables is created by fixating masses 1 and 2 to the outside of the pulleys. This configuration combines the use of linked cable actuation and unlinked pre-

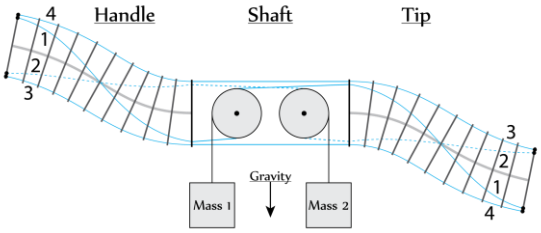

Figure 32: The handle and tip are placed inline, opposite and mirrored to each other. Cables 1 and 2 are indirectly connected by two pulleys. Cables 3 and 4 are directly connected.

loaded cable actuation into a hibryd cable actuation solution.

The masses now create a constant moment around the axis of the pulleys. To create a higher similarity to a handheld surgical instrument, it would be best to exclude these masses in the prototype. In that case one must find another manner for creating these constant moments.

A moment can be created by fixating one end of a spring to the outside of the pulley and guiding the spring along the pulley's circumference before fixating its other end to a stationary point on the shaft. The resulting spring force F_s is then equal to:

$$F_s = \frac{k}{l_0} \cdot (l_x - l_0) \qquad \textbf{Eq. 3-1}$$

where k denotes length unspecific spring stiffness, and l_x and l_0 respectively represent the deflected and initial spring length. The formula shows that a change of l_x will lead to a change in F_s.

Rotating the pulley will influence $l_{x,}$ and therefore F_s. The force should however preferably be constant, because the moment it creates should preferably be constant. A clever way of creating approximating a constant spring force is by increasing its deflected length l_x. This working principle comes clear when Eq. 3-1 is rewritten into:

$$F_s = k \cdot \left(\frac{l_x}{l_0} - 1\right) \qquad \textbf{Eq. 3-2}$$

Thus the effect of changing l_x on the change of F_s is determined by $l_{0.}$ A longer spring will therefore reduce the change of F_s. When using a spring with sufficient length, the generated force can be approximated constant for a certain domain of l_x. The masses can therefore successfully be replaced by long springs and the prototype is ready to be designed.

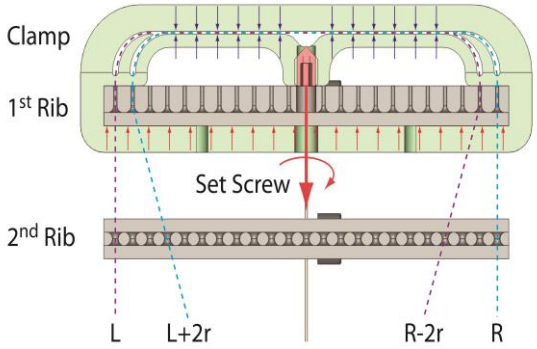

Figure 33: Cable clamp positioned on the top of the validation models. The set screw is screwed outward and thereby incorporates three functions: the fixation of the cables and the centering and fixation of the clamp onto the top rib.

3.4 Prototype design

3.4.1 Design solutions and materials

The construction of the prototype consists out of two validation models, fixated on an acrylic box that contains the pulley-spring mechanism. The complete construction, an exploded view and the parts list is illustrated in
Figure 34.

One can see that the pulleys are guided by bronze bearings. Furthermore, the springs are curved over the pulleys in order to contain a near constant moment arm during rotation and to enable the incorporation of long springs. Further discussion of the design will focus on three features: the fixation of the cables, the construction of the acrylic box and the dimensioning of the springs.

Cable Fixation

The prototype includes four cables in two mirrored pairs i.e. cables L & R and cables L+2r & R-2r. These cables need to be fixated at the end the handle and the tip. The helix cables also need to be fixated at the pulleys. The fixation of all the four cables at the handle and tip is realized with a single clamp system, illustrated by a cross-section view in Figure 33. The cables L & R-2r and R & L+2r are both actually one cable that runs through the clamping construction. In order not to break or damage the cables it is

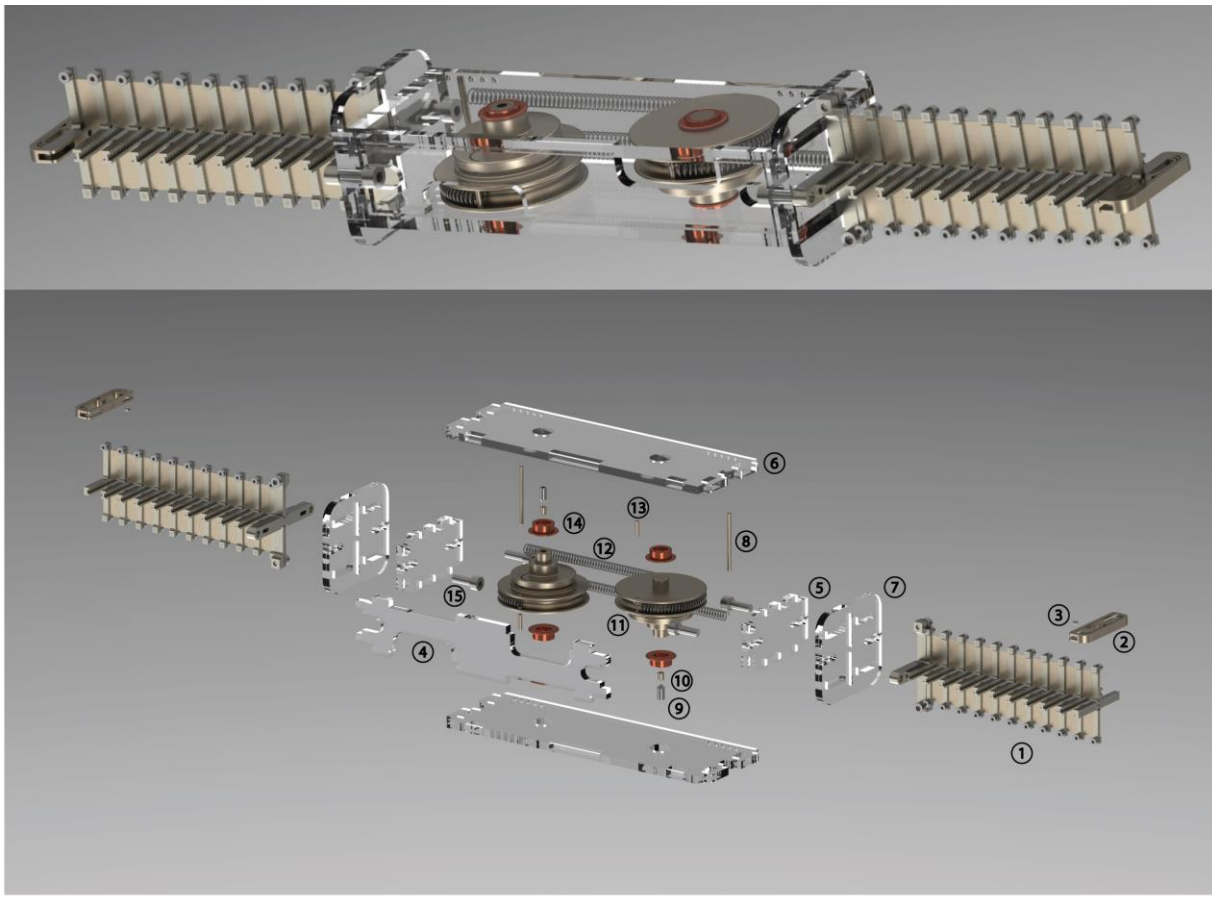

Figure 34: Top: Solidworks model of the demonstration prototype. Bottom: Exploded view of the demonstration model with a partlist

crucial that the bending radii of the cables do not become too small. The cables are therefore guided by arched slots. The clamping of the cables relies on one set screw, which pushes against the 1st rib and thereby performs three functions. First, it clamps the cables by deforming the clamp through the forces indicated with the blue arrows. Secondly it fixates the clamp and the 1st rib together by the forces indicated with the red arrows.

Thirdly, because the set screw is slightly chamfered at the bottom (as viewed in the figure) and the center hole of the 1st rib is slightly smaller than the set screw, it centers the clamp on the rib. The figure also illustrates the rounding of the cable holes in the 2nd rib.

The fixation in the pulley system is illustrated in Figure 35 by a side view and a cross-sectional view of the pulley. The cables are positioned on the pulley by a v-shaped cable slot. The end of each cable runs through the milled arc that connects the cable slot with a drilled hole through which the cables exit the pulley. The cable fixation rod and set screw press the cables against the inside of the pulley at the center of the pulley. It should be noted that in the left picture of Figure 35 the cable fixation rod and set screw are positioned outside the pulley, while on the right picture they are positioned inside the sectioned pulley.

Figure 35 also shows how the spring runs through a slot in the pulley and is fixated to the pulley by a small rod.

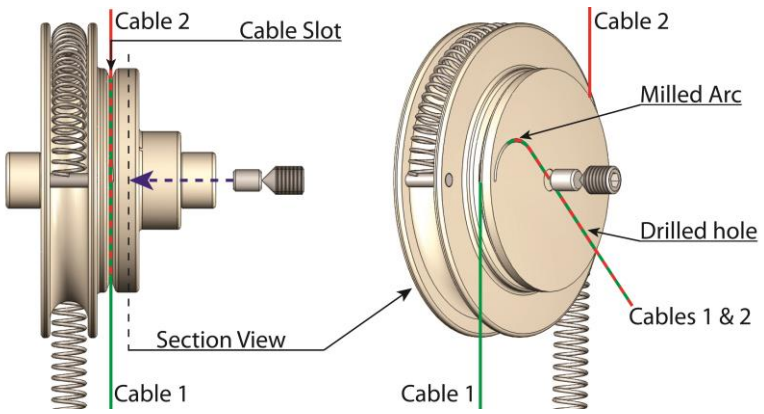

Figure 35: Cable clamping system in the pulleys. The set screw fixates the cables that run through the milled arc and leave the pulley through the drilled hole.

Acrylic Box

The acrylic box consists of seven plates with slots designed to fit into one another. Figure 36 illustrates the four steps in which the box is put together. The first stage shows all seven plates numbered and in an exploded view. In the second stage, plates 2 are placed against plate 1. In the third stage the plates 3 enclose and secure plates 1 & 2. In the fourth and final stage plates 4 slides over plates 3 thereby enclosing all the plates into a sturdy box.

Springs

The springs are used to create the initial load on the cables. While the initial load delivers the actuation force of the helix cables of the tip, the maximum deformation of the tip is determined by the magnitude of the initial force. If the springs are weak, the maximum deformation of the tip will be small. A relatively high spring force would increase the maximum deformation of the tip, but would also increase the overall friction in the prototype.

During the validation process it was determined that the validation model with cable L+2r could safely handle 5 N before plastic deformation of the leaf springs would occur. A value of 5N was therefore set as the initial load.

The cables and the springs are situated around the pulley with different radii. The force generated by the spring is therefore transferred to the cables through the following ratio:

$$F_{spring} = F_{cable} \cdot \frac{r_{cable}}{r_{spring}}$$

Radii r_{cable} and r_{spring} are 14.5 and 22.5 mm respectively, resulting in an initial desired spring

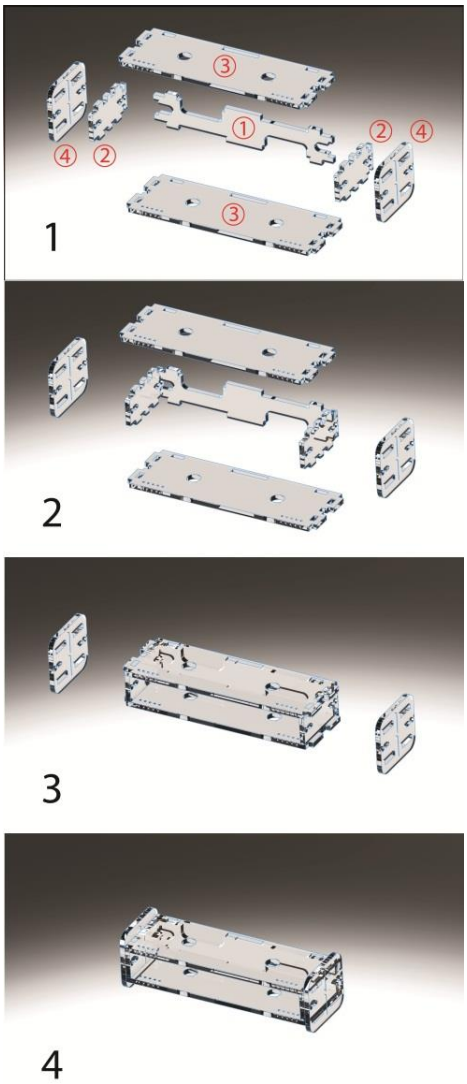

Figure 36: 1) Acrylic box consisting of seven plates. 2) Plates 2 slide into plate 1. 3) Plates 3 slide over plates 1 and 2. 3) Plates 4 slide over plates 3 and thereby enclose the box.

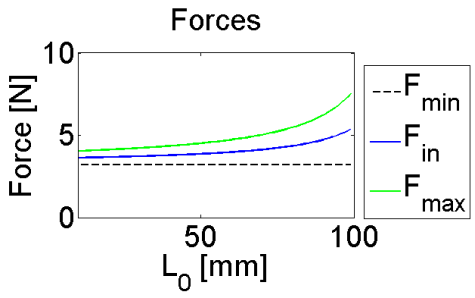

Figure 37: Forces F_{min}, F_{in} and F_{max} against l_0.

force of 3.22 N.

This spring force must be delivered when the prototype is at this maximum deformation. The simulation model was used to calculate the change of cable length at this maximum deformation, which is equal to 10.5 mm. By the ratio of r_{cable} and r_{spring} this results in a spring deflection of 14 mm. With Eq. 3-1 one can therefore state:

$$3.22\ \mathrm{N} = \frac{\mathrm{k}}{\mathrm{l_0}} \cdot (\mathrm{l_x} - \mathrm{l_0})$$
$$\mathrm{F_{in}} = \frac{\mathrm{k}}{\mathrm{l_0}} \cdot (\mathrm{l_x} - \mathrm{l_0} + 14\ \mathrm{mm})$$
$$\mathrm{F_{max}} = \frac{\mathrm{k}}{\mathrm{l_0}} \cdot (\mathrm{l_x} - \mathrm{l_0} + 28\ \mathrm{mm}) \qquad \textbf{Eq. 3-3}$$

Where l_x is the length of the spring at maximum deformation of the prototype and is equal to 120 mm. Variable l_0 is the initial spring length, k the length unspecific stiffness, F_{in} the force at the initial straight position and F_{max} maximum deformation in the opposite direction. One can see in Figure 37 that at an initial length of 50 mm the deviation between the forces becomes reasonable small, meaning that the created moment around the pulley approximates a constant value. The corresponding spring stiffness is 0.053 N/mm.

It should be noted that springs used in the actual prototype are not based on these calculations, since the used leaf springs were not the same as the ones in the validation model.

3.5 Prototype behavior

The prototype has been successfully built and works precisely as described. The finished result can be seen in the photos of Figure 40. The behavior of the prototype will be described based on its shape domain and its reaction to external forces.

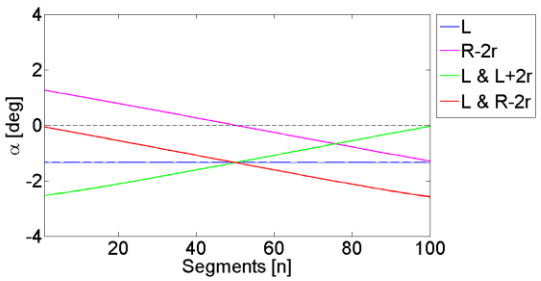

Figure 38: Four α-graphs of the demonstration prototype's shape domain.

Shape domain

The shape domain of the demonstration model defines all the possible shapes that can be passed on by the handle to the tip. This domain is based on the possible combined actuation outputs of the four cables. In the α-graph this basically includes all linear α-lines and is only bounded by a maximal value of α. This allows for a fluent motion between different shapes. Four of those α-lines are illustrated in Figure 38 and their resulting shapes are shown in Figure 40.

External forces

The reaction of the prototype to external forces will be evaluated based on the fixation of the handle in a certain position, as Figure 39. It should be noted that by fixating the shape of the handle the lengths of the cables in the tip are fixated as well. One can now identify three different external forces to which the prototype can be exposed as illustrated in Figure 39. F_{E1} and F_{E2} propose a directional and positional change of rib 1 respectively. F_{E3} proposes a shape change of the entire steerable element. Each of these external forces reveals an interesting behavior of the prototype.

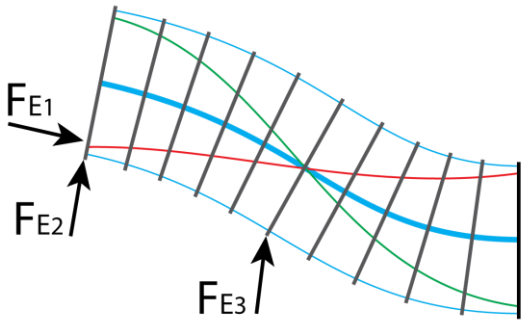

Figure 39: External Forces. F_{E1} is proposes a directional change of rib 1. F_{E2} proposes a positional change rib 1. F_{E3} proposes a shape change of the steerable element.

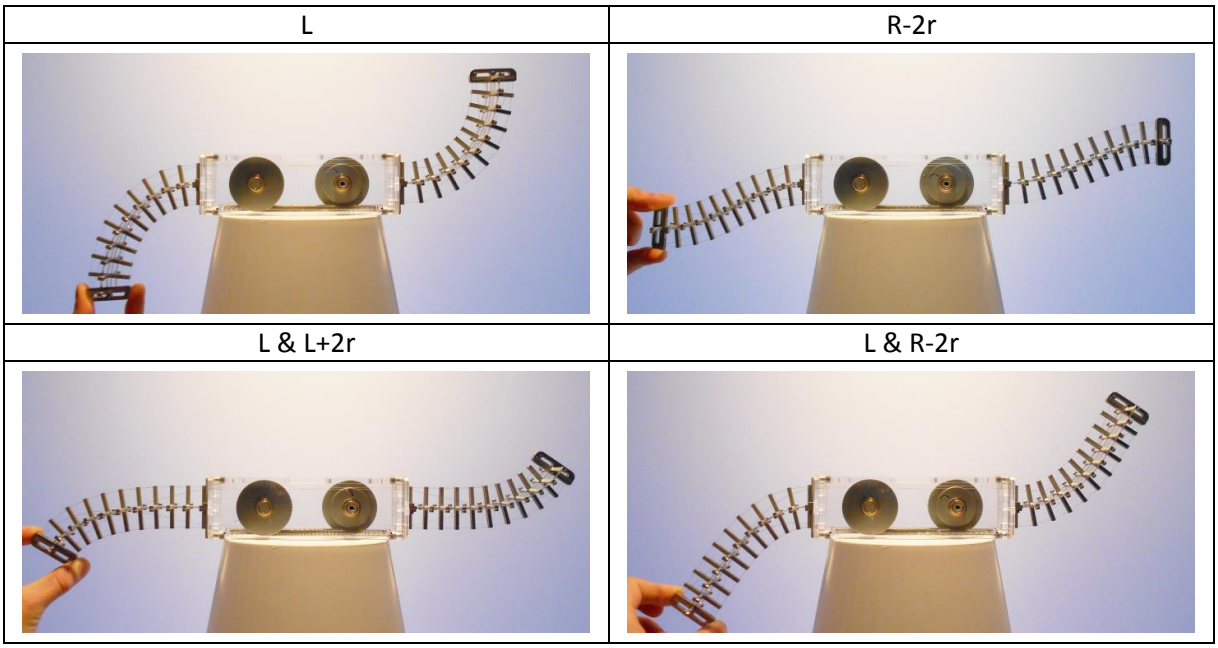

Figure 40: The four deformed shapes of the prototype as describe by the α-graph of Figure 38.

Directional stiffness

When the prototype is exposed to F_{E1} of Figure 39, the prototype resists to the directional change of rib 1 proposed by F_{E1}. This resistance is referred to as the directional stiffness.

The directional stiffness can be explained by realizing that F_{E1} has the same direction as F_{C1} of the bottom parallel cable during actuation. It can therefore be seen as actuating the bottom parallel cable, which would shorten. The linear cable change of mirrored parallel cables as discussed in section 3.2 dictates that the shortening of one cable is coupled to an equal elongation of the other. Since the lengths of the cables are fixated as the shape of the handle is fixated, this elongation cannot occur and thus the steerable element is directionally stiff.

Positional stiffness

When the prototype is exposed to F_{E2} of Figure 39, the prototype resists to the positional change of rib 1 proposed by F_{E1}. This resistance is referred to as the positional stiffness.

The same analogy used to explain the directional stiffness can be used to explain the positional stiffness. The direction of F_{E2} is namely equal to the direction of F_{C1x} of the red helix cable during actuation. The actuation of the red helix cable results in a shortening of the cable. Even though the relation between the length changes of mirrored helix cables is not linear, a shortening of one cable still results in an (unequal) elongation of the other. The elongation of the green cable can however not occur as the shape of the handle is fixated, thus the steerable element is positional stiff.

The positional stiffness is a lot more compliant than the direction al stiffness. This is due to the fact that the positional stiffness is exclusively based on the helix cables, whereas the directional stiffness is based on the parallel cables as well. The parallel cables are fixated at rib 1 at the handle, while the helix cables are loaded by the springs. The magnitude of the positional stiffness is therefore dependent on the load in the helix cables.

Shape flexibility

When the model is exposed to F_{E3} of Figure 39, a third interesting behavior reveals itself. The external force results in a deformation of the steerable element while the position and direction of rib 1 is preserved. This effect will be referred to as the shape flexibility of the steerable element.

The shape flexibility is analyzed based on a straight and a sine-shape steerable element exposed to F_{E3} on rib 6 and 4 respectively. The initial and deformed shapes are illustrated in Figure 41. The figure shows a deformation of certain segments, which inevitably means that the cable lengths in those segments change.

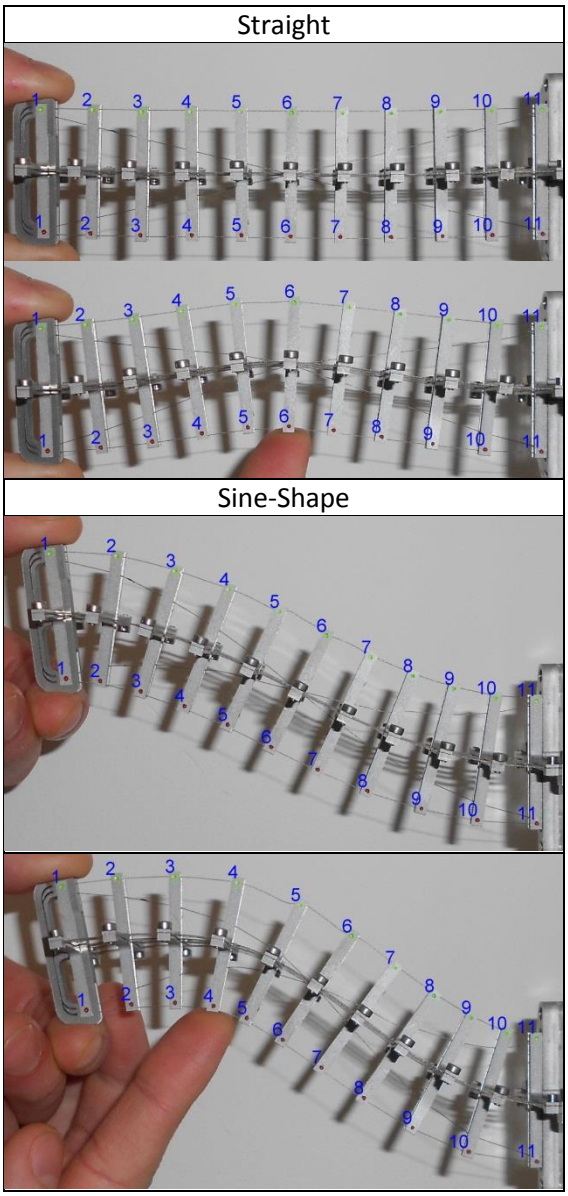

Figure 41: The straight shape of the steerable element is deformed by an external force on rib 6. The sine shaped steerable element is deformed by an external force on rib 4. Note that the fixation of rib 1 is purely to supply good data for shape flexibility analysis. The prototype does show the same shape flexibility behavior without the fixation, although the positional stiffness is to weak to keep rib 1 exactly in place.

The position and direction of rib 1 remains unaltered through its directional stiffness and positional stiffness. For the directional stiffness and positional stiffness it was found that the total lengths of the cables do not change. From the direction preservation of rib 1 also follows that the overall angle of the steerable element is preserved and

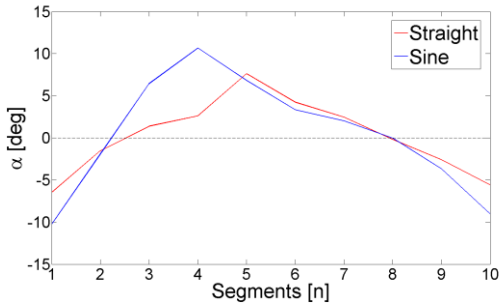

Figure 42: The α-changes per segment at load F_{E3}. (do notice that this is not the α-line, but the change in α).

therefore the sum of all α-values for the initial and deformed shape should be equal. A positive α-change as the result of F_{E3} must therefore be compensated by an equal negative α-change. This manner of compensation between segments differs between the parallel cables and the helix cables.

Parallel cables lie at a constant distance r_{cn} from the flexible axis. This means that for every segment the ratio between α and the length of the cable in a segment is equal. The deformation of a certain segment can therefore be compensated for by every other segment of the steerable element.

For helix cables, this is not the case. An α-change in segment 1 will result in a larger change in the cable length than an equal α-change in segment 4. In order for segment 4 to compensate the cable length change of segment 1, it must therefore deform with a higher α-change. This would however mean that the overall angle of the steerable element should change, which is resisted through the directional stiffness of rib 1.

For segment 10 however the ratio is equal to that of segment 1, since the absolute distances r_{C1} and r_{C10} are equal. Furthermore, a helix cable positioned on the right of the flexible axis in segment 1 is positioned on the left in segment 10. One can therefore state that the change of α in segment 1 should be compensated for by an equal α-change in segment 10. The same can be said about the other segments with equal values of r_{cn}. This relation will be referred to as the compensation relation by equal segments.

The α-values of the steerable elements of Figure 41 have been retrieved by the imaging process used for the validation process, using the blue markers on the ribs. Figure 42 shows the α-change per segment for the straight and sine-shape. One can see that the line representing the straight case approaches

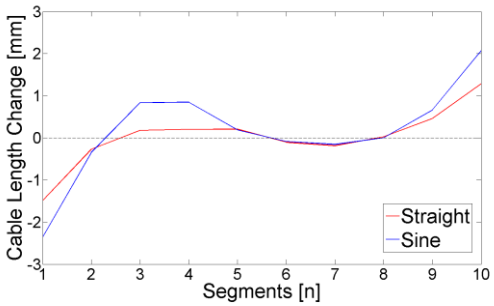

Figure 43: Cable length change per segment.

symmetry. This means that the deformation of for example segment 1 is equal to the deformation of segment 10. This is exactly what is expected.

The line representing the α-change for the sine-shape is not a symmetrical shape, since the external force is not placed in the middle of the steerable element. One can however still see that the α-change of segment 1 is equal to the α-change of segment 10.

The analysis based on the α-change of the other segments is a bit more difficult. Figure 43 therefore presents the cable length change per segment. Figure 43 also reveals that the absolute cable length change in segments 7 and 8 is not equal to those of segments 3 and 4 respectively. This is not in agreement with the compensation relation of equal segments.

This mismatch can however be explained by analyzing what happens at segments 5 and 6. In Figure 42 one can see that these segments do deform, while Figure 43 shows no significant cable length change in those segments. This is because the helix cables in these segments cross the flexible axis and their length are therefore not affected by a change of α. Segments 7 and 8 do therefore no longer have to deform equally to segments 3 and 4 respectively in order to contain the summed values of α.

This does, however, not explain the fact that the cable length changes caused in segments 3 and 4 are not compensated for. This could be explained by the clearance in the validation model. The cable holes of the validation model are 0.5 mm while the cables are 0.15 mm. This clearance could be the reason why segments 5 and 6 are allowed to bend to compensate for segments 7 and 8.

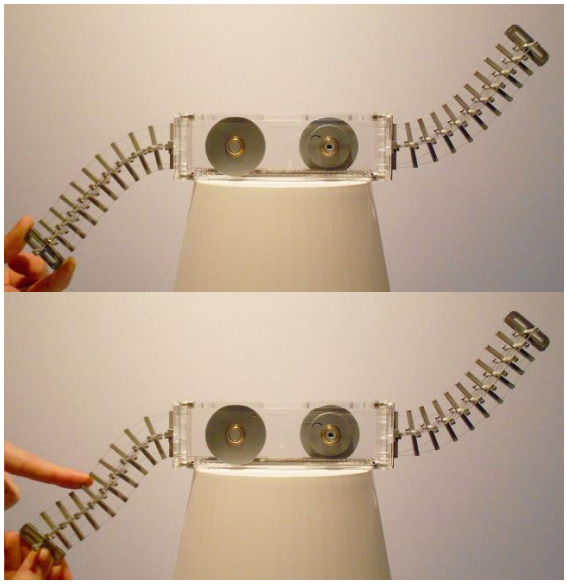

Figure 44: Not all alterations of the shape in the handle are transferred to the tip of the prototype. This phenomenon is referred to as sampling.

Sampling

The shape flexibility results in another interesting behavior of the prototype as illustrated in Figure 44. While the rib 1 of the handle is fixated, the shape of the handle can be altered without influencing the shape of the tip. This effect can be explained by the fact that the cable lengths in the handle do not change due to the shape flexibility of the steerable element.

In Section 2.7 it was already mentioned that the deformed shapes of the steerable element actuated by helix cables can be interpreted as a sine function. By introducing an external force to the handle, the handle deforms by the compensation relation of equal segments. In Figure 42 one can see that the α-changes due to the external force show a linear behavior with a direction change at the externally loaded rib. The angle of the actual α-line of the deformed steerable element will therefore be skewed and bended due to these α-changes, as illustrated in Figure 45. The α-line has now become similar to the pyramid shape of the α-line cable R-4r.

The external force can therefore be compared to the peak force caused by the direction change of a cable. While the angle of the α-line determines the frequency of the sine-shape, one can interpret the effect of F_{E3} as an increase of steerable elements shape frequency.

This additional sine is however not passed on to

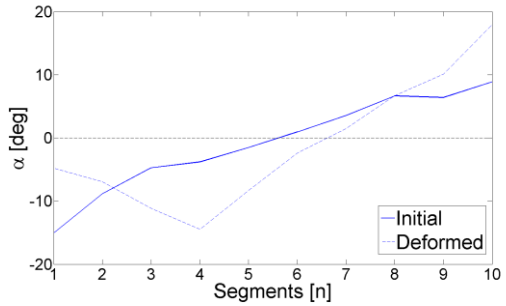

Figure 45: The α-graph of the initial sine-shape steerable element and after it is deformed by F_{E3}. These α-graphs are based on the photos of Figure 41.

the tip, as can be seen in Figure 44. The demonstration model therefore contains a sampling behavior that only allows the lowest frequencies to be passed on to the tip.

3.6 Discussion

3.6.1 Positioning and directing the tip

As discussed in the introduction, a surgeon needs the ability of positioning and directing the tool of the instrument. In segmented parallel cable actuated instrumentation like the cable ring forceps of Figure 3, the alteration of the direction and the position of the tip are coupled. With the prototype it has become apparent that the use of helix cables can decouple these two functions.

For the use in laparoscopic surgery, this type of behavior is really interesting, since it would allow the surgeon to reposition the tip of the instrument without altering its direction, i.e. in other words allowing the surgeon to 'pan'. Especially in surgeries like ESBS, were the operation area is limited and reached after a curved path, this type of behavior can potentially be very beneficial.

3.6.2 Local positional stiffness

The positional stiffness is unique for helix cables actuated steerable elements, with its magnitude based on the tension in the springs. Increasing the initial load of the springs would therefore result in a higher positional stiffness.

The positional stiffness can also be described as a local stiffness, since it only involves the position of rib 1. This sort of positional stiffness is not yet included in any of the known steerable instrumentation. In these instruments, a positional stiffness of the tip is always accomplished by creating a fully stiff steerable element. The local positional stiffness could however prove to be a beneficial quality during surgery. The reason is that fully stiff instruments will be immovable when the side of the steerable segment is exposed to an external force. This lack of adaptation to external forces at the side of the steerable element can cause damage if the steerable element is forced against tissue. The local positional stiffness does, however, allow external forces to deform the steerable element without altering the direction of the tip's very end. The compliant behavior could therefore reduce the risk of tissue damage.

It could also be interesting to see whether the positional stiffness can be extended by the inclusion of cables L+4r and R-4r. One could argue that the cable force due to the direction change of the cables would introduce an additional local stiffness at the middle of the steerable element.

3.6.3 Multiple segments

The prototype demonstrates a very useful shape behavior. The combination of cables L and L+2r and their mirrored pairs seems very suitable for the use in steerable instrumentation. However, during procedures as ESBS the path to the operation area could consist out of a sequence of multiple curves. The functionality of the cable combination only allows a maximum number of two sequential curves and could therefore prove insufficient.

A solution could lie in the expansion of the shape domain of the steerable element. This can be done by including additional cables, for example cable R-4r, following a steerable element with three different sets of cables. Each cable set would however require its own positional plane, whilst otherwise the cables would interfere with each other. This cable configuration could therefore prove difficult to miniaturize.

Another solution for increasing the shape domain of the instrument is to increase its number of steerable elements. The elements will be placed in series, equal to the configuration of the Multiflex of Figure 26. These different elements could be created by fixating the cables at different ribs. It should be noted that in this case the cables of the first element will influence the deformation of the second element as well. Therefore the following cable configuration is proposed.

One begins with one set of helix cables at the top. If these two helix cables reach the other side of

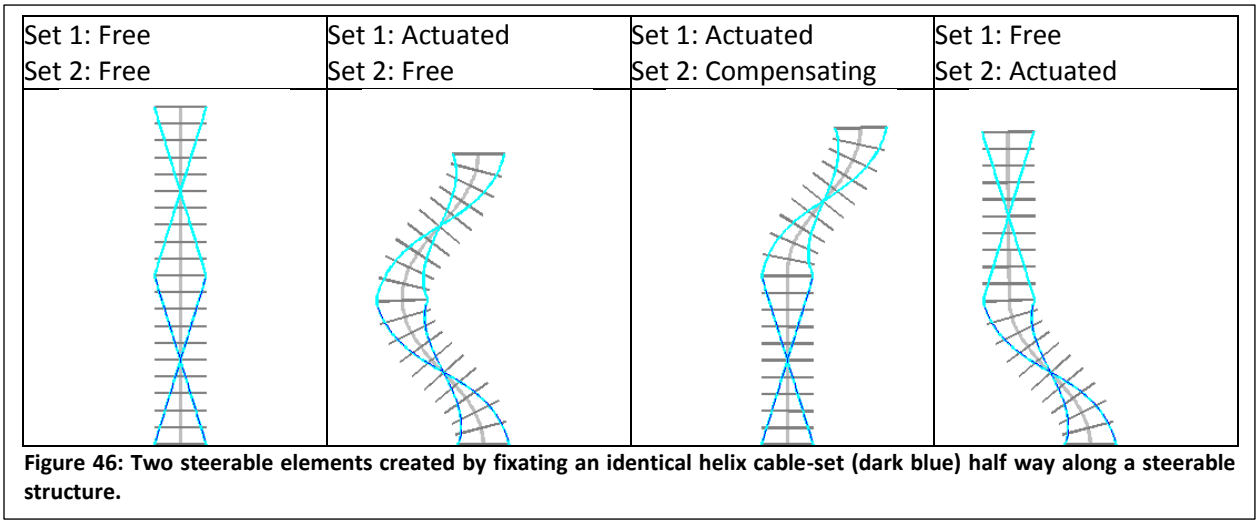

Figure 46: Two steerable elements created by fixating an identical helix cable-set (dark blue) half way along a steerable structure.

the steerable structure and therefore change direction, a second set of equally skewed helix cables are introduced. These new cables will deform only the bottom half of the structure. This cable configuration is illustrated in Figure 46.

The most left figure shows the un-deformed shapes of both steerable elements. If a cable of the first cable-set is actuated without compensation by the cables of the second cable-set, the two steerable elements are deformed as illustrated by the second figure on the left.

By adequately compensating with the cables of the second set, it would be possible to resist the deformation of the second steerable element. This means one would be able to control the first steerable element independently from the second element, as is illustrated by the second figure from the right.

In order to realize the independent control of the second segment as well, one can use the same cable configuration principles used in the Multiflex of Figure 28. In the handle, the cables of the first element must follow the exact same path as the cables of the second element. This will ensure that the cables of the first element will adequately elongate or shorten to compensate for the deformation of the second steerable element and not influence the shape of the first element. The resulting deformation of both segments is illustrated in the right figure of Figure 46.

Whilst the paths of the first and second cable sets are now equal, no additional cable planes are required. The result is an easier to miniaturized construction than the inclusion of differently skewed helix cables.

4 Conclusions

The main goal of this paper was to investigate the behavior of a steerable element actuated by helix cables. A two-dimensional simulation model based on a segmented structure of a steerable element was developed. The evaluation of its results gave insight in the influence of actuation cable placement on the shape of the steerable element. It was found that helix cables have the ability to deform a steerable element with a non-constant bending radius. Parallel cables do not have this ability. Furthermore it was found that the combined actuation of multiple differently placed helix cables can result in deformed shapes that single helix cables are not able to create.

This knowledge was used for the construction of a mechanical control mechanism. Two steerable elements were placed inline and opposite to one another. This configuration was fitted two pairs of mirrored parallel and helix cables. To cope with the non-linear cable change of the helix cables, a pulley spring system was incorporated into the system.

The resulting prototype enables the steerable element to be steered in a multitude of direction and position combinations. The coupling between the direction and position of the tip as seen for parallel cable actuated instruments is thereby decoupled.

Next to a directional stiffness of the tip as already included in parallel cable actuated instruments, the prototype also contains a local positional stiffness of

the tip.

The prototype also revealed a quality referred to as shape flexibility. This quality results from the additional positional stiffness at the tip and means that the steerable element can be reshaped by external forces without effecting the position and direction of the tip. Shape flexibility leads to a sampling behavior between handle an tip, wherein only the lowest shape frequencies in the handle are passed on to the tip.

The demonstration prototype is the first known segmented cable actuated system that is able to create a multitude of shapes.

5 References

[1] T. Nai, Steerable arthroscopic punch: Methods to steer a surgical cutter, Delft, 2009.

[2] P. Henselmans, "Multi-branchend, multi-steerable instruments for endonasal brain surgery," 2012.

[3] "www.intuitivesurgical.com," Intuitive Surgical, 2013. [Online].

[4] Intuitive Surgical, "EndoWrist - instrument & accessory calalog," januari 2013. [Online].

[5] J. Bodner, F. Augustin, H. Wykypiel, J. Fish, G. Meuhlmann, G. Wetscher and T. Schmid, "The da Vinci robotic system for general surgical applications: a critical interim appraisal," *Swiss Med Weekely,* vol. 135, pp. 674-678, 2005.

[6] D. Stefanchik, O. Vakharia and J. Spivey, "Braided Endoscope Accessories". US Patent US 2008097152 A1,, 20 07 2006.

[7] P. Breedveld, J. Scheltes, E. Blom and J. Verheij, "A New, Easily Miniaturized Steerable Endoscope.," *IEEE Engineering in Medicine and Biology Magazine,* pp. 40-47, 2005.

[8] V. M., Mechanics of Materials, 2012.

[9] M. Malcolm, G. Forsythe and C. Moler, Computer Methods for Mathematical Computations, Prentice-Hall, 1976.

[10] F. Chunman, D. Dodou and P. Breedveld, "Review of manual control methods for handheld maneuverable instruments," *Minimally Invasive Therapy,* no. Early Online 1-9, 2012.

[11] P. Breedveld, "Vici: Grant application form.," 2011.

[12] "http://www.obgynreno.com/," [Online].

Appendix A. Simulation Model

A.1 Equations

Segment 1

Equation 3-4

$$\angle\delta_1 = t^{-1}\left(\frac{|C_2D_2|}{|C_1D_2|}\right)$$

Distance $|C_1D_2|$ is rewritten as:

$$|C_1D_2| = |C_1O_1| \cdot s(\alpha_1)$$
$$|C_1O_1| = |A_1O_1| - r_{C_1}$$

Distance $|A_1O_1|$ is the bending radius of the segment. The curved distance $|A_1A_2|$ is equal to the fixed length of the segment (ℓ) and equal to a fraction $\alpha_1/2\cdot\pi$ of the complete circumference of the circle described by distance $|A_1O_1|$. By using the circumference formula of a circle one can therefore state:

$$\ell = 2\cdot\pi\cdot|A_1O_1|\cdot\frac{\alpha_1}{2\cdot\pi}$$
$$|A_1O_1| = \frac{\ell}{\alpha_1}$$

And therefore:

$$|C_1D_2| = \left(\frac{\ell}{\alpha_1} - r_{C_1}\right)\cdot s(\alpha_1)$$

Distance $|C_2D_2|$ is equal to:

$$|C_2D_2| = |B_2D_2| + |C_2B_2|$$

Distance $|B_2D_2|$ can be determined by realizing distance $|C_1O_1|$ is equal distance $|B_2O_1|$ meaning triangle $\Delta B_2C_1O_1$ is isosceles. Therefore one can state that $\angle B_2C_1O_1$ is equal to $\angle C_1B_2O_1$. Since the sum of all angles of a triangle is equal to π, one can state:

$$\angle C_1B_2O_1 = \angle B_2C_1O_1 = \frac{\pi - \alpha_1}{2}$$

Using the sum of triangles for $\Delta B_2C_1O_1$ angle $\angle B_2D_2C_1$ is equal to half π, one can now describe $\angle B_2C_1D_2$ by:

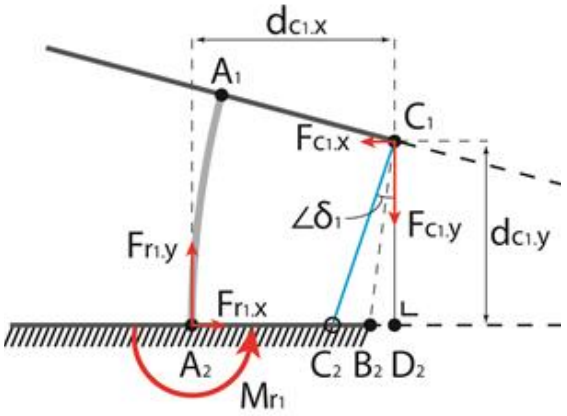

Figure 47: Moments, forces and moment arms of segment 1.

$$\angle B_2C_1D_2 = \frac{\alpha_1}{2}$$

Distance $|B_2D_2|$ can now be described by the product of distance $|C_1D_2|$ and the tangent of $\angle B_2C_1D_2$:

$$|B_2D_2| = \left(\frac{\ell}{\alpha_1} - r_{C_1}\right)\cdot s(\alpha_1)\cdot t\left(\frac{\alpha_1}{2}\right)$$

Distance $|C_2B_2|$ is the difference between the r_1 and r_2. Since the initial position of the cable from segment *1* to *n* is a straight line, the difference between r_{n-1} and r_n is constant and will be denoted by *dr*:

$$dr = \ell\cdot t\left(\frac{\pi}{2} - \beta\right)$$

In where $\angle\beta$ stands for the initial angle of the cable (Figure 7), for a parallel cable $\angle\beta$ is equal to half π which reduces *dr* to zero. $\angle\delta_1$ can now be written as:

$$\angle\delta_1 = t^{-1}\left(\frac{\left(\frac{\ell}{\alpha_1} - r_{C_1}\right)\cdot s(\alpha_1)\cdot t\left(\frac{\alpha_1}{2}\right) + dr}{\left(\frac{\ell}{\alpha_1} - r_{C_1}\right)\cdot s(\alpha_1)}\right)$$

This simplifies to:

$$\angle\delta_1 = t^{-1}\left(t\left(\frac{\alpha_1}{2}\right) + \frac{dr}{\left(\frac{\ell}{\alpha_1} - r_{C_1}\right)\cdot s(\alpha_1)}\right)$$

Equation 3-5

The moment arm d_{C1x} is equal to the difference between $|A_2O_1|$ and $|D_2O_1|$. Noticing $|A_2O_1|$is already described for equation 3-4 as the bending radius of the segment:

$$|A_1O_1| = \frac{\ell}{\alpha_1}$$

$|D_2O_1|$ is the product of $|C_1O_1|$ and the cosine of $\angle\alpha_1$. $|C_1O_1|$ is equal to the bending radius $|A_2O_1|$ minus r_{C1}:

$$|C_1O_1| = \frac{\ell}{\alpha_1} - r_{C_1}$$

Moment arm d_{C1x} is therefore equal to:

$$d_{C_1x} = \frac{\ell}{\alpha_1} - \left(\frac{\ell}{\alpha_1} - r_{C_{1.1}}\right) \cdot c(\alpha_1)$$

The moment arm d_{C1y} is the product of $|C_1O_1|$ and the sine of $\angle\alpha_1$:

$$d_{C_1y} = \left(\frac{\ell}{\alpha_1} - r_{C_{1.1}}\right) \cdot s(\alpha_1)$$

Equation 3-6

The moment balance starts as:

$$\sum M_{A_2} = 0 : \; M_{r_1} - F_{C_1x} \cdot d_{C_1y} + F_{C_1y} \cdot d_{C_1x} = 0$$

Each element is described by:

Moment:

$$M_{r_1} = c \cdot \alpha_1$$

Cable forces:

$$F_{C_1x} = -F_{C_1} \cdot s(\delta_1)$$

$$F_{C_1y} = -F_{C_1} \cdot c(\delta_1)$$

$$\angle\delta_1 = t^{-1}\left(\frac{\left(\frac{\ell}{\alpha_1} - r_{C_1}\right) \cdot s(\alpha_1) \cdot t\left(\frac{\alpha_1}{2}\right) + dr}{\left(\frac{\ell}{\alpha_1} - r_{C_1}\right) \cdot s(\alpha_1)}\right)$$

This is the description of $\angle\delta_1$ before the simplification done in the above explanation of equation 3-4.

Moment arms:

$$d_{C_1x} = \frac{\ell}{\alpha_1} - \left(\frac{\ell}{\alpha_1} - r_{C_{1.1}}\right) \cdot c(\alpha_1)$$

$$d_{C_1y} = \left(\frac{\ell}{\alpha_1} - r_{C_{1.1}}\right) \cdot s(\alpha_1)$$

The moment balance can now be written as Eq. A-1. It includes arctangent terms inside sinus and cosine terms. In order to simplify the moment balance, the arctangent is rewritten into arcsines and arccosine

$$\sum M_{A_2} = 0 : \; c \cdot \alpha_1 + F_{C_1} \cdot \sin\left(\tan^{-1}\left(\frac{\left(\frac{\ell}{\alpha_1} - r_{C_1}\right) \cdot \sin(\alpha_1) \cdot \tan\left(\frac{\alpha_1}{2}\right) + dr}{\left(\frac{\ell}{\alpha_1} - r_{C_1}\right) \cdot \sin(\alpha_1)}\right)\right) \cdot \left(\left(\frac{\ell}{\alpha_1} - r_{C_{2.1}}\right) \cdot \sin(\alpha_1)\right) - F_{C_1}$$

$$\cdot \cos\left(\tan^{-1}\left(\frac{\left(\frac{\ell}{\alpha_1} - r_{C_1}\right) \cdot \sin(\alpha_1) \cdot \tan\left(\frac{\alpha_1}{2}\right) + dr}{\left(\frac{\ell}{\alpha_1} - r_{C_1}\right) \cdot \sin(\alpha_1)}\right)\right) \cdot \left(\frac{\ell}{\alpha_1} - \left(\frac{\ell}{\alpha_1} - r_{C_{1.1}}\right) \cdot \cos(\alpha_1)\right) = 0 \quad \textbf{Eq. A-1}$$

$$\sum M_{A_2} = 0 : \; c \cdot \alpha_1 + F_{C_1} \cdot \frac{\left(\frac{\ell}{\alpha_1} - r_{C_1}\right) \cdot s(\alpha_1) \cdot t\left(\frac{\alpha_1}{2}\right) + dr}{\sqrt{\left(\left(\frac{\ell}{\alpha_1} - r_{C_1}\right) \cdot s(\alpha_1) \cdot t\left(\frac{\alpha_1}{2}\right) + dr\right)^2 + \left(\left(\frac{\ell}{\alpha_1} - r_{C_1}\right) \cdot s(\alpha_1)\right)^2}} \cdot \left(\left(\frac{\ell}{\alpha_1} - r_{C_1}\right) \cdot s(\alpha_1)\right)$$

$$- F_{C_1} \cdot \frac{\left(\frac{\ell}{\alpha_1} - r_{C_1}\right) \cdot s(\alpha_1)}{\sqrt{\left(\left(\frac{\ell}{\alpha_1} - r_{C_1}\right) \cdot s(\alpha_1) \cdot t\left(\frac{\alpha_1}{2}\right) + dr\right)^2 + \left(\left(\frac{\ell}{\alpha_1} - r_{C_1}\right) \cdot s(\alpha_1)\right)^2}} \cdot \left(\frac{\ell}{\alpha_1} - \left(\frac{\ell}{\alpha_1} - r_{C_1}\right) \cdot c(\alpha_1)\right) \quad \textbf{Eq. A-2}$$

terms by:

$$t^{-1}\left(\frac{a}{b}\right) = s^{-1}\left(\frac{a}{\sqrt{a^2+b^2}}\right)$$
$$t^{-1}\left(\frac{a}{b}\right) = c^{-1}\left(\frac{b}{\sqrt{a^2+b^2}}\right)$$

This leads to arcsines term within a sine and a arccosine term within a cosine, leaving just the terms inside the arcsines and arccosine. The moment balance can therefore be written as Eq. A-2.

Segment 2

Equation 3-7

F_a is always equal but opposite to F_r. Through the change in local coordinate system and the deformation of segment 2, the direction of reaction force F_{r1} is altered. This alteration can be visualized by:

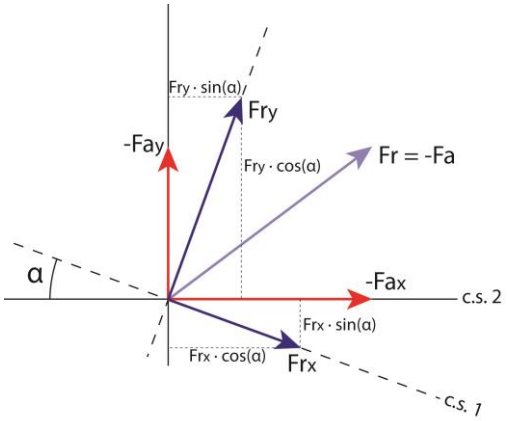

The decomposition of F_{a1} should therefore be written as:

$$F_{a_1x} = -F_{r_1x}\cdot c(\alpha_2) - F_{r_1y}\cdot s(\alpha_2)$$
$$F_{a_1y} = -F_{r_1y}\cdot c(\alpha_2) + F_{r_1x}\cdot s(\alpha_2)$$

Equation 3-8

The description of $\angle\gamma_2$ starts by realizing that:

$$\begin{aligned}\angle\gamma_2 &= \angle C_{2.3} + \angle C_{2.4}\\ &= \angle C_{2.1} + \angle C_{2.2}\\ &= \frac{\angle C_{2.1} + \angle C_{2.2} + \angle C_{2.3} + \angle C_{2.4}}{2}\end{aligned}$$

The description of $\angle C_{2.1}$ can be deducted from the evaluation of segment 1 and since $\Delta C_1C_2D_2$ is rectangular is equal to:

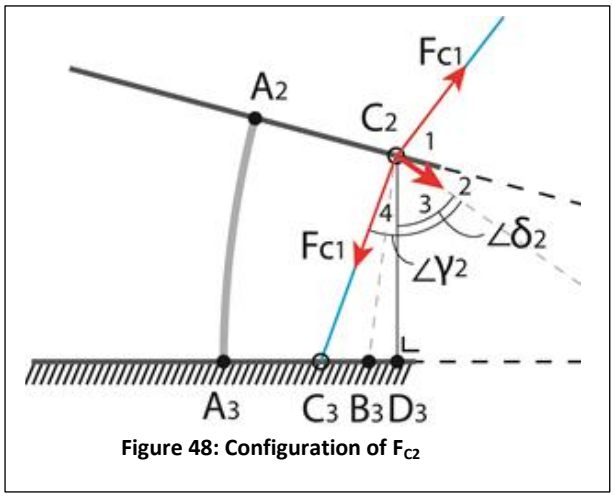

Figure 48: Configuration of F_{C2}

$$\angle C_{2.1} = \frac{\pi}{2} - \angle\delta_1$$
$$\angle C_{2.1} = \frac{\pi}{2} - t^{-1}\left(t\left(\frac{\alpha_1}{2}\right) + \frac{dr}{\left(\frac{\ell}{\alpha_1} - r_{C_1}\right)\cdot s(\alpha_1)}\right)$$

The description of $\angle C_{2.4}$ derived in the same manner as $\angle\delta_1$ and can therefore be copied and adequately altered into:

$$\angle C_{2.4} = t^{-1}\left(t\left(\frac{\alpha_2}{2}\right) + \frac{dr}{\left(\frac{\ell}{\alpha_2} - r_{C_2}\right)\cdot s(\alpha_2)}\right)$$

Since triangle $\Delta C_2O_2D_3$ is rectangular on can state:

$$\angle C_{2.2} + \angle C_{2.3} = \frac{\pi}{2} - \alpha_2$$

The description of $\angle\gamma_2$ can now be written as Eq. A-3.

Equation 3-9

Force F_{C2} is decomposed by $\angle\delta_2$ which is equal to:

$$\angle\delta_2 = \angle\gamma_2 - \angle C_{2.4}$$

The full description of $\angle\delta_2$ is giving by Eq. A-4.

$$\angle\gamma_2 = \frac{\pi - t^{-1}\left(t\left(\frac{\alpha_1}{2}\right) + \frac{dr}{\left(\frac{\ell}{\alpha_1} - r_{C_1}\right)\cdot s(\alpha_1)}\right) - \alpha_2 + t^{-1}\left(t\left(\frac{\alpha_2}{2}\right) + \frac{dr}{\left(\frac{\ell}{\alpha_2} - r_{C_2}\right)\cdot s(\alpha_2)}\right)}{2} \qquad \textbf{Eq. A-3}$$

$$\angle\delta_2 = \frac{\pi - t^{-1}\left(t\left(\frac{\alpha_1}{2}\right) + \frac{dr}{\left(\frac{\ell}{\alpha_1} - r_{C_1}\right)\cdot s(\alpha_1)}\right) - \alpha_2 - t^{-1}\left(t\left(\frac{\alpha_2}{2}\right) + \frac{dr}{\left(\frac{\ell}{\alpha_2} - r_{C_2}\right)\cdot s(\alpha_2)}\right)}{2} \qquad \textbf{Eq. A-4}$$

Equation 3-10

The decomposition of forces F_{C2x} and F_{C2y} is realized by:

$$F_{C_2x} = F_{C_2}\cdot s(\angle\delta_2)$$
$$F_{C_2y} = -F_{C_2}\cdot c(\angle\delta_2)$$

In where F_{C2} is equal to:

$$\mathrm{F_{C_2}} = 2\cdot \mathrm{F_{C_1}}\cdot \mathrm{c}(\gamma_2)$$

The full descriptions of the decomposed forces F_{C2x} and F_{C2y} thereby becomes a rather large functions. They can however be simplified with the use of several sine and cosine rules. First the composition of F_{C2x} is explained.

$\underline{\mathbf{F_{C2x}}}$

The full description is equal to:

$$F_{C_2x} = 2\cdot F_{C_1}\cdot c\left(\frac{\pi - t^{-1}\left(t\left(\frac{\alpha_1}{2}\right) + \frac{dr}{\left(\frac{\ell}{\alpha_1} - r_{C_{1.1}}\right)\cdot s(\alpha_1)}\right) - \alpha_2 + t^{-1}\left(t\left(\frac{\alpha_2}{2}\right) + \frac{dr}{\left(\frac{\ell}{\alpha_1} - r_{C_{1.2}}\right)\cdot s(\alpha_2)}\right)}{2}\right)$$
$$\cdot s\left(\frac{\pi - t^{-1}\left(t\left(\frac{\alpha_1}{2}\right) + \frac{dr}{\left(\frac{\ell}{\alpha_1} - r_{C_{1.1}}\right)\cdot s(\alpha_1)}\right) - \alpha_2 - t^{-1}\left(t\left(\frac{\alpha_2}{2}\right) + \frac{dr}{\left(\frac{\ell}{\alpha_1} - r_{C_{1.2}}\right)\cdot s(\alpha_2)}\right)}{2}\right)$$

For ease of notation the arctangent terms will for now be noted by:

$$A = t^{-1}\left(t\left(\frac{\alpha_1}{2}\right) + \frac{dr}{\left(\frac{l}{\alpha_1} - r_{C_{1.1}}\right)\cdot s(\alpha_1)}\right)$$
$$B = t^{-1}\left(t\left(\frac{\alpha_2}{2}\right) + \frac{dr}{\left(\frac{l}{\alpha_1} - r_{C_{1.2}}\right)\cdot s(\alpha_2)}\right)$$

$$F_{C_2x} = 2\cdot F_{C_1}\cdot c\left(\frac{\pi - A - \alpha_2 + B}{2}\right)\cdot s\left(\frac{\pi - A - \alpha_2 - B}{2}\right)$$

This equation can be rewritten to:

$$F_{C_2x} = 2\cdot F_{C_1}\cdot c\left(\frac{\pi}{2} + \frac{B - (A + \alpha_2)}{2}\right)\cdot s\left(\frac{\pi}{2} - \frac{B + (A + \alpha_2)}{2}\right)$$

The sine and cosine terms can be simplified:

$$F_{C_2x} = -2\cdot F_{C_1}\cdot s\left(\frac{B - (A + \alpha_2)}{2}\right)\cdot c\left(\frac{B + (A + \alpha_2)}{2}\right)$$

With the following equations of sine and cosine the terms can be further rewritten.

$$2\cdot c\left(\frac{a+b}{2}\right)\cdot s\left(\frac{a-b}{2}\right) = s(a) - s(b)$$
$$-2\cdot s\left(\frac{a+b}{2}\right)\cdot s\left(\frac{a-b}{2}\right) = s(b) - s(a)$$

The force can therefore be written as:

$$F_{C_2x} = F_{C_1}\cdot(s(A + \alpha_2) - s(B))$$

And can be rewritten into:

$$F_{C_2x} = F_{C_1}\cdot\big((s(A)\cdot c(\alpha_2) + c(A)\cdot s(\alpha_2)) - s(B)\big)$$

By filling in descriptions for A and B, one gets:

$$F_{C_2x} = F_{C_1}\cdot\left(s\left(t^{-1}\left(t\left(\frac{\alpha_1}{2}\right) + \frac{\mathrm{dr}}{\left(\frac{\ell}{\alpha_1} - r_{C_{1.1}}\right)\cdot s(\alpha_1)}\right)\right)\cdot c(\alpha_2) + c\left(t^{-1}\left(t\left(\frac{\alpha_1}{2}\right) + \frac{dr}{\left(\frac{\ell}{\alpha_1} - r_{C_{1.1}}\right)\cdot s(\alpha_1)}\right)\right)\cdot s(\alpha_2)\right)$$
$$- s\left(t^{-1}\left(t\left(\frac{\alpha_2}{2}\right) + \frac{dr}{\left(\frac{\ell}{\alpha_1} - r_{C_{1.2}}\right)\cdot s(\alpha_2)}\right)\right)$$

The arctangent terms inside the sine and cosine terms can be rewritten into arcsines and arccosine terms by:

$$\mathrm{t}^{-1}\left(\frac{\mathrm{a}}{\mathrm{b}}\right) = \mathrm{s}^{-1}\left(\frac{\mathrm{a}}{\sqrt{\mathrm{a}^2 + \mathrm{b}^2}}\right)$$

$$t^{-1}\left(\frac{a}{b}\right) = c^{-1}\left(\frac{b}{\sqrt{a^2+b^2}}\right)$$

Rewriting the arctangent terms in arcsines and arccosine terms:

$$t^{-1}\left(t\left(\frac{\alpha_1}{2}\right) + \frac{dr}{\left(\frac{\ell}{\alpha_1} - r_{C_{1.1}}\right)\cdot s(\alpha_1)}\right) = t^{-1}\left(\frac{\left(\frac{\ell}{\alpha_1} - r_{C_{1.1}}\right)\cdot s(\alpha_1)\cdot t\left(\frac{\alpha_1}{2}\right) + dr}{\left(\frac{\ell}{\alpha_1} - r_{C_{1.1}}\right)\cdot s(\alpha_1)}\right)$$

$$= s^{-1}\left(\frac{\left(\frac{\ell}{\alpha_1} - r_{C_{1.1}}\right)\cdot s(\alpha_1)\cdot t\left(\frac{\alpha_1}{2}\right) + dr}{\sqrt{\left(\left(\frac{\ell}{\alpha_1} - r_{C_{1.1}}\right)\cdot s(\alpha_1)\cdot t\left(\frac{\alpha_1}{2}\right) + dr\right)^2 + \left(\left(\frac{\ell}{\alpha_1} - r_{C_{1.1}}\right)\cdot s(\alpha_1)\right)^2}}\right)$$

$$= \cos^{-1}\left(\frac{\left(\frac{\ell}{\alpha_1} - r_{C_{1.1}}\right)\cdot s(\alpha_1)}{\sqrt{\left(\left(\frac{\ell}{\alpha_1} - r_{C_{1.1}}\right)\cdot s(\alpha_1)\cdot t\left(\frac{\alpha_1}{2}\right) + dr\right)^2 + \left(\left(\frac{\ell}{\alpha_1} - r_{C_{1.1}}\right)\cdot s(\alpha_1)\right)^2}}\right)$$

The final description of F_{C2x} is now equal to:

$$F_{C_2x} = F_{C_1}\cdot\left(\frac{\left(\frac{\ell}{\alpha_1} - r_{C_{1.1}}\right)\cdot s(\alpha_1)\cdot t\left(\frac{\alpha_1}{2}\right) + dr}{\sqrt{\left(\left(\frac{\ell}{\alpha_1} - r_{C_{1.1}}\right)\cdot s(\alpha_1)\cdot t\left(\frac{\alpha_1}{2}\right) + dr\right)^2 + \left(\left(\frac{\ell}{\alpha_1} - r_{C_{1.1}}\right)\cdot s(\alpha_1)\right)^2}}\cdot c(\alpha_2)\right.$$
$$+\frac{\left(\frac{\ell}{\alpha_1} - r_{C_{1.1}}\right)\cdot s(\alpha_1)}{\sqrt{\left(\left(\frac{\ell}{\alpha_1} - r_{C_{1.1}}\right)\cdot s(\alpha_1)\cdot t\left(\frac{\alpha_1}{2}\right) + dr\right)^2 + \left(\left(\frac{\ell}{\alpha_1} - r_{C_{1.1}}\right)\cdot s(\alpha_1)\right)^2}}\cdot s(\alpha_2)$$
$$\left.-\frac{\left(\frac{\ell}{\alpha_1} - r_{C_{1.2}}\right)\cdot s(\alpha_2)\cdot t\left(\frac{\alpha_2}{2}\right) + dr}{\sqrt{\left(\left(\frac{\ell}{\alpha_2} - r_{C_{1.2}}\right)\cdot s(\alpha_3)\cdot t\left(\frac{\alpha_2}{2}\right) + dr\right)^2 + \left(\left(\frac{\ell}{\alpha_2} - r_{C_{1.2}}\right)\cdot s(\alpha_2)\right)^2}}\right)$$

F_{C2y}

The full description is equal to:

$$F_{C_2y} = -2 \cdot F_{C_1} \cdot c\left(\frac{\pi - t^{-1}\left(t\left(\frac{\alpha_1}{2}\right) + \frac{\mathrm{dr}}{\left(\frac{\ell}{\alpha_1} - r_{C_{1.1}}\right) \cdot s(\alpha_1)}\right) - \alpha_2 + t^{-1}\left(t\left(\frac{\alpha_2}{2}\right) + \frac{dr}{\left(\frac{\ell}{\alpha_1} - r_{C_{1.2}}\right) \cdot s(\alpha_2)}\right)}{2}\right) \cdot c\left(\frac{\pi - t^{-1}\left(t\left(\frac{\alpha_1}{2}\right) + \frac{\mathrm{dr}}{\left(\frac{\ell}{\alpha_1} - r_{C_{1.1}}\right) \cdot s(\alpha_1)}\right) - \alpha_2 - t^{-1}\left(t\left(\frac{\alpha_2}{2}\right) + \frac{dr}{\left(\frac{\ell}{\alpha_1} - r_{C_{1.2}}\right) \cdot s(\alpha_2)}\right)}{2}\right)$$

The notations of the arctangent terms are simplified:

$$F_{C_2y} = -2 \cdot F_{C_1} \cdot c\left(\frac{\pi - A - \alpha_2 + B}{2}\right) \cdot c\left(\frac{\pi - A - \alpha_2 - B}{2}\right)$$

The sine and cosine terms are rewritten in order to single out $\angle\alpha_2$:

$$F_{C_2y} = -2 \cdot F_{C_1} \cdot c\left(\frac{\pi}{2} + \frac{B - (A + \alpha_2)}{2}\right) \cdot c\left(\frac{\pi}{2} - \frac{B + (A + \alpha_2)}{2}\right)$$

Rewritting:

$$F_{C_2y} = 2 \cdot F_{C_1} \cdot s\left(\frac{B - (A + \alpha_2)}{2}\right) \cdot s\left(\frac{B + (A + \alpha_2)}{2}\right)$$

Now the following sine and cosine rules are used:

$$-2 \cdot s\left(\frac{a + b}{2}\right) \cdot s\left(\frac{a - b}{2}\right) = c(a) - c(b)$$
$$2 \cdot s\left(\frac{a + b}{2}\right) \cdot s\left(\frac{a - b}{2}\right) = c(b) - c(a)$$

This results in the following description of F_{C2y}:

$$F_{C_2y} = F_{C_1} \cdot c(A + \alpha_2) - c(B)$$

Rewriting the cosine:

$$F_{C_2y} = F_{C_1} \cdot (c(A) \cdot c(\alpha_2) - s(A) \cdot s(\alpha_2)) - c(B)$$

Filling in A en B:

$$F_{C_2y} = F_{C_1} \cdot \left(c\left(t^{-1}\left(t\left(\frac{\alpha_1}{2}\right) + \frac{dr}{\left(\frac{\ell}{\alpha_1} - r_{C_{1.1}}\right) \cdot s(\alpha_1)} \right) \right) \cdot c(\alpha_2) - s\left(t^{-1}\left(t\left(\frac{\alpha_1}{2}\right) + \frac{dr}{\left(\frac{\ell}{\alpha_1} - r_{C_{1.1}}\right) \cdot s(\alpha_1)} \right) \right) \cdot s(\alpha_2) \right.$$
$$\left. - c\left(t^{-1}\left(t\left(\frac{\alpha_2}{2}\right) + \frac{dr}{\left(\frac{\ell}{\alpha_1} - r_{C_{1.2}}\right) \cdot s(\alpha_2)} \right) \right) \right)$$

The arctangent terms inside the sine and cosine terms can be rewritten into arcsines and arccosine terms by:

$$t^{-1}\left(\frac{a}{b}\right) = s^{-1}\left(\frac{a}{\sqrt{a^2 + b^2}}\right)$$
$$t^{-1}\left(\frac{a}{b}\right) = c^{-1}\left(\frac{b}{\sqrt{a^2 + b^2}}\right)$$

The final description of F_{C2y} is therefore:

$$F_{C_2y} = F_{C_1} \cdot \left(\frac{\left(\frac{\ell}{\alpha_1} - r_{C_{1.1}}\right) \cdot s(\alpha_1)}{\sqrt{\left(\left(\frac{\ell}{\alpha_1} - r_{C_{1.1}}\right) \cdot s(\alpha_1) \cdot t\left(\frac{\alpha_1}{2}\right) + dr\right)^2 + \left(\left(\frac{\ell}{\alpha_1} - r_{C_{1.1}}\right) \cdot s(\alpha_1)\right)^2}} \cdot c(\alpha_2) \right.$$
$$- \frac{\left(\frac{\ell}{\alpha_1} - r_{C_{1.1}}\right) \cdot s(\alpha_1) \cdot t\left(\frac{\alpha_1}{2}\right) + dr}{\sqrt{\left(\left(\frac{\ell}{\alpha_1} - r_{C_{1.1}}\right) \cdot s(\alpha_1) \cdot t\left(\frac{\alpha_1}{2}\right) + dr\right)^2 + \left(\left(\frac{\ell}{\alpha_1} - r_{C_{1.1}}\right) \cdot s(\alpha_1)\right)^2}} \cdot s(\alpha_2)$$
$$\left. - \frac{\left(\frac{l}{\alpha_2} - r_{C_{1.2}}\right) \cdot s(\alpha_2)}{\sqrt{\left(\left(\frac{\ell}{\alpha_2} - r_{C_{1.2}}\right) \cdot s(\alpha_2) \cdot t\left(\frac{\alpha_2}{2}\right) + dr\right)^2 + \left(\left(\frac{\ell}{\alpha_2} - r_{C_{1.2}}\right) \cdot s(\alpha_2)\right)^2}} \right)$$

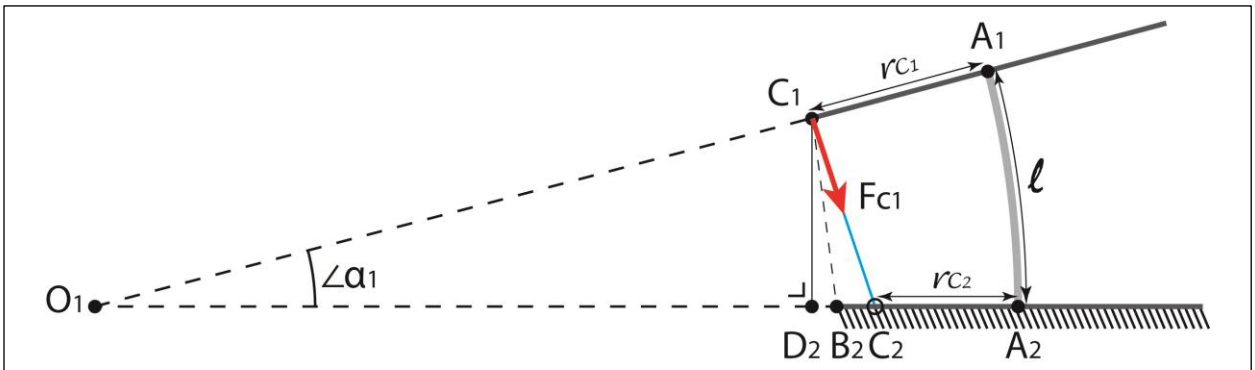

Figure 49: Deformed segment 1.

A.2 Negative α

The Figure 49 shows segment 1 bended by a helix cable to the left. This results in a negative value for $\angle\alpha_1$. The question is if the derived equations for segment 1 can still be applied in this configuration.

First realize that the values of r_{C1} and r_{C2} will be negative if positioned on the left side of the flexible axis. Now each term of the moment balance of segment 1 is going to be evaluated for a negative value of α_1 as illustrated in Figure 50.

$$\sum \mathrm{M_{A_2}} = 0 : \ \mathrm{M_{r_1}} - \mathrm{F_{C_1x}} \cdot \mathrm{d_{C_1y}} + \mathrm{F_{C_1y}} \cdot \mathrm{d_{C_1x}} = 0$$

$$\boldsymbol{M_{r_1} = c \cdot \alpha_1}$$

Since $\angle\alpha_1$ is now negative, the bending moment will also be negative. While the flexible axis is bended in the opposite direction, this is exactly what is expected.

$$\boldsymbol{F_{C_1x} = F_{C_1} \cdot s(\delta_1)}$$

The magnitude of F_{C1x} will be equal to the positive α_1-case, but have an opposite direction. From the sine it is known that:

$$-\mathrm{s(x)} = \mathrm{s(-x)}$$

This means that for an equal magnitude but opposite direction the angle $\angle\delta_1$ should change sign. The description of $\angle\delta_1$ is:

$$\angle\delta_1 = \mathrm{t^{-1}}\left(\mathrm{t}\left(\frac{\alpha_1}{2}\right) + \frac{\mathrm{dr}}{\left(\frac{\ell}{\alpha_1} - \mathrm{r_{C_{1.1}}}\right) \cdot \mathrm{s}(\alpha_1)}\right)$$

From the tangent one knows that:

$$-t^{-1}(x) = t^{-1}(-x)$$

So in order for angle $\angle\delta_1$ to change its sign, the term inside the arctan() should change its sign. For the first term this is true because:

$$-t\left(\frac{\alpha_1}{2}\right) = t\left(\frac{-\alpha_1}{2}\right)$$

For the second term is:

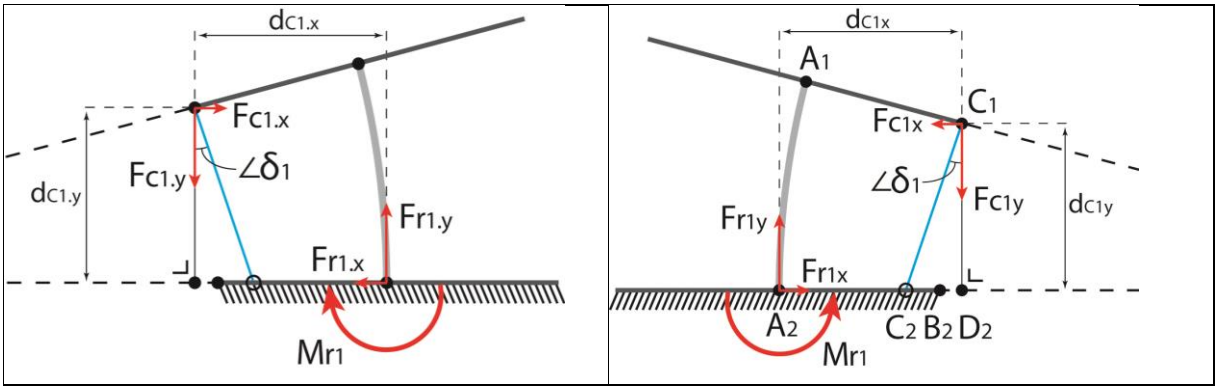

Figure 50: Left: Moment, forces and moment arm of segment 1 with negative $\angle\alpha_1$. Right: Moment, forces and moment arm of segment 1 with positive $\angle\alpha_1$.

$$\frac{dr}{\left(\frac{\ell}{\alpha_1} - r_{C_{1.1}}\right) \cdot sin(\alpha_1)}$$

One should realize that the *dr* is equal to $r_{C1.1}$ minus $r_{C1.2}$, which will be negative. The numerator of the division therefore becomes negative. The denominator stays positive, because one can state for a negative value of $\angle\alpha_1$:

$$\left(\frac{\ell}{\alpha_1} - r_{C_{1.1}}\right) < 0$$

$$s(\alpha_1) < 0$$

Noting that length ℓ divided by $\angle\alpha_1$ will always have a higher magnitude then $r_{c1.1}$. The decomposition of F_{C1} into F_{C1x} is therefore correct for negative values of $\angle\alpha_1$.

$$\boldsymbol{d_{C_1 y}} = \left(\frac{\ell}{\boldsymbol{\alpha_1}} - \boldsymbol{r_{C_{1.1}}}\right) \cdot \boldsymbol{s(\alpha_1)}$$

The moment created by F_{c1x} and d_{C1y} should change direction, as is seen Figure 50. Since F_{C1x} changes direction, d_{C1y} should stay equal. The function of d_{C1y} was already seen in the evaluation of force F_{C1x} and was found to stay positive.

$$\boldsymbol{F_{C_1 y}} = -\boldsymbol{F_{C_1}} \cdot \boldsymbol{c(\delta_1)}$$

From the evaluation of force F_{C1x} one has seen that angle $\angle\delta_1$ changes from sign if $\angle\alpha_1$ becomes negative. From the cosine it is know that:

$$c(x) = c(-x)$$

This means that F_{C1y} correctly does not change direction.

$$\boldsymbol{d_{C_1 x}} = \frac{\ell}{\boldsymbol{\alpha_1}} - \left(\frac{\ell}{\boldsymbol{\alpha_1}} - \boldsymbol{r_{C_{1.1}}}\right) \cdot \boldsymbol{c(\alpha_1)}$$

From Figure 50 it can be deducted that the moment created by F_{C1y} and d_{C1x} should change direction. Since $\angle\alpha_1$ and $r_{C1.1}$ are both negative and $c(\alpha_1)$ will stay positive, the value of d_{C1x} stays equal in magnitude, but correctly changes sign.

The equations of segment 1 are therefore suitable for negative values of α_1. Since the equations of segment 2 are based on the same principles it is safe to state these equations are also suitable. (this statement is checked but the math is not noted)

A.3 α_1 & α_2 opposite signs

In Figure 51 a case is presented in where $\angle\alpha_1$ is absolutely larger but opposite to $\angle\alpha_2$. One can see that the direction of F_{C2} is completely different to the example case discussed in the paper. One can therefore ask the question if the derived equations are still applicable in this particular case.

The magnitude of F_{C2} is determined by:

$$\mathrm{F_{C_2}} = 2 \cdot \mathrm{F_{C_1}} \cdot \mathrm{c}(\gamma_2)$$

With $\angle\gamma_2$ defined by:

$$\begin{aligned}\angle\gamma_2 &= \angle C_{2.3} + \angle C_{2.4} \\ &= \angle C_{2.1} + \angle C_{2.2} \\ &= \frac{\angle C_{2.1} + \angle C_{2.2} + \angle C_{2.3} + \angle C_{2.4}}{2}\end{aligned}$$

In where $\angle C_{2.1}$ was originally defined as:

$$\angle C_{2.1} = \frac{\pi}{2} - \angle\delta_1$$

In this case however, since $\angle\alpha_1$ is negative, $\angle\delta_1$ is equal to $\angle C_{1.1}$ and therefore

$$\angle C_1 C_2 O_1 = \frac{\pi}{2} - \angle\delta_1$$

and $\angle C_{2.1}$ should be defined as:

$$\angle C_{2.1} = \frac{\pi}{2} + \angle\delta_1$$

However, earlier in the negative α-case presented above it was found that $\angle\delta_1$ will have the same magnitude but an opposite sign. This means that the original description of $\angle C_{2.1}$ will still provide the correct value. The original equation for $\angle\gamma_2$ will therefore give the angle defined by $\angle C_{2.3} + \angle C_{2.4}$.

From Figure 51 one can however deduct that the magnitude of F_{C2} is determined by $\angle C_{2.5}$ and not by $\angle C_{2.3} + \angle C_{2.4}$. The angle is however placed inside a cosine term, for which the following rule applies:

$$cos(\pi \pm c) = -cos(c)$$

Since the summation of $\angle C_{2.3,}$ $\angle C_{2.4}$ and $\angle C_{2.5}$ define a straight line, one can state:

$$\angle C_{2.5} = \pi - (\angle C_{2.3} + \angle C_{2.4})$$

$$cos(\angle C_{2.5}) = -cos(\angle C_{2.3} + \angle C_{2.4})$$

So the magnitude of the force will be equal for both angles.

The cosine will be negative if $\angle\gamma_2$ lies between ½ π and 1½ π, which is the case for this particular cable position. Therefore if $\angle C_{2.3} + \angle C_{2.5}$ is used as $\angle\gamma_2$, the magnitude of F_{C2} will be negative. This is what one would expect since the force is directed to the other side of the cable. The original equation for calculating the magnitude of F_{C2} will therefore still be correct.

The following equations are used for the decomposition of F_{C2}:

$$\begin{aligned}F_{C_2 x} &= F_{C_2} \cdot s(\angle\delta_2) \\ F_{C_2 y} &= -F_{C_2} \cdot c(\angle\delta_2)\end{aligned}$$

With $\angle\delta_2$ originally equal to:

$$\begin{aligned}\angle\delta_2 &= \angle\gamma_2 - \angle C_{2.4} \\ \angle\delta_2 &= \angle C_{2.3}\end{aligned}$$

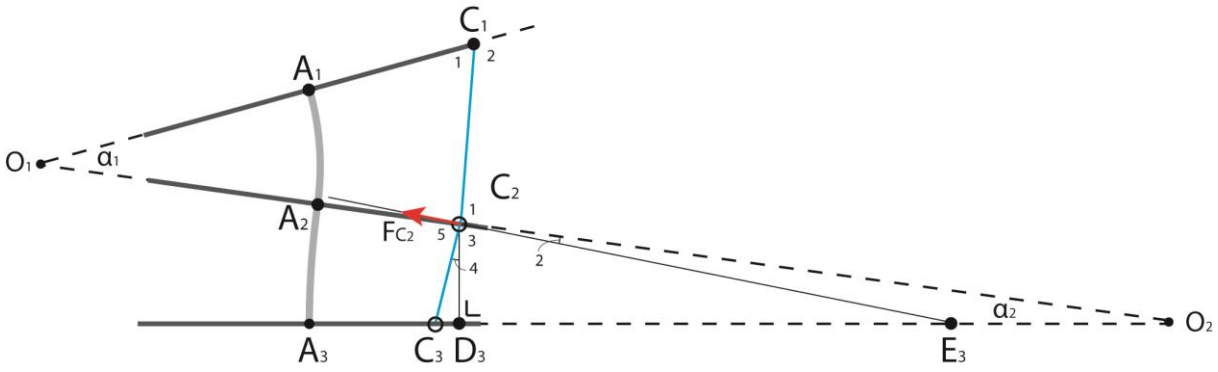

Figure 51: Deformed segments 1 and 2. Segment 1 with a negative α-value and segment 2 with a positive α-value.

However, from Figure 51 one can see that for the decomposition of F_{C2} one should use:

$$\angle\delta_2 = \angle C_{2.4} + \angle C_{2.5}$$

Since the summation of $\angle C_{2.3,}$ $\angle C_{2.4}$ and $\angle C_{2.5}$ define a straight line, one can state:

$$\angle C_{2.4} + \angle C_{2.5} = \pi - \angle C_{2.3}$$

The following rules apply to sine and cosine terms:

$$cos(\pi \pm c) = -cos(c)$$
$$sin(\pi \pm c) = \mp sin(c)$$

So again if the angles of the original equations are used, the magnitude of the decomposed forces would be correct.

Now if F_{C2} is negative, F_{C2x} should be negative as well. Since the sine of $\angle C_{2.3}$ is positive for 0 to π, this will be the case. If F_{C2} is negative and $\angle C_{2.3}$ is smaller than ½ π, the cosine of the decomposition into F_{C2y} will be positive. This means F_{C2y} positive and from Figure 51 one can see that this is correct. If however $\angle C_{2.3}$ is greater than ½ π, the cosine would be negative, resulting in a negative value of F_{C2y}. Again this is confirms the expectations.

So the equations presented in the paper correctly handle the case in where $\angle\alpha_{n-1}$ and $\angle\alpha_n$ have opposite signs.

A.4 Convexity of the moment balances

A function is convex if its derivative does not changed sign, so it is either zero and/or positive or zero and/or negative. If one can prove that the moment balance is convex, it means that it will only cross the zero-line once and the Matlab function *fzero* can be used to find this point.

The moment balance of segment 1 is equal to:

$$\sum \mathrm{M_{A_2}} = 0 : \ \mathrm{M_{r_1}} - \mathrm{F_{C_1x}} \cdot \mathrm{d_{C_1y}} + \mathrm{F_{C_1y}} \cdot \mathrm{d_{C_1x}} = 0$$

Bending moment:
$\mathrm{M_{r_1}} = \mathrm{c} \cdot \alpha_1$

Cable forces:
$\mathrm{F_{C_1x}} = -\mathrm{F_{C_1}} \cdot \mathrm{s}(\delta_1)$
$\mathrm{F_{C_1y}} = -\mathrm{F_{C_1}} \cdot \mathrm{c}(\delta_1)$
$$\angle\delta_1 = \mathrm{t}^{-1}\left(\mathrm{t}\left(\frac{\alpha_1}{2}\right) + \frac{dr}{\left(\frac{\ell}{\alpha_1} - r_{C_1}\right) \cdot \mathrm{s}(\alpha_1)} \right)$$

Moment arms:
$\mathrm{d_{C_1x}} = \frac{\ell}{\alpha_1} - \left(\frac{\ell}{\alpha_1} - \mathrm{r_{C_1}}\right) \cdot \mathrm{c}(\alpha_1)$
$\mathrm{d_{C_1y}} = \left(\frac{\ell}{\alpha_1} - \mathrm{r_{C_1}}\right) \cdot \mathrm{s}(\alpha_1)$

Now one wants to find the derivatives of each moment component. The case of a parallel cable is evaluated, since it reduces the mathematical complexity while still providing a good impression of the process. This means dr will be equal to zero and $\angle\delta_1$ can therefore be written as:

$$\angle\delta_1 = \frac{\alpha_1}{2}$$

If the segment size is large enough, $\angle\alpha_1$ will become small. To further simplify the process, the sine and cosine terms can be approximated for small values of $\angle\alpha_1$ by:

$$\sin(\alpha) \approx \alpha$$
$$\cos(\alpha) \approx 1$$
$$\tan(\alpha) \approx \alpha$$
$$\tan^{-1}(\alpha) \approx \alpha$$

This results in the following simplifications:

$\mathrm{F_{C_1x}} = -\mathrm{F_{C_1}} \cdot \frac{\alpha_1}{2}$
$\mathrm{F_{C_1y}} = -\mathrm{F_{C_1}}$
$\mathrm{d_{C_1x}} = \mathrm{r_{C_1}}$
$\mathrm{d_{C_1y}} = \ell - \mathrm{r_{C_1}} \cdot \alpha_1$

The derivatives of each moment are now given by:

$\mathrm{M_{r_1}} = \mathrm{c} \cdot \alpha_1$

$$\mathbf{\frac{d}{d\alpha_1}} = \mathbf{c} = \mathbf{\frac{E \cdot I}{\ell}}$$

$$\mathrm{F_{C_1x}} \cdot \mathrm{d_{C_1y}} = \frac{-\mathrm{F_{C_1}} \cdot \alpha_1 \cdot \left(\ell - \mathrm{r_{C_1}} \cdot \alpha_1\right)}{2}$$
$$= \frac{\mathrm{F_{C_1}} \cdot \left(\mathrm{r_{C_1}} \cdot {\alpha_1}^2 - \alpha_1 \cdot \ell\right)}{2}$$

$$\mathbf{\frac{d}{d\alpha_1}} = \mathbf{F_{C_1} \cdot r_{C_1} \cdot \alpha_1 - \frac{F_{C_1} \cdot \ell}{2}}$$

$\mathrm{F_{C_1y}} \cdot \mathrm{d_{C_1x}} = -\mathrm{F_{C_1}} \cdot \mathrm{r_{C_1}}$

$$\mathbf{\frac{d}{d\alpha_1}} = \mathbf{0}$$

If the amount of segments is increased, the segment length ℓ will decrease. One can therefore analyze the behavior of the derivatives by taking their limit for l goes to zero:

$$\lim_{\ell \to 0} \mathbf{\frac{E \cdot I}{\ell}} = \infty$$
$$\lim_{\ell \to 0} \mathbf{F_{C_1} \cdot r_{C_1} \cdot \alpha_1 - \frac{F_{C_1} \cdot \ell}{2}} = \mathbf{F_{C_1} \cdot r_{C_1} \cdot \alpha_1}$$

By realizing that $\angle\alpha_1$ goes to zero when ℓ goes to zero, one can confidently state the following.

$$\mathbf{\frac{E \cdot I}{\ell}} \gg \mathbf{F_{C_1} \cdot r_{C_1} \cdot \alpha_1 - \frac{F_{C_1} \cdot \ell}{2}}$$

So for a parallel cable the derivative of bending moment M_{r1} is always greater than that of the moments created by F_{Cx1} and F_{C1y}. Because it is also constant in respect to $\angle\alpha_1$, one can also confidently state that the moment balance for a parallel cable is a convex function and thereby crosses the zero-line for $\angle\alpha_1$ only once.

For a helix cable, d_{C1x} and d_{C1y} are equal to those

of a parallel cable and only F_{C1x} and F_{C1y} will differ. This will however not change the fact that the limit of the derivative of M_{r1} for ℓ goes to zero approaches infinity, while those of the moments of F_{C1x} and F_{C1y} do not. Therefore one can also safely state that the moment balance of segment 1 will also be convex for helix cables.

For segment 2, the math will become more complex, but the end result will stay the same. The derivatives of the moments created by the forces F_{a1} and F_{C1} are all influenced by ℓ and α which approach zero if one would increase the amount of segments. Therefore the derivatives will approach zero, while the derivative of the bending moment would approach infinity. The moment balance will therefore always be convex if the amount of segments is high enough.

Appendix B. Matlab code

The matlab code contains two parts: the simulation model and the imaging algorithm for retrieving the data of the validation model.

B.1 The simulation model

Run.m

One starts by running run.m. The m-files that are run in this script are listed in chronological order. The plotting files are not presented while they do not contain interesting information.

```
%%% Simulation Model %%%
% 2D-Model of a segmented steerable segment actuated by parallel and helix
% cables.

% Created in 2012-2013
% by P.W.J. Henselmans

clc, clear all, close all

% Enter the amount of cables and segments
amount_of_cables = 2
amount_of_segments = 100

% Initial values based on the dimensions and characteristics of the model
run Parameters

% Initial cable parameters. Each column divines a cable. The number of column is not limited.
Force_cables   : defines the pulling force
r_cable        : the starting position. A negative number represents a starting           position at the
              left.
Direction      : defines the direction of the helix cable, a negative value   indicates a direction to the
              left.
Beta           : is the angle of the helix cable. It can be divined a number of as r0,r1,r2,r4 which
              represent the horizontal distance a cable travels and is created in Parameters.m
```

```
Force_cables        = [0.3     0.1      0.5         0.1       ]*9.81; %N
r_cable             = [15      -15      -10         0            ];%m
direction           = [-1       1        -1         1         ];
beta                = [r4       r2       r4         r0        ];%rad

% Running the model
run Model

% Creating the data used for plotting
run Create_Plotting_Data

% Plot the deformed steerable element, alpha, moments and forces
run Plot

% Plot the deformed steerable element, the alpha graph and the forces
% individually
run Plot_Deformed_Shape
run Plot_Alpha
run Plot_Forces

% Plots the summation of the moments M_Fa and M_Fc along the flexible axis to create an
% intuitive view of their contribution to Mr. Best for 1 cable.
run Plot_Summation_of_Moments

% Calculate the lengths of the cables
run Cable_length
```

Parameters.m

```
%% Parameters

l_total             = 130;           %total length steerable element [mm]
l                   = l_total/amount_of_segments;   %length of a segment [mm]
r                   = 16;            %radius of the steerable element [mm]
b                   = 30;            %width of the flexible axis [mm]
h                   = 0.2;           %thickness of the flexible axis [mm]
E                   = 210E3;         %modulus of elasticity of the flexible
                                      axis [N/mm^2]
I                   = (b*(h^3))/12;  %moment of inertia of the flexible axis
```

```
                                        [mm^4]
c                   = E*I/l;          %stiffness of the flexible axis [Nmm/rad]

% beta angles based on the horizontal distance of a cable.
r0 = 0;
r1 = atan((1*r)/l_total);
r2 = atan((2*r)/l_total);
r4 = atan((4*r)/l_total);
```

Model.m

Model.m is divided into a part for segment 1 and segments 2 to n. It uses four functions: alpha_1_function, Forces_1, alpha_n_function and Forces_n.

```
% Simulation Model
for m = 1:amount_of_cables
    % Determine distance dr per segment
    dr(m) = l * tan(beta(m));

    % Setting the force for each cable. This function allows to set Force
    % to zero for calculating the individual outputs of cables for
    % approximating alpha during combined actuation.
    Force(m) = Force_cables(1,m);

    % Configurating r_cable for all segments
    for n = 2:amount_of_segments
        r_cable(n,m) = r_cable(n-1,m) + direction(m) * dr(m);
        r_cable(n+1,m) = r_cable(n,m) + direction(m) * dr(m);

        if abs(r_cable(n+1,m)) > r +0.001
            direction(1,m) = -direction(1,m);
            r_cable(n+1,m) = r_cable(n,m) + direction(m) * dr(m);
        end
    end
end
% Searching for alpha of segment 1 by a line search along the domain of alpha.
% FMINBND is used to minimize the outcome of the moment balance by varying
% alpha
    options = optimset('MaxFunEvals',5000,'MaxIter',10000,'TolFun',0.1e-50,'TolX',1e-50);
```

```
    alpha(1,1) = fzero(@(alpha_1) alpha_1_function(alpha_1,c, Force, l, r_cable, amount_of_cables),[-0.5
    0.5], options);

% Calculating the reaction and cable forces with the newly found alpha of
% segment 1
    [Fr,Fa, Fc, M_Fa, M_Fc] = Forces_1(Force, l, r_cable, amount_of_cables, alpha(1,1));

% Calculating segments 2 to n
for n = 2:amount_of_segments
        % Searching for alpha of segment n by a line search along the domain of alpha.
        % the fzero function is used to minimize the outcome of the moment balance by varying
        % alpha
       alpha(n,1) = fzero(@(alpha_n) alpha_n_function(alpha_n,alpha,Fr,Fc,n,c,l,r_cable,amount_of_cables),
       [-0.5 0.5], options);

        % Calculating the reaction and cable forces with the newly found alpha of
        % segment n
            [Fr, Fa, Fc, M_Fa, M_Fc] = Forces_n(alpha,Fr,Fa,Fc,n,l,r_cable, amount_of_cables,M_Fa,M_Fc);
end
```

alpha_function_1

```
function Moment_Balance = alpha_1_function(alpha_1,c, Force, l, r_cable, amount_of_cables)

for m = 1:amount_of_cables
     % Force - cable
     Fc(1,1,m) = Force(1,m);

     % For alpha 1 is zero, the moment arms and distances of trianlge
     % C1C2D2 are not effected by a deformation.
     if alpha_1 == 0
         % Moment arms - cable
         d_cx(m) = r_cable(1,m);
         d_cy(m) = l;

         % Distances of the triangle C1D2C2
         c1d2 = l;
         c2d2 = r_cable(1,m) - r_cable(2,m);
         c1c2 = sqrt(c1d2^2 + c2d2^2);
     else
```

```
        % Moment arms - cable
        d_cx(m) = (l/alpha_1) - ((l/alpha_1)-r_cable(1,m)) * cos(alpha_1);
        d_cy(m) = ((l/alpha_1)-r_cable(1,m)) * sin(alpha_1);

       % Distances of the triangle C1D2C2
        c1d2 = ((l/alpha_1) - r_cable(1,m))*sin(alpha_1);
        c2d2 = (((l/alpha_1) - r_cable(1,m))*sin(alpha_1)) * tan(alpha_1/2) + r_cable(1,m) - r_cable(2,m);
        c1c2 = sqrt(c1d2^2 + c2d2^2);
    end

    % The sine and consine term for the decomposition of the cable forces
    sin_decomposition = c2d2/c1c2;
    cos_decomposition = c1d2/c1c2;

    % Moments generated by the cable forces. Mc1_x is Mc(1,1), Mcy is
    % Mc1_y(1,2)
    MFc(m)     = Fc(1,1,m) * (sin_decomposition * d_cy(m) - cos_decomposition * d_cx(m));

end

% Complete moment balance
Moment_Balance  = alpha_1*c + sum(MFc(:));
```

Forces_1

```
function Moment_Balance = alpha_1_function(alpha_1,c, Force, l, r_cable, amount_of_cables)

for m = 1:amount_of_cables
    % Force - cable
    Fc(1,1,m) = Force(1,m);

    % For alpha 1 is zero, the moment arms and distances of trianlge
    % C1C2D2 are not effected by a deformation.
    if alpha_1 == 0
        % Moment arms - cable
        d_cx(m) = r_cable(1,m);
        d_cy(m) = l;
```

```
        % Distances of the triangle C1D2C2
        c1d2 = l;
        c2d2 = r_cable(1,m) - r_cable(2,m);
        c1c2 = sqrt(c1d2^2 + c2d2^2);
    else
        % Moment arms - cable
        d_cx(m) = (l/alpha_1) - ((l/alpha_1)-r_cable(1,m)) * cos(alpha_1);
        d_cy(m) = ((l/alpha_1)-r_cable(1,m)) * sin(alpha_1);

       % Distances of the triangle C1D2C2
        c1d2 = ((l/alpha_1) - r_cable(1,m))*sin(alpha_1);
        c2d2 = (((l/alpha_1) - r_cable(1,m))*sin(alpha_1)) * tan(alpha_1/2) + r_cable(1,m) - r_cable(2,m);
        c1c2 = sqrt(c1d2^2 + c2d2^2);
    end

    % The sine and consine term for the decomposition of the cable forces
    sin_decomposition = c2d2/c1c2;
    cos_decomposition = c1d2/c1c2;

    % Moments generated by the cable forces. Mc1_x is Mc(1,1), Mcy is
    % Mc1_y(1,2)
    MFc(m)     = Fc(1,1,m) * (sin_decomposition * d_cy(m) - cos_decomposition * d_cx(m));

end

% Complete moment balance
Moment_Balance  = alpha_1*c + sum(MFc(:));
```

alpha_function_n

```
function Moment_Balance = alpha_n_function(alpha_n,alpha,Fr,Fc,n,c,l,r_cable, amount_of_cables,Ma,Mc)

% Calculate the action forces of segment n based on Fr and the direction
% change of the local coordinate system. They are named F_a instead of Fa
% in order not to distort the actual array of Fa created in Forces_n. The
% same is done for moments M_Fa to MFa and M_Fc to MFc
F_a(1,1) = -Fr(n-1,1);
F_a(1,2) = -(Fr(n-1,2) * cos(alpha_n) + Fr(n-1,3) * sin(alpha_n));
F_a(1,3) = -(Fr(n-1,3) * cos(alpha_n) - Fr(n-1,2) * sin(alpha_n));

% % Moment arms of the action forces
if alpha_n == 0
    d_ax = 0;
    d_ay = l;
else
    d_ax = (l/alpha_n) -(l/alpha_n)* cos(alpha_n);
    d_ay = (l/alpha_n)* sin(alpha_n);
end

% Calculate the combined moments of the action force components
MFa = -F_a(1,2)*d_ay + F_a(1,3)*d_ax;

for m = 1:amount_of_cables
    % The moment arms or distance c2c3, c2d3 and c3d3 are not effect by
    % deformation for alpha_n is zero
    if alpha_n == 0
        % Moment arms - cable
         d_cx(m) = r_cable(n,m);
         d_cy(m) = l;

        % Distances segment n
         c2d3  = l;
         c3d3  = r_cable(n,m) - r_cable(n+1,m);
         c2c3  = sqrt(c2d3^2 + c3d3^2);
    else
        % Moment arms - cable
         d_cx(m) = (l/alpha_n) - ((l/alpha_n)-r_cable(n,m)) * cos(alpha_n);
         d_cy(m) = ((l/alpha_n)-r_cable(n,m)) * sin(alpha_n);
```

```
        % Distances segment n
         c2d3  = ((l/alpha_n) - r_cable(n,m)) * sin(alpha_n);
         c3d3  = ((l/alpha_n) - r_cable(n,m)) * sin(alpha_n) * tan(alpha_n/2) + r_cable(n,m) -
r_cable(n+1,m);
         c2c3  = sqrt(c2d3^2 + c3d3^2);
    end

    % The moment distances c1c2, c1d2 and c2d2 are not effect by
    % deformation for alpha_n-1 is zero
    if alpha(n-1,1) == 0
         % Distances segment n-1
         c1d2  = l;
         c2d2  = r_cable(n-1,m) - r_cable(n,m);
         c1c2  = sqrt(c1d2^2 + c2d2^2);
    else
         % Distances segment n-1
         c1d2  = ((l/alpha(n-1,1)) - r_cable(n-1,m)) * sin(alpha(n-1,1));
         c2d2  = ((l/alpha(n-1,1)) - r_cable(n-1,m)) * sin(alpha(n-1,1)) * tan(alpha(n-1,1)/2) + r_cable(n-
1,m) - r_cable(n,m);
         c1c2  = sqrt(c1d2^2 + c2d2^2);
    end

    % Decomposition terms for the decomposition of the cable forces
     x_decomposition      = (c2d2/c1c2)*cos(alpha_n) + (c1d2/c1c2)*sin(alpha_n) - (c3d3/c2c3);
     y_decomposition      = (c1d2/c1c2)*cos(alpha_n) - (c2d2/c1c2)*sin(alpha_n) - (c2d3/c2c3);

    % Combined moment of the cable force components
     MFc(n,m)     = Fc(1,1,m) * (-x_decomposition * d_cy(m) + y_decomposition * d_cx(m));

end

% Complete moment balance
 Moment_Balance = alpha_n*c - alpha(n-1,1)*c + MFa + sum(MFc(n,:));
```

Forces_n

```
function [Fr, Fa, Fc, M_Fa, M_Fc] = Forces_n(alpha,Fr,Fa,Fc,n,l,r_cable, amount_of_cables,M_Fa,M_Fc)

% Calculate the action forces of segment n
Fa(n,1) = -Fr(n-1,1);
Fa(n,2) = -(Fr(n-1,2) * cos(alpha(n,1)) + Fr(n-1,3) * sin(alpha(n,1)));
Fa(n,3) = -(Fr(n-1,3) * cos(alpha(n,1)) - Fr(n-1,2) * sin(alpha(n,1)));

% Moment arms of the action forces
if alpha(n,1) == 0
    d_ax = 0;
    d_ay = l;
else
    d_ax = (l/alpha(n,1)) -(l/alpha(n,1))* cos(alpha(n,1));
    d_ay = (l/alpha(n,1))* sin(alpha(n,1));
end

% Moments created by Fa
M_Fa(n,1) = -Fa(n,2)*d_ay;
M_Fa(n,2) = Fa(n,3)*d_ax;

for m = 1:amount_of_cables

    % Calcuation of the moment arms and distances c2d3, c2c3 and c3d3.
    % Again the difference is made for alpha is zero
    if alpha(n,1) == 0
         % Moment arms - cable
         d_cx(m) = r_cable(n,m);
         d_cy(m) = l;

        % Distances segment n
         c2d3  = l;
         c3d3  = r_cable(n,m) - r_cable(n+1,m);
         c2c3  = sqrt(c2d3^2 + c3d3^2);
    else
        % Moment arms - cable
         d_cx(m) = (l/alpha(n,1)) - ((l/alpha(n,1))-r_cable(n,m)) * cos(alpha(n,1));
         d_cy(m) = ((l/alpha(n,1))-r_cable(n,m)) * sin(alpha(n,1));
```

```
        % Distances segment n
         c2d3  = ((l/alpha(n,1)) - r_cable(n,m)) * sin(alpha(n,1));
         c3d3  = ((l/alpha(n,1)) - r_cable(n,m)) * sin(alpha(n,1)) * tan(alpha(n,1)/2)
          + r_cable(n,m) - r_cable(n+1,m);
         c2c3  = sqrt(c2d3^2 + c3d3^2);
    end

    if alpha(n-1,1) == 0
         % Distances segment n-1
         c1d2  = l;
         c2d2  = r_cable(n-1,m) - r_cable(n,m);
         c1c2  = sqrt(c1d2^2 + c2d2^2);
    else
         % Distances segment n-1
         c1d2  = ((l/alpha(n-1,1)) - r_cable(n-1,m)) * sin(alpha(n-1,1));
          c2d2  = ((l/alpha(n-1,1)) - r_cable(n-1,m)) * sin(alpha(n-1,1)) * tan(alpha(n-1,1)/2)
         + r_cable(n-1,m) - r_cable(n,m);
         c1c2  = sqrt(c1d2^2 + c2d2^2);
    end

    % Decomposition terms
     x_decomposition      = (c2d2/c1c2)*cos(alpha(n,1)) + (c1d2/c1c2)*sin(alpha(n,1)) - (c3d3/c2c3);
     y_decomposition      = (c1d2/c1c2)*cos(alpha(n,1)) - (c2d2/c1c2)*sin(alpha(n,1)) - (c2d3/c2c3);

    % Combined moment of the cable force components
     Fc(n,2,m) = Fc(1,1,m) * x_decomposition;
     Fc(n,3,m) = Fc(1,1,m) * y_decomposition;
     Fc(n,1,m) = sqrt(Fc(n,2,m)^2 + Fc(n,3,m)^2);

    % Combined moment of the cable force components
     M_Fc(n,:,m)     = Fc(1,1,m) * [-x_decomposition * d_cy(m)  y_decomposition * d_cx(m)];
end

% Calculate the reaction forces
Fr(n,2) = -(Fa(n,2) + sum(Fc(n,2,:)));
Fr(n,3) = -(Fa(n,3) + sum(Fc(n,3,:)));
Fr(n,1) = sqrt(Fr(n,2)^2 + Fr(n,3)^2);
```

Create_Plotting_Data.m

Create_Plotting_Data takes the alpha values of the model and creates data to enable to plot the deformed shape. In contrary to the model it starts at segment n, which is why certain data is flipped.

```
% Creating Plotting Data

% Determine the amount of ribs to be plotted. This is needed since for high
% amount of segments it is not preferable to plot all ribs
teller = 1;
amount_of_ribs = amount_of_segments;
skip = 0.85;
while amount_of_ribs > 20 || floor(amount_of_ribs)~=ceil(amount_of_ribs) || floor(skip)~=ceil(skip)
    teller = teller +1;
    amount_of_ribs = (amount_of_segments/teller);
    skip = amount_of_segments/amount_of_ribs;
end
amount_of_ribs = amount_of_ribs+1;

% Data is flipped because the plotting proces starts at the bottom rib, in
% contrairy to the shape calcuation proces
alpha_flipped = flipud(alpha(:,1));
r_cable_flipped(:,:) = flipud(r_cable(:,:));

% Starting potitions
point_axis(1,:) = [0 0];
% point_cable

% Plot central axis
for i = 2:amount_of_segments+1
    % Determine the shift in x and y for the new cable point
    if alpha == 0
        d_x = 0;
        d_y = 1;
    else
        d_x = (l/alpha_flipped(i-1,1)) -(l/alpha_flipped(i-1,1))* cos(alpha_flipped(i-1,1));
        d_y = (l/alpha_flipped(i-1,1))* sin(alpha_flipped(i-1,1));
    end
    % Adjust d_x and d_y for the global coordination system
        dx = d_x * cos(sum(alpha_flipped(1:i-2,1))) + d_y * sin(sum(alpha_flipped(1:i-2,1)));
        dy = d_y * cos(sum(alpha_flipped(1:i-2,1))) - d_x * sin(sum(alpha_flipped(1:i-2,1)));
```

```
    point_axis(i,:) = point_axis(i-1,:) + [dx dy];
end

% Plot the ribs
for i = 1 : amount_of_ribs
    % Skip certain ribs
    j = i*skip - (skip -1);

    dx_cylinder = r * cos(sum(alpha_flipped(1:j-1,1)));
    dy_cylinder = r * sin(sum(alpha_flipped(1:j-1,1)));

    % The right and left rib coordinates
    point_rib(1,:,i) = point_axis(j,:) + [dx_cylinder -dy_cylinder];
    point_rib(2,:,i) = point_axis(j,:) + [-dx_cylinder  dy_cylinder];
end


% Plot cable points
for i = 1:amount_of_cables
    for j = 1:amount_of_segments+1
        % Determine the cable point positions on the ribs
        r_cable_x(j,i) = r_cable_flipped(j,i) * cos(sum(alpha_flipped(1:j-1,1)));
        r_cable_y(j,i) = r_cable_flipped(j,i) * sin(sum(alpha_flipped(1:j-1,1)));
        % Relocate the cable points to the axis points
        point_cable(j,:,i) = point_axis(j,:) + [r_cable_x(j,i) -r_cable_y(j,i)];
    end
end
```

Cable_Length

Can be used to calculate the lengths of the cables. The cable lengths per segment is presented by cable_length_per_segment.

```
% Calculation of the cables lengths
for i = 1:amount_of_cables
    r_cable_x(1,i) = r_cable_flipped(1,i);
    r_cable_y(1,i) = 0;

    for j = 2:amount_of_segments+1
        r_cable_x(j,i) = r_cable_flipped(j,i) * cos(sum(alpha_flipped(1:(j-1),1)));
        r_cable_y(j,i) = r_cable_flipped(j,i) * sin(sum(alpha_flipped(1:(j-1),1)));
    end
    for j = 1:amount_of_segments+1
        point_cable_length(j,:,i) = point_axis(j,:) + [r_cable_x(j,i) -r_cable_y(j,i)];
    end
end
cable_length(1,1:amount_of_cables) = 0;

for i = 1:amount_of_cables
    for j = 1:amount_of_segments
        cable_length(j,i) = sqrt((point_cable_length(j,1,i)-point_cable_length(j+1,1,i))^2 +
(point_cable_length(j,2,i)-point_cable_length(j+1,2,i))^2);
    end
end

cable_length_per_segment = cable_length;
cable_length = sum(cable_length)
```

Combined_Actuation.m

One can use this file to plot the individual cables and their combined result.

```
% Combined Actuation
clc, clear all, close all

% Enter the amount of cables you want to combine
amount_of_cables = 4
% Enter the amount of segments
amount_of_segments = 100

for cn = 1:amount_of_cables+1
run Parameters

% Initial cable parameters
Force_cables        = [4       4      4       4     4         5       ]; %N%N
r_cable             = [-15      15      -15     15    0         0       ];%m
direction           = [-1       -1       1      -1     -1        -1     ];
beta                = [ r0     r2      r2      r2     r1        r2   ];%rad

if cn ~= amount_of_cables+1
    for i = 1:amount_of_cables
        if i ~= cn
        Force_cables(1,i)        = 0;
        end
    end
end
run Model

clearvars 'm'

save(['Data/' [num2str(cn)] '.mat'])
end


run Plot_Combined_Cables
```

B.2 Imaging algorithm

The algorithm uses an imaging package called dipimage to evaluate the photos. This can be downloaded for free at: http://www.diplib.org/.

The validation photos are placed in a directory. In this directory, each validated cable has its own directory wherein the photos of underloading and overloading are saved, each marked with the number and the letter a or b respectively.

The imaging algorithm allows for multiple photos to be evaluated in one single run. One starts with taking a sample of a red marker and a green marker of a photo of the validation model:

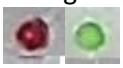

These markers must be loaded in `Find_RGB_Values.m`. One must therefore type in the name of the marker one wants to evaluate in rule 10 `filename` and then define the folder in which these samples are place by altering `path` the rule 11.

By running `Find_RGB_Values.m` the algorithm presents a grey picture of the sample. By holding the left mouse button and dragging one can define the area of the sample that needs to be evaluated on its RGB values. All the pixels are then presented in two figures of Red, Green and Blue. The mean values are given in the command window.

One must now open `Image_Processing.m` and manually fill in the found RGB values for the green and red markers on the top of the file.

The imagine algorithm is started by `Retrieving_Images.m`. One can select which cable(s) must be processed by defining the value of i. This directory is then opened and all the photos of that cable are processed by `Image_Processing.m`. The results of the imaging process are one file with the marker positions and the segment angles and a figure of the photo with the markers so one can check if the process has succeeded. Both the file and the figure is saved in the same directory as the original photo.

The algorithm of `Image_Processing.m` works in the following steps:

- The image is loaded and turned into the RGB color space, resulting in three matrixes for the red, green and blue values. The matrixes are as big as the amount of pixels of the image. The three matrixes are defined in `image_rgb`
- The green markers will be searched for first since they are the easiest to find. Their positions will later be used to indicate the positions of the red markers.
- A domain around the RGB-values of the green makers is created. The size is defined by `threshold`
- The number of green markers must be equal to 11, otherwise the algorithm adjusts the threshold accordingly. The threshold increases if the number of markers is lower than 11 and decreases if the number of markers is higher than 11.
- The Red-matrix is scanned for pixels that belong to the R-domain. The same is done for the Green-matrix and Blue-matrix.
- The resulting matrixes are combined; meaning that if a pixel belongs to all three domains it is marked with a 1. Else the pixel is given the value 0. This creates the matrix `image_array_binary`
- Pixels with a 1 value are now grouped together. This is done because a marker in the photo will consist of multiple pixels which must be grouped to form one marker. The grouping is done by checking around a pixel if it is surrounded by other pixels marked by 1. If so, the area between

the pixels is also marked with a 1. If this was not done, the algorithm will see the initial pixels with value 1 as individual markers. Also a single pixel that falls into the RGB-domain but does not belong to an actual marker could be falsely identified as a marker. The grouping process does not let this happen since a group must contain at least 10 pixels that belong the RGB-domain.

- The algorithm now determines the center of these groups and labels this center point as a marker.
- If 11 markers are found, the algorithm continues to finding the red markers. If not, the thresholds are adjusted accordingly and the process repeats itself. If after 10 repeating still no 11 markers are found, the RGB-domains are adjusted based on the mean RGB-values of the markers that where identified.
- The red markers are more difficult to find, since the screws on the flexible axis can be falsely identified as a marker. Therefore a circle around found green markers is colored black, resulting in a matrix defining the following grey figure:

- This image is now used to find the positions of the red markers.
- If all the red markers are found, the markers are sorted based on their heights.
- The positions of the markers are used to calculate the angles of the ribs, save in the m-file as segment_angles
- Finally the photo with the identified markers is plotted and saved:

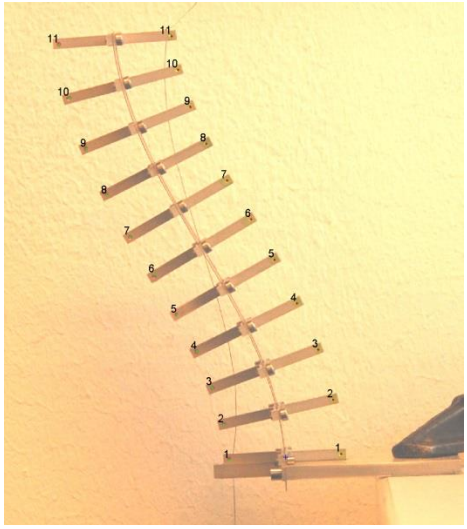

Find_RGB_Values

```
% Find RGB Values

clc, clear all, close all
% Start the imaging software package.
addpath('C:\Program Files\DIPimage 2.4.1\common\dipimage');
dip_initialise;
dipsetpref('ImageFilePath', 'C:\Program Files\DIPimage 2.4.1\images');

% Load image
filename = ['green']
path =
['C:\Users\T\Dropbox\Afstuderen\Afstuderen\Verslag\Matlab\Matlab\Validation -
kopie\' [filename] '.png']
[image_out,map] = readim(path);

% Turn into RGB color space
image_rgb = colorspace(image_out,'RGB');

% Converting image into matlab matrix
image_array_original = dip_array(image_rgb);
size_x = size(image_array_original,2);
size_y = size(image_array_original,1);

% Crop a sample of the marker
H = dipshow(image_array_original);
[B,C] = dipcrop(H);

% Converting the marker sample into matlab matrix
B_array = dip_array(B);

% Determine the mean RGB-values of the marker sample
Red = mean(mean(B_array(:,:,1)))
Green = mean(mean(B_array(:,:,2)))
Blue = mean(mean(B_array(:,:,3)))


% Plot the u and v values of the image and the ball sample
% plot(image_array_original(:,:,2), image_array_original(:,:,3),'r.');
% hold on
figure(1)
plot(B_array(:,:,1), B_array(:,:,2),'b.');
xlabel ('R')
ylabel ('G')
figure(2)
plot(B_array(:,:,2), B_array(:,:,3),'b.');
xlabel ('G')
ylabel ('B')
```

Retrieving_Images.m

```
clc, clear all

% The imaging software package is started
run dip_image

% The algorithm defines the directory in where the photos of the validation
% model are placed. Then the algoritm Image_Processing is run which identifies
% the red and green markers.
for i = 15

if i == 1
directory = 'Initial Position\Chronological';
else if i == 2
directory = 'L';
else if i == 3
directory = 'L+r';
else if i == 4
directory = 'L+2r\Load 1';
else if i == 5
directory = 'L+2r\Load 2';
else if i == 6
directory = 'L+2r\Load 3';
else if i == 7
directory = 'L+2r\Load 4';
else if i == 8
directory = 'L+2r\Load 5';
else if i == 9
directory = 'L+4r\Load 1';
else if i == 10
directory = 'L+4r\Load 2';
else if i == 11
directory = 'L+4r\Load 3';
else if i == 12
directory = 'L+4r\Load 4';
else if i == 13
directory = 'L+4r\Load 5';
else if i == 14
directory = 'R';
else if i == 15
directory = 'R-2r';
else if i == 16
directory = 'R & R-2r';
else if i == 17
directory = 'R & L+4r & R-2r';
    end
    end
    end
    end
    end
    end
    end
    end
    end
    end
```

```
    end
    end
    end
    end
    end
end
    % Define the number of photos per cable
    for j = 1:10
        % Defines the under and overloading photos
        for p = 1:2
            close all
            if j == 1
                loading = 'a';
            else if j == 2
                    loading = 'b';
                end
            end

    % Define the directory wherein the directories of the photos are placed
    path_basis =
'C:\Users\T\Dropbox\Afstuderen\Afstuderen\Verslag\Foto\Photoshop\';
    path_extra = [directory '\'];

    file_name = [loading ' (' num2str(p) ')'];
    load_name = [path_basis path_extra file_name '.jpg']
    save_name = [path_basis path_extra file_name];

    % First is checked if the photo can be found, if it is found, the
    % image_Processing is run
    if exist(load_name, 'file') == 2
        run Image_Processing
    end
    end
    end
end
```

Image_Processing.m

```
% Image Processing
close all

% Green marker RGB values
R_green = 162;
G_green = 201;
B_green = 98;

% Red marker RGB values
R_red = 209;
G_red = 104;
B_red = 88;

% Load the image
[image_out,map] = readim(load_name);

% Turn into RGB color space
image_rgb = colorspace(image_out,'RGB');

% Converting image into matlab matrix
image_array_original = dip_array(image_rgb);
size_x = size(image_array_original,2);
size_y = size(image_array_original,1);

% Define after how many runs the RGB values of the makers should be updated
% into the mean values of the markers that are found.
new_rgb = 10;

% First the algorithm searches for the green markers. These markers are the
% easiest to find and the positions will be used to eliminate errors when the
algorithm
% searches for the red markers.
for p = 2

    % Set initial values
    error = 0;
    num_markers = 0;
    r = 0;
    R_value = 0;
    g = 0;
    G_value = 0;
    b = 0;
    B_value = 0;

    if p == 2
        % RGB values: Right - Green
        threshold = 25;
        threshold_green = threshold;
        R_threshold = R_green;
        G_threshold = G_green;
        B_threshold = B_green;
    end

% If the number of markers is not equal to 11, the threshold in adjusted
```

```
while num_markers ~= 11
    image_array = image_array_original;
    num_markers
    p;
if num_markers < 11
    threshold = threshold+1;
    error = error+1;
else if num_markers > 11
    error = error+1;
    threshold = threshold-1;
    end
end

% if after 10 threshold adjustments the number of markers is still not equal
to 11,
% the RGB-values are adjusted based on the average RGB-values of the
% markers that are identified
if error == new_rgb
    error = 0;
    threshold = 25;
    R_threshold = ceil(mean(R_value))
    G_threshold = ceil(mean(G_value))
    B_threshold = ceil(mean(B_value))
end

% Filtering the image. image_array consists of three matrixes, one for the
% R-values, one for the G-values and one for the B-values. Each matrix is
% scanned for values that fall into the RGB-domains, defined by
% R_threshold_down and R_threshold_up. If a certain pixel falls into all
% three domains, the pixel is identified as belonging to a marker.
r = 0;
R_threshold_down = image_array(:,:,1) > R_threshold-threshold;
R_threshold_up = image_array(:,:,1) < R_threshold+threshold;
for i=1:size_y
    for j=1:size_x
        if R_threshold_down(i,j) ~= 1 || R_threshold_up(i,j) ~= 1
            image_array(i,j,1) = 0;
        else if error == new_rgb-1 && randi(10,1) == 5
            r = r+1;
            R_value(r) = image_array(i,j,1);
            end
        end
    end
end

g = 0;
G_threshold_down = image_array(:,:,2) > G_threshold-threshold;
G_threshold_up = image_array(:,:,2) < G_threshold+threshold;
for i=1:size_y
    for j=1:size_x
        if G_threshold_down(i,j) ~= 1 || G_threshold_up(i,j) ~= 1
            image_array(i,j,2) = 0;
        else if error == new_rgb-1 && randi(10,1) == 8
            g = g+1;
            G_value(g) = image_array(i,j,2);
            end
```

```
        end
    end
end

b = 0;
B_threshold_down = image_array(:,:,3) > B_threshold-threshold;
B_threshold_up = image_array(:,:,3) < B_threshold+threshold;
for i=1:size_y
    for j=1:size_x
        if B_threshold_down(i,j) ~= 1 || B_threshold_up(i,j) ~= 1
            image_array(i,j,3) = 0;
        else if error == new_rgb-1 && randi(10,1) == 3
            b = b+1;
            B_value(b) = image_array(i,j,3);
            end
        end
    end
end

% The three matrixes of image_array are combined to form one binary matrix.
% A pixel that belongs to a marker is given the value 1, other pixels get
% the value 0.
for i=1:size_y
    for j=1:size_x
        if image_array(i,j,1) == 0 || image_array(i,j,2) == 0 ||
image_array(i,j,3) == 0
            image_array_binary(i,j) = 0;
        else
            image_array_binary(i,j) = 1;
        end
    end
end

% A square area around each marker pixel is scanned for other marker
% pixels. If a group of at least 15 marker pixels are identified for lying
% in the square defined by i_min, i_max, j_min and j_max, all pixels in
% that square are identified as a marker-pixel. This is done to ensure that
% one marker is not identified as multiple markers.
image_binary = zeros(size_x,size_y);
group_image_binary = zeros(size_x,size_y);
group_amount = 0;

for i=1:size_y
    for j=1:size_x
        group_amount = 0;
        image_group = [0 0];
        if image_array_binary(i,j) == 1
            for k = i-15:i+15
                for l = j-15:j+15
                    if k >= 1 && k<= size_y && l >= 1 && l<= size_x
                        if image_array_binary(k,l) == 1
                            group_amount = group_amount +1;
                            image_group(group_amount,:) = [k l];
                        end
                    end
                end
```

```
            end

            i_min(1) = min(image_group(:,1));
            i_max(1) = max(image_group(:,1));
            j_min(1) = min(image_group(:,2));
            j_max(1) = max(image_group(:,2));

            if group_amount > 10
                for m = i_min:i_max
                    for n = j_min:j_max
                        group_image_binary(m,n) = 1;
                    end
                end
            else
                group_image_binary(i,j) = 0;
            end
        end
    end
end

% The marker pixels are now clustered and the centerpoint of a cluster is
% calculated and will be used as a marker.
L=bwlabel(group_image_binary);
if p == 2
    markers_right = regionprops(L,'Centroid');
    num_markers = numel(markers_right);
end

end
end

% The markers are sorted on their height.
for k = 1:numel(markers_right)
    markers_unsorted(k,:,2) = markers_right(k).Centroid;
end

% The marker are fliped upside down.
markers(:,:,2) = sortrows(markers_unsorted(:,:,2),2);
markers(:,:,2) = flipud(markers(:,:,2));


% Now the algorithm will search for the red markers.
for p = 1
    error = 0;

    num_markers = 0;
    r = 0;
    R_value = 0;
    g = 0;
    G_value = 0;
    b = 0;
    B_value = 0;

    if p == 1
        % RGB values: Left - Red
```

```
        threshold = 25;
        threshold_red = threshold;
        R_threshold = R_red;
        G_threshold = G_red;
        B_threshold = B_red;
    end

    % The known positions of the green markers are used to color in the
    % area between the green and red marker. This eliminates the
    % possibility of a rib, knut or the flexible axis beining identified as
    % a marker.
    image_array_blacked = image_array_original;
     for n = 1:11
        for i = 1:290
            for j=1:290
                if sqrt(i^2 + j^2) <= 290
                    if  (round(markers(n,2,2))+i) < size_y &&
(round(markers(n,1,2))+j) < size_x

image_array_blacked(round(markers(n,2,2))+i,round(markers(n,1,2))+j,:) = 0;
                    end

                    if  (round(markers(n,2,2))+i) < size_y &&
(round(markers(n,1,2))-j) > 0

image_array_blacked(round(markers(n,2,2))+i,round(markers(n,1,2))-j,:) = 0;
                    end

                    if  (round(markers(n,2,2))-i) > 0 &&
(round(markers(n,1,2))+j) < size_x
                        image_array_blacked(round(markers(n,2,2))-
i,round(markers(n,1,2))+j,:) = 0;
                    end

                    if  (round(markers(n,2,2))-i) > 0 &&
(round(markers(n,1,2))-j) > 0
                        image_array_blacked(round(markers(n,2,2))-
i,round(markers(n,1,2))-j,:) = 0;
                    end
                end
            end
        end
     end

    image_aangepast = dip_image(image_array_blacked)
    image_aangepast


% If the number of markers is not equal to 11, the threshold in adjusted
while num_markers ~= 11
    image_array = image_array_blacked;
    num_markers
    p;
if num_markers < 11
    threshold = threshold+1;
    error = error+1;
```

```
else if num_markers > 11
    error = error+1;
    threshold = threshold-1;
    end
end
if error == new_rgb
    error = 0;
    threshold = 15;
    R_threshold = ceil(mean(R_value))
    G_threshold = ceil(mean(G_value))
    B_threshold = ceil(mean(B_value))
end


% Filtering the image
r = 0;
R_threshold_down = image_array(:,:,1) > R_threshold-threshold;
R_threshold_up = image_array(:,:,1) < R_threshold+threshold;
for i=1:size_y
    for j=1:size_x
        if R_threshold_down(i,j) ~= 1 || R_threshold_up(i,j) ~= 1
            image_array(i,j,1) = 0;
        else if error == new_rgb-1 && randi(10,1) == 5
            r = r+1;
            R_value(r) = image_array(i,j,1);
            end
        end
    end
end

g = 0;
G_threshold_down = image_array(:,:,2) > G_threshold-threshold;
G_threshold_up = image_array(:,:,2) < G_threshold+threshold;
for i=1:size_y
    for j=1:size_x
        if G_threshold_down(i,j) ~= 1 || G_threshold_up(i,j) ~= 1
            image_array(i,j,2) = 0;
        else if error == new_rgb-1 && randi(10,1) == 8
            g = g+1;
            G_value(g) = image_array(i,j,2);
            end
        end
    end
end

b = 0;
B_threshold_down = image_array(:,:,3) > B_threshold-threshold;
B_threshold_up = image_array(:,:,3) < B_threshold+threshold;
for i=1:size_y
    for j=1:size_x
        if B_threshold_down(i,j) ~= 1 || B_threshold_up(i,j) ~= 1
            image_array(i,j,3) = 0;
        else if error == new_rgb-1 && randi(10,1) == 3
            b = b+1;
            B_value(b) = image_array(i,j,3);
            end
```

```
        end
    end
end

for i=1:size_y
    for j=1:size_x
        if image_array(i,j,1) == 0 || image_array(i,j,2) == 0 ||
image_array(i,j,3) == 0
            image_array_binary(i,j) = 0;
        else
            image_array_binary(i,j) = 1;
        end
    end
end

image_binary = zeros(size_x,size_y);
group_image_binary = zeros(size_x,size_y);
group_amount = 0;

for i=1:size_y
    for j=1:size_x
        group_amount = 0;
        image_group = [0 0];
        if image_array_binary(i,j) == 1
            for k = i-15:i+15
                for l = j-15:j+15
                    if k >= 1 && k<= size_y && l >= 1 && l<= size_x
                        if image_array_binary(k,l) == 1
                            group_amount = group_amount +1;
                            image_group(group_amount,:) = [k l];
                        end
                    end
                end
            end

            i_min(1) = min(image_group(:,1));
            i_max(1) = max(image_group(:,1));
            j_min(1) = min(image_group(:,2));
            j_max(1) = max(image_group(:,2));

            if group_amount > 30 && (i_max - i_min) < 25  && (j_max - j_min) <
25
                for m = i_min:i_max
                    for n = j_min:j_max
                        group_image_binary(m,n) = 1;
                    end
                end
            else
                group_image_binary(i,j) = 0;
            end
        end
    end
end


L=bwlabel(group_image_binary);
```

```
if p == 1
    markers_left = regionprops(L,'Centroid');
    num_markers = numel(markers_left);
end
if p == 2
    markers_right = regionprops(L,'Centroid');
    num_markers = numel(markers_right);
end

end
end

% The markers are sorted based on their height and fliped upside down.
for k = 1:numel(markers_left)
    markers_unsorted(k,:,1) = markers_left(k).Centroid;
    markers_unsorted(k,:,2) = markers_right(k).Centroid;
end

markers(:,:,1) = sortrows(markers_unsorted(:,:,1),2);
markers(:,:,1) = flipud(markers(:,:,1));

% The angles of the ribs and the angle between two ribs are calculated.
% The angle of the bottom rib is used as the horizontal refference line.
marker_angles(1)= atan((markers(1,2,2)-markers(1,2,1))/abs(markers(1,1,2)-
markers(1,1,1)));

for i = 2:numel(markers_left)
    marker_angles(i) = atan((markers(i,2,2)-
markers(i,2,1))/abs(markers(i,1,2)-markers(i,1,1)));
    segment_angles(i-1) = marker_angles(i)-marker_angles(i-1);
end

% The angles are rewritten from rad to degrees.
marker_angles_degrees = marker_angles*360/(2*pi)
segment_angles_degrees = segment_angles*360/(2*pi)

marker_center(1,1) = markers(1,1,1) + round((markers(1,1,2) -
markers(1,1,1))/2);
marker_center(1,2) = markers(1,2,1) - round((markers(1,2,1) -
markers(1,2,2))/2);

% The markers are rotated based on the angle of the bottom rib.
for i = 1:numel(markers_left)
    markers_rotated(i,1,1) = ((markers(i,1,1)-
    marker_center(1,1))*cos(marker_angles(1)) + (marker_center(1,2)-
    markers(i,2,1))*sin(marker_angles(1)));
    markers_rotated(i,2,1) = ((marker_center(1,2)-
    markers(i,2,1))*cos(marker_angles(1)) + (markers(i,1,1)-
    marker_center(1,1))*sin(marker_angles(1)));
    markers_rotated(i,1,2) = ((markers(i,1,2)-
    marker_center(1,1))*cos(marker_angles(1)) + (marker_center(1,2)-
    markers(i,2,2))*sin(marker_angles(1)));
    markers_rotated(i,2,2) = ((marker_center(1,2)-
    markers(i,2,2))*cos(marker_angles(1)) + (markers(i,1,2)-
    marker_center(1,1))*sin(marker_angles(1)));
```

```
end
savefile = [save_name '.mat'];
save(savefile, 'segment_angles','markers', 'marker_center', 'markers_rotated',
'marker_angles');

% the image is plotted with the markers.
image_out
hold all
for k = 1:numel(markers_left)
    plot(markers(k,1,1), markers(k,2,1), 'g.');
    text(markers(k,1,1), markers(k,2,1), num2str(k),'FontSize', 15,
'VerticalAlignment','bottom', ...
                             'HorizontalAlignment','right')
end
hold all
for k = 1:numel(markers_right)
    plot(markers(k,1,2), markers(k,2,2), 'r.');
    text(markers(k,1,2), markers(k,2,2), num2str(k),'FontSize', 15,
'VerticalAlignment','bottom', ...
                             'HorizontalAlignment','right')
end
hold all
plot(marker_center(1,1),marker_center(1,2),'b+')
hold all

savefigure = [save_name '- marked'];
saveas(gcf,savefigure,'jpg')
```

Initial_Angles_Calculation.m

Used to calculate the initial position of the flexible axis out of the multiple photos.

```
% initial angles calculation
clc, clear all

for p = 1:23
    path =
'C:\Users\T\Dropbox\Afstuderen\Afstuderen\Verslag\Foto\Photoshop\Initial
Position\';
    filename = [path 'IP (' num2str(p) ').mat'];
    load(filename);
    segment_angles(1,:) = fliplr(segment_angles(1,:));
    angles_matrix(p,:) = segment_angles(1,:);
    angles_degrees(p,:) = (segment_angles(1,:)*360)/(2*pi);
end

for q = 1:10
    initial_angles(q) = mean(angles_matrix(:,q));
    u(q) = mean((angles_matrix(:,q)*360)/(2*pi));
    plot_zero(q) = 0;
end

for w = 1:14
    difference(w,:) = u - angles_degrees(w,:);
    MD_per_image(w) = mean(difference(w,:));
    MAD_per_image(w) = mean(abs(difference(w,:)));
    MD_d_MAD_per_image(w) = MD_per_image(w)/MAD_per_image(w);

    std_per_image(w) = std(difference(w,:),1);
end

for n = 1:10
    variance(n) = var(difference(:,n));
end



figure(1)
plot(u(1,:),'r','linewidth', 3)
hold all
for p = 1:23

plot(angles_degrees(p,:),'b','linewidth', 0.1)
hold all

end
plot(plot_zero,'k--')
title ('Average Initial Angles', 'Fontsize', 18)
xlabel ('Segment (n)', 'Fontsize', 15)
ylabel ('Angle (degrees)', 'Fontsize', 15)
```

Combine_Angles

Combines the angles found for the underloading and overloading procedures.

```
clc, clear all

% Load the initial position
load ('Initial_Angles.mat')

excel_file_name = 'Combined_Angles.xls'

% Delete existing excel file
if exist(excel_file_name, 'file') == 2
    delete(excel_file_name)
end


% The algorithm defines the directory in where the photos of the validation
% model are placed. Then the algoritm Read_Images is run which identifies
% the red and green markers.
for i = 2:17

if i == 1
directory = 'Initial Position';
else if i == 2
directory = 'L';
cable_name = 'L';
else if i == 3
directory = 'L+r';
cable_name = 'L+r';
else if i == 4
directory = 'L+2r\Load 1';
cable_name = 'L+2r - Load 1';
else if i == 5
directory = 'L+2r\Load 2';
cable_name ='L+2r - Load 2';
else if i == 6
directory = 'L+2r\Load 3';
cable_name = 'L+2r - Load 3';
else if i == 7
directory = 'L+2r\Load 4';
cable_name = 'L+2r - Load 4';
else if i == 8
directory = 'L+2r\Load 5';
cable_name = 'L+2r - Load 5';
else if i == 9
directory = 'L+4r\Load 1';
cable_name = 'L+4r - Load 1';
else if i == 10
directory = 'L+4r\Load 2';
cable_name = 'L+4r - Load 2';
else if i == 11
directory = 'L+4r\Load 3';
cable_name = 'L+4r - Load 3';
else if i == 12
directory = 'L+4r\Load 4';
```

```
cable_name = 'L+4r - Load 4';
else if i == 13
directory = 'L+4r\Load 5';
cable_name = 'L+4r - Load 5';
else if i == 14
directory = 'R';
cable_name = 'R';
else if i == 15
directory = 'R-2r';
cable_name = 'R-2r';
else if i == 16
directory = 'R & R-2r';
cable_name =  'R & R-2r';
else if i == 17
directory = 'R & L+4r & R-2r';
cable_name = 'R & L+4r & R-2r';
    end
    end
    end
    end
    end
    end
    end
    end
    end
    end
    end
    end
    end
    end
    end
end

    for j = 1:2
        for p = 1:10
            close all
            if j == 1
                loading = 'a';
            else if j == 2
                    loading = 'b';
                end
            end


    path_basis =
'C:\Users\T\Dropbox\Afstuderen\Afstuderen\Verslag\Foto\Photoshop\';
    path_extra = [directory '\'];

    file_name = [loading ' (' num2str(p) ')'];
    load_name = [path_basis path_extra file_name '.mat'];
    save_name = [path_basis path_extra cable_name];

    if exist(load_name, 'file') == 2
        load (load_name)
        segment_angles_degrees = fliplr(segment_angles)*360/(2*pi);
```

```
        if j == 1
            underloaded_angles(p,:) = segment_angles_degrees -
initial_angles_degrees;
        else if j == 2
            overloaded_angles(p,:) = segment_angles_degrees -
initial_angles_degrees;
            end
        end
        clearvars segment_angles
    end
    end
    end

    angles_combined = [underloaded_angles; overloaded_angles];

    for w = 1:10
        combined_angles(1,w) = mean(angles_combined(:,w));
        underloaded_mean(1,w) = mean(underloaded_angles(:,w));
        overloaded_mean(1,w) = mean(overloaded_angles(:,w));
        underloaded_deviation(:,w) =  combined_angles(1,w) -
underloaded_angles(:,w);
        overloaded_deviation(:,w) =  combined_angles(1,w) -
overloaded_angles(:,w);
        difference(1,w) = overloaded_mean(1,w) - underloaded_mean(1,w)
        plot_zero(w) = 0;
    end
% underloaded_deviation
% overloaded_deviation
    MD = mean(difference)
    MAD = mean(abs(difference))
    std_dif = std(difference,1)
    deviation(:,:) = [underloaded_deviation; overloaded_deviation];

    mean_deviation_ps = mean(deviation)
    mean_deviation = mean(mean_deviation_ps)
    mean_underloaded_deviation_ps = mean(underloaded_deviation)
    mean_underloaded_deviation = mean(mean_underloaded_deviation_ps)
    mean_overloaded_deviation_ps = mean(overloaded_deviation)
    mean_overloaded_deviation = mean(mean_overloaded_deviation_ps)


    std_ps = std(deviation,1)
    std = mean(std_ps)

    screen_size = get(0, 'ScreenSize');
    f1 = figure(1);
    set(f1, 'Position', [0 0 screen_size(3)/2 screen_size(4)/2 ] );
    for q = 1:size(underloaded_angles(:,1),1)
%     for q = 4
        h(1) = plot(1:10,underloaded_angles(q,:),'g');
        hold all
        g(1) = plot(1:10,overloaded_angles(q,:),'b');
        hold all
    end
%     h(1) = plot(1:10,underloaded_mean(1,:),'g--','linewidth', 1);
%     hold all
```

```
%     g(1) = plot(1:10,overloaded_mean(1,:),'b--','linewidth', 1);
%     hold all
    v(1) = plot(1:10,combined_angles(1,:),'r','linewidth', 1.5);
    hold all
    plot(1:10,plot_zero(:),'k-.')
    hold all
    title (cable_name, 'Fontsize', 18)
    xlabel ('Segment (n)', 'Fontsize', 15)
    ylabel ('Angle (degrees)', 'Fontsize', 15)
    Leg1 = legend([h(1), g(1), v(1)],'Underloaded','Overloaded','Average',
'Location', 'Best');
%     Leg1 = legend([h(1), g(1)],'Underloaded','Overloaded', 'Location',
'SouthEast');
    set(Leg1, 'Fontsize',14)

    save_figure =
['C:\Users\T\Dropbox\Afstuderen\Afstuderen\Verslag\Foto\Photoshop\Combined
Angles\' cable_name]
    saveas(gcf,save_figure,'bmp')

    save_file =
['C:\Users\T\Dropbox\Afstuderen\Afstuderen\Verslag\Foto\Photoshop\Combined
Angles\' cable_name ' - Combined_Angles']
    save(save_file,'combined_angles', 'underloaded_mean', 'overloaded_mean')

    name_cable = {cable_name};

    xlswrite(excel_file_name,[name_cable],'Combined Angles',['A'
num2str(i+1)])
    xlswrite(excel_file_name,[std],'Combined Angles',['B' num2str(i+1)])
    xlswrite(excel_file_name,[{'Std'}],'Combined Angles',['B' num2str(2)])
    xlswrite(excel_file_name,[std_ps],'Combined Angles',['D' num2str(i+1)])
    xlswrite(excel_file_name,[{'per
seg:'},{'S1'},{'S2'},{'S3'},{'S4'},{'S5'},{'S6'},{'S7'},{'S8'},{'S9'},{'S10'}]
,'Combined Angles',['C' num2str(2)])
%

    clearvars std_ps std mean_variance variance mean_overloaded_deviation
mean_underloaded_deviation underloaded_angles overloaded_angles
combined_angles segment_angles deviation underloaded_deviation
overloaded_deviation
%     close all
End
```

Validation_model_vs_Simualtion_model.m

Compares the outputs of the simulation model to those of the validation model.

```
clc, clear all, close all

excel_file_name = 'Model_vs_Validaton.xls'

% Delete existing excel file
if exist(excel_file_name, 'file') == 2
    delete(excel_file_name)
end

for as = 1:2
    if as == 1
    amount_of_segments = 10;
    else if as == 2
         amount_of_segments = 1000;
    else if as == 3
         amount_of_segments = 50;
    else if as == 4
         amount_of_segments = 100;
    else if as == 5
         amount_of_segments = 1000;
    else if as == 6
         amount_of_segments = 3000;
        end
        end
        end
        end
        end
    end


%     close all
for i = 2:17
close all
run Parameters

if i == 2
    directory = 'L';
    cable_name = 'L';
    amount_of_cables = 1;
    Force_cables    = load_2;
    r_cable         = -16.5;
    direction       = 1;
    beta            = r0;
else if i == 3
    directory = 'L+r';
    cable_name = 'L+r';
    amount_of_cables = 1;
    Force_cables    = load_4;
    r_cable         = -15;
    direction       = 1;
    beta            = r1;
else if i == 4
```

```
    directory = 'L+2r\Load 1';
    cable_name = 'L+2r - Load 1';
    amount_of_cables = 1;
    Force_cables    = load_1;
    r_cable         = -15;
    direction       = 1;
    beta            = r2;
else if i == 5
    directory = 'L+2r\Load 2';
    cable_name ='L+2r - Load 2';
    amount_of_cables = 1;
    Force_cables    = load_2;
    r_cable         = -15;
    direction       = 1;
    beta            = r2;
else if i == 6
    directory = 'L+2r\Load 3';
    cable_name = 'L+2r - Load 3';
    amount_of_cables = 1;
    Force_cables    = load_3;
    r_cable         = -15;
    direction       = 1;
    beta            = r2;
else if i == 7
    directory = 'L+2r\Load 4';
    cable_name = 'L+2r - Load 4';
    amount_of_cables = 1;
    Force_cables    = load_4;
    r_cable         = -15;
    direction       = 1;
    beta            = r2;
else if i == 8
    directory = 'L+2r\Load 5';
    cable_name = 'L+2r - Load 5';
    amount_of_cables = 1;
    Force_cables    = load_5;
    r_cable         = -15;
    direction       = 1;
    beta            = r2;
else if i == 9
    directory = 'L+4r\Load 1';
    cable_name = 'L+4r - Load 1';
    amount_of_cables = 1;
    Force_cables    = load_1;
    r_cable         = -15;
    direction       = 1;
    beta            = r4;
else if i == 10
    directory = 'L+4r\Load 2';
    cable_name = 'L+4r - Load 2';
    amount_of_cables = 1;
    Force_cables    = load_2;
    r_cable         = -15;
    direction       = 1;
    beta            = r4;
else if i == 11
    directory = 'L+4r\Load 3';
```

```
    cable_name = 'L+4r - Load 3';
    amount_of_cables = 1;
    Force_cables    = load_3;
    r_cable         = -15;
    direction       = 1;
    beta            = r4;
else if i == 12
    directory = 'L+4r\Load 4';
    cable_name = 'L+4r - Load 4';
    amount_of_cables = 1;
    Force_cables    = load_4;
    r_cable         = -15;
    direction       = 1;
    beta            = r4;
else if i == 13
    directory = 'L+4r\Load 5';
    cable_name = 'L+4r - Load 5';
    amount_of_cables = 1;
    Force_cables    = load_5;
    r_cable         = -15;
    direction       = 1;
    beta            = r4;
else if i == 14
    directory = 'R';
    cable_name = 'R';
    amount_of_cables = 1;
    Force_cables    = load_2;
    r_cable         = 16.5;
    direction       = 1;
    beta            = r0;
else if i == 15
    directory = 'R-2r';
    cable_name = 'R-2r';
    amount_of_cables = 1;
    Force_cables    = load_4;
    r_cable         = 15;
    direction       = -1;
    beta            = r2;
else if i == 16
    directory = 'R & R-2r';
    cable_name =  'R & R-2r';
    amount_of_cables = 2;
    Force_cables    = [load_3 load_5];
    r_cable         = [16.5 15];
    direction       = [-1 -1];
    beta            = [r0 r2];
else if i == 17
    directory = 'R & L+4r & R-2r';
    cable_name = 'R & L+4r & R-2r';
    amount_of_cables = 3;
    Force_cables    = [load_3 load_2 load_3];
    r_cable         = [16.5 -15 15];
    direction       = [-1 1 -1];
    beta            = [r0 r4 r2];
    end
    end
    end
```

```
    end
    end
    end
    end
    end
    end
    end
    end
    end
    end
    end
    end
end

% Run Model
run Model_line_search

% If the amount of segment is higher then 10, summarize alpha on intervals
if amount_of_segments ~= 10

    interval = amount_of_segments/10;
    alpha_summed(1,1) = sum(alpha(1:interval));
    for d = 2:10
        j = (d-1)*interval + 1;
        alpha_summed(1,d) = sum(alpha(j:d*interval));
    end
    alpha = alpha_summed'
end

alpha_model = (flipud(alpha')*360)/(2*pi);

% Load validation data
    path_basis =
'C:\Users\T\Dropbox\Afstuderen\Afstuderen\Verslag\Foto\Photoshop\Combined
Angles\';

    load_name = [path_basis cable_name ' - Combined_Angles.mat'];
    load(load_name);
    alpha_validation = combined_angles;

% Create zero line
    zero_line(1:10) = 0;

    abs_max_model = max(abs(alpha_model));
    screen_size = get(0, 'ScreenSize');

% Plot Model against Validation data
    f1 = figure(1);
    set(f1, 'Position', [0 0 screen_size(3) screen_size(4)] );
    H = plot(alpha_model,'b', 'Linewidth', 2);
    hold all
    G(1) = plot(alpha_validation, 'r', 'Linewidth', 2);
    hold all
    plot(zero_line,'k--')
```

```
    % text(l_place ,alpha_model(l_place), ['L' weight],'FontSize', 14,
'VerticalAlignment','top', ...
    %                           'HorizontalAlignment','right')

%     title([cable_name ' - Model vs Validation - '
num2str(amount_of_segments) ' Segments'], 'FontSize', 50)
    title([cable_name], 'FontSize', 70)
%     title('L+4r', 'FontSize', 70)
%     title('L+2r', 'FontSize', 70)
    xlabel('Segment [n]', 'FontSize', 60)
    ylabel('\alpha [deg]', 'FontSize', 60)
    axis([1 10 -1.5*abs_max_model 1.5*abs_max_model])
%     Leg1 = legend([H,G],'Model','Validation','Location',
'Northeastoutside');
%     set(Leg1, 'Fontsize',45)
    set(gca,'fontsize',45)
    hold all

    save_figure =
['C:\Users\T\Dropbox\Afstuderen\Afstuderen\Verslag\Figuren\Validation\Results\
' num2str(amount_of_segments) ' Segments\' cable_name]
    saveas(gcf,save_figure,'bmp')

    clearvars r_cable

% Determine mean deviation and variance
    abs_max_model = max(abs(alpha_model));
    error_ps = alpha_model - alpha_validation;
    ME = mean(error_ps);
    MAE = mean(abs(error_ps));
    ME_perc = (ME/abs_max_model)*100;
    MAE_perc = (MAE/abs_max_model)*100;
    Std = std(error_ps,1);
    Std_perc = (Std/abs_max_model)*100;

    name_cable = {cable_name};
%
    xlswrite(excel_file_name,[name_cable],['Segments '
num2str(amount_of_segments)],['A' num2str(i+1)])
    xlswrite(excel_file_name,[ME, ME_perc, MAE, MAE_perc, Std,
Std_perc],['Segments ' num2str(amount_of_segments)],['B' num2str(i+1)])
    xlswrite(excel_file_name,[{'ME'},{'% ME'},{'MAE'},{'% MAE'},{'Std'},{'%
Std'}],['Segments ' num2str(amount_of_segments)],['B' num2str(2)])
    xlswrite(excel_file_name,[error_ps],['Segments '
num2str(amount_of_segments)],['I' num2str(i+1)])
    xlswrite(excel_file_name,[{'ME per
seg:'},{'S1'},{'S2'},{'S3'},{'S4'},{'S5'},{'S6'},{'S7'},{'S8'},{'S9'},{'S10'}]
,['Segments ' num2str(amount_of_segments)],['G' num2str(2)])
end
end
```

Appendix C. Validation pilot study

The data from the validation model is retrieved by taken a photo, as illustrated by the figure below. These photos were then scanned by the imaging process as described in Appendix B.2.

Initial position

In unloaded position the validation model will ideally be in a straight position and the data collected from the validation model would reveal all segments angles to be zero. however, the validation model might not be completely straight, the markers on the ribs might not be completely centered or/and the imaging process might not be completely free of error. These reasons can result in a deviation from the ideal all zero segment angles position. To monitor this deviation, the validation model is captured in unloaded position throughout the validation process.

The mean angle per segment will be used as the reference of the initial position for all measurements. This means that the initial position is subtracted from every measurement.

In order to determine the initial position, a number of measurements of an unloaded validation model are taken between the evaluations of different cable positions. The needed amount of measurements to assure a valid initial position is calculated from the pilot study. 14 Measurements are available from the pilot study, which are shown the figure below. The table shows the mean value and the variance of each segment.

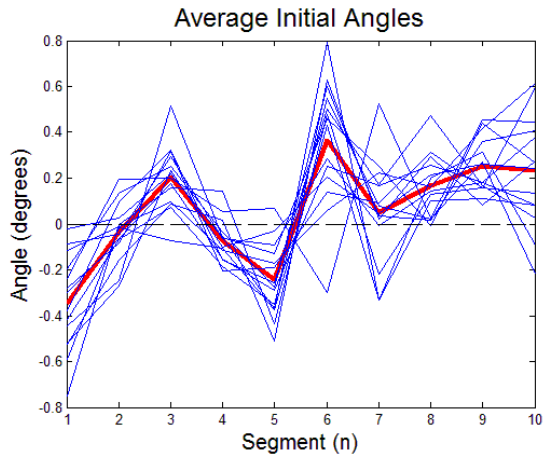

Segments:	1	2	3	4	5	6	7	8	9	10
Mean: μ	-0.34	-0.03	0.20	-0.07	-0.24	0.36	0.05	0.16	0.25	0.23
Var: σ^2	0.04	0.01	0.02	0.009	0.026	0.078	0.053	0.018	0.015	0.060

The sample size of an experiment determines at which confidence level (ε) one can state whether a certain margin of error (w) is reached. The sample size of a standard normal distribution can be calculated by:

$$w \leq 2 \cdot z_{\epsilon/2} \cdot \frac{\sigma}{\sqrt{n}}$$

Where $z_{\epsilon/2}$ stands for the critical value and is determined by ε and the standard normal distribution.

$$P(Z \geq z_{\epsilon/2}) = {}^{\varepsilon}/_{2}$$

The confidence level is set on 0.05, resulting in $z_{\epsilon/2}$ being equal to 1.645. Now this critical value is based on a standard normal distribution. In order to translate the critical value to the normal distribution of the initial values, one has to do the following:

$$x_{\epsilon/2} = \frac{z_{\epsilon/2} - \mu}{\sigma}$$

Where in $x_{\epsilon/2}$ is the critical value belonging to the normal distribution. Now sample size n can be determined by:

$$n \geq \left(\frac{2 \cdot x_{\epsilon/2} \cdot \sigma}{w}\right)^2$$

Based on these values the minimal sample size is 5. This feels quite low and since it is not time consuming, the unloaded position will be evaluate more often.

Underloaded and overloaded

The figure below represents the underloaded and overloaded evaluation of cable L+2r of the pilot study. One can see that the lines are positioned close to one another and even overlap.

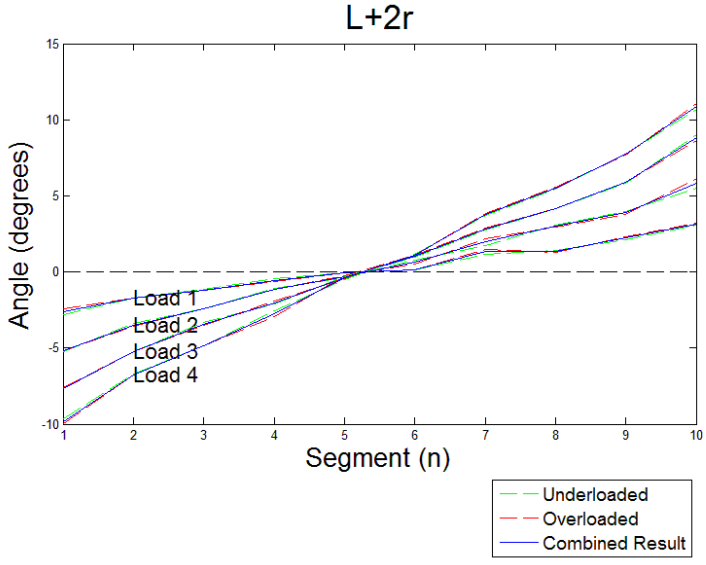

The evaluation of a cable position will be consisting of out of n times an underloaded and an overloaded measurement. The mean of a segment will become the evaluation angle of that segment.

In order to determine the needed sample size n, the underloaded and overloaded values of the pilot study are used. The sample size is calculated for every cable position. This revealed very different values varying from 4 for cable L+r to 15 for cable L+4r. These values are based on only 1 underloaded and 1 overloaded evaluation. The sample size is therefore not actually based on these evaluations. The sample size is therefore set on 10 underloaded and 10 overloaded evaluations. Judging on the results of the pilot study this seems sufficient.

Validated cable positions

There are a couple of features that need to be evaluated, namely the symmetry of the model itself, the behavior of single cables, the behavior of combined cables and the effect of different loads.

Symmetry

L+2r is compared to the results of R-2r for a single load.

Behavior: single cable

This examination includes the following four cables: L, L+r, L+2r and L+4r. These cables will be evaluated in one position, or in other words for one load. Cables L+r, L+2r and L+4r will be loaded with 400 gr and in order to prevent damage due to overloading, cable L will be loaded with 200 gr.

Behavior: combined cables

For the validation of combined cables a single cable combination will be evaluated. That combination will be L & R-2r. This cable combination is chosen because it is used in the demonstration prototype.

Force

To force behavior of the validation model is studied by the examination of the two cable positions L+2r and L+4r. The choice is fallen on these particular positions because it allows the evaluation of the sideway forces that arise by the cable direction change in cable position L+4r.

The following table represents the validated cable positions.

Cable	Load	Underloading	Overloading
Symmetry			
L	2	10	10
Initial position			
R	2	10	10
Initial position			
R-2r	4	10	10
Initial position			
Behavior			
L+r	4	10	10
Initial position			
R & R-2r	3 & 5	10	10
Initial position			
R & L+4r & R-2r	3 & 2 & 3	10	10
Initial position			
Force			
L+2r	1	10	10
L+2r	2	10	10
L+2r	3	10	10
L+2r	4	10	10
L+2r	5	10	10
Initial position			
L+4r	1	10	10
L+4r	2	10	10
L+4r	3	10	10
L+4r	4	10	10
L+4r	5	10	10

Appendix D. Drawings

D.1 Validation model

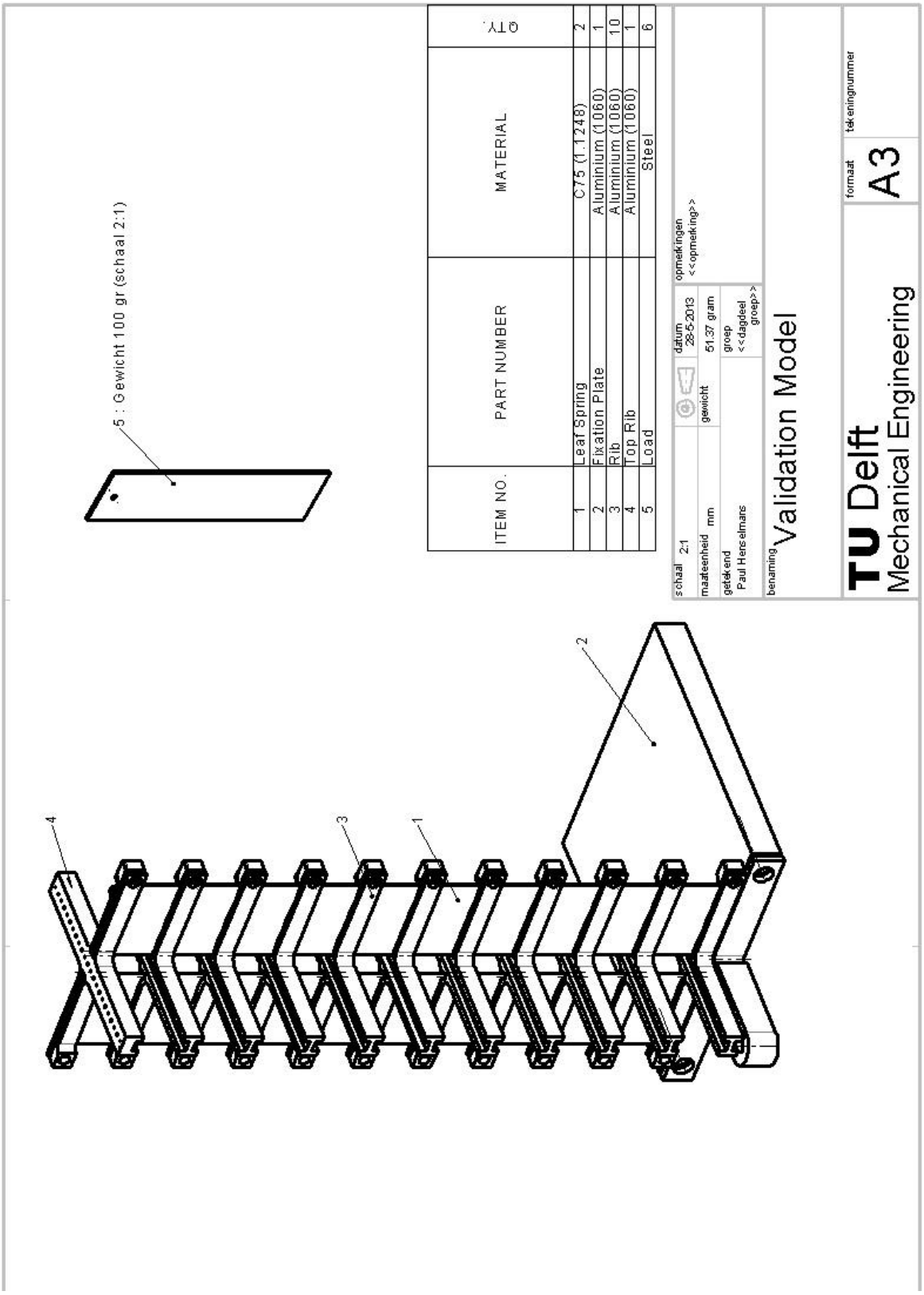

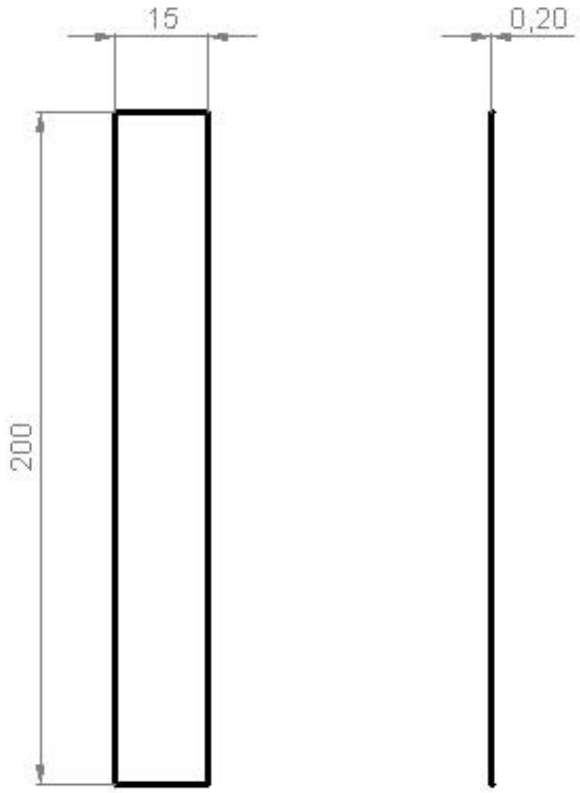

benaming Leaf Spring			maateenheid mm
		formaat A4	tekeningnummer 1
TU Delft Mechanical Engineering	schaal 1:1 / datum 28-5-2013 / gewicht 2.56 gram		
	getekend Paul Henselmans		groep <<dagdeel>>

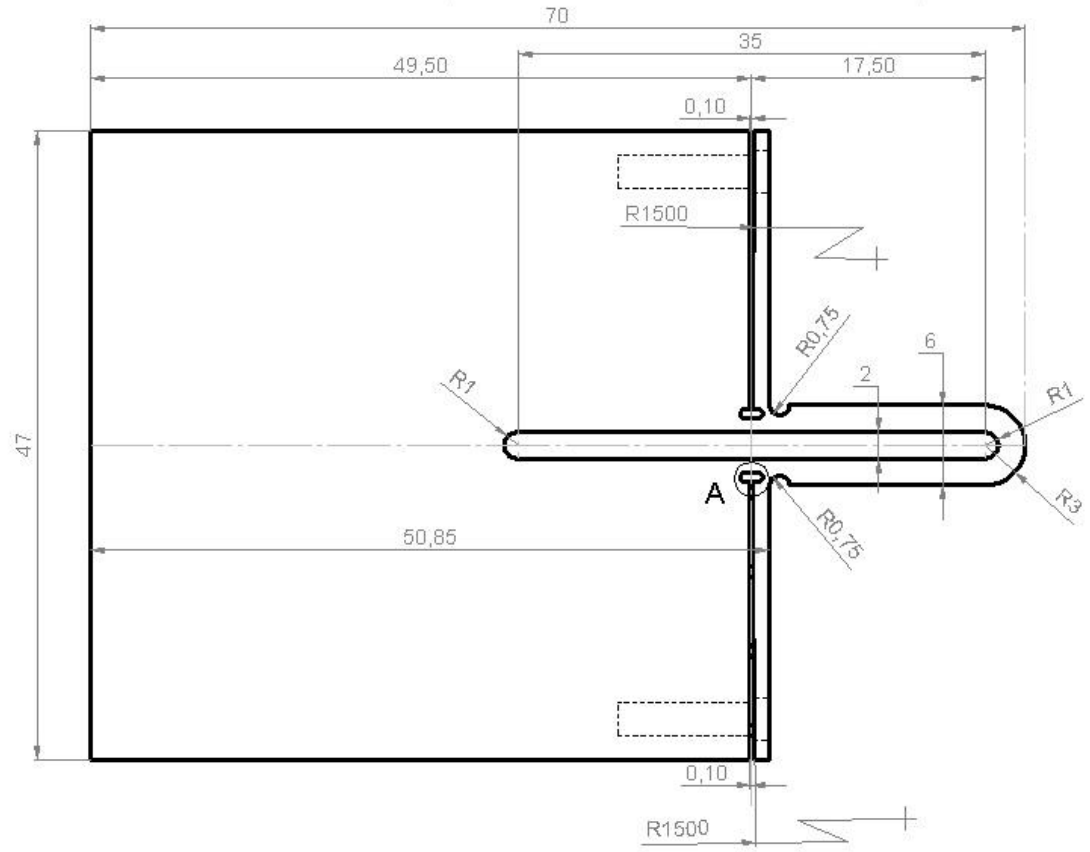

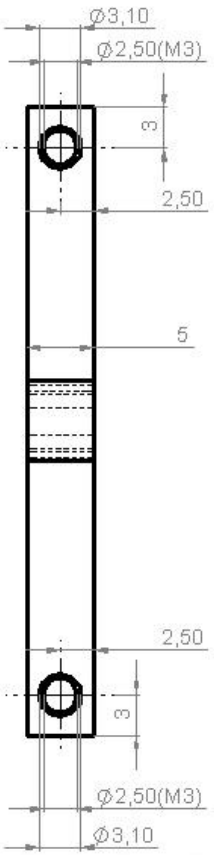

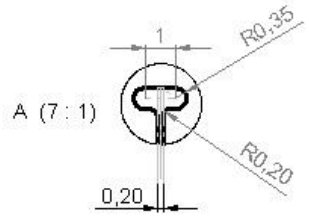

schaal 3:1		datum 28-5-2013	opmerkingen <<opmerking>>
maateenheid mm	gewicht	32.27 gram	
getekend Paul Henselmans		groep <<dagdeel groep>>	

benaming **Fixation Plate**

TU Delft
Mechanical Engineering

formaat	tekeningnummer
A3	2

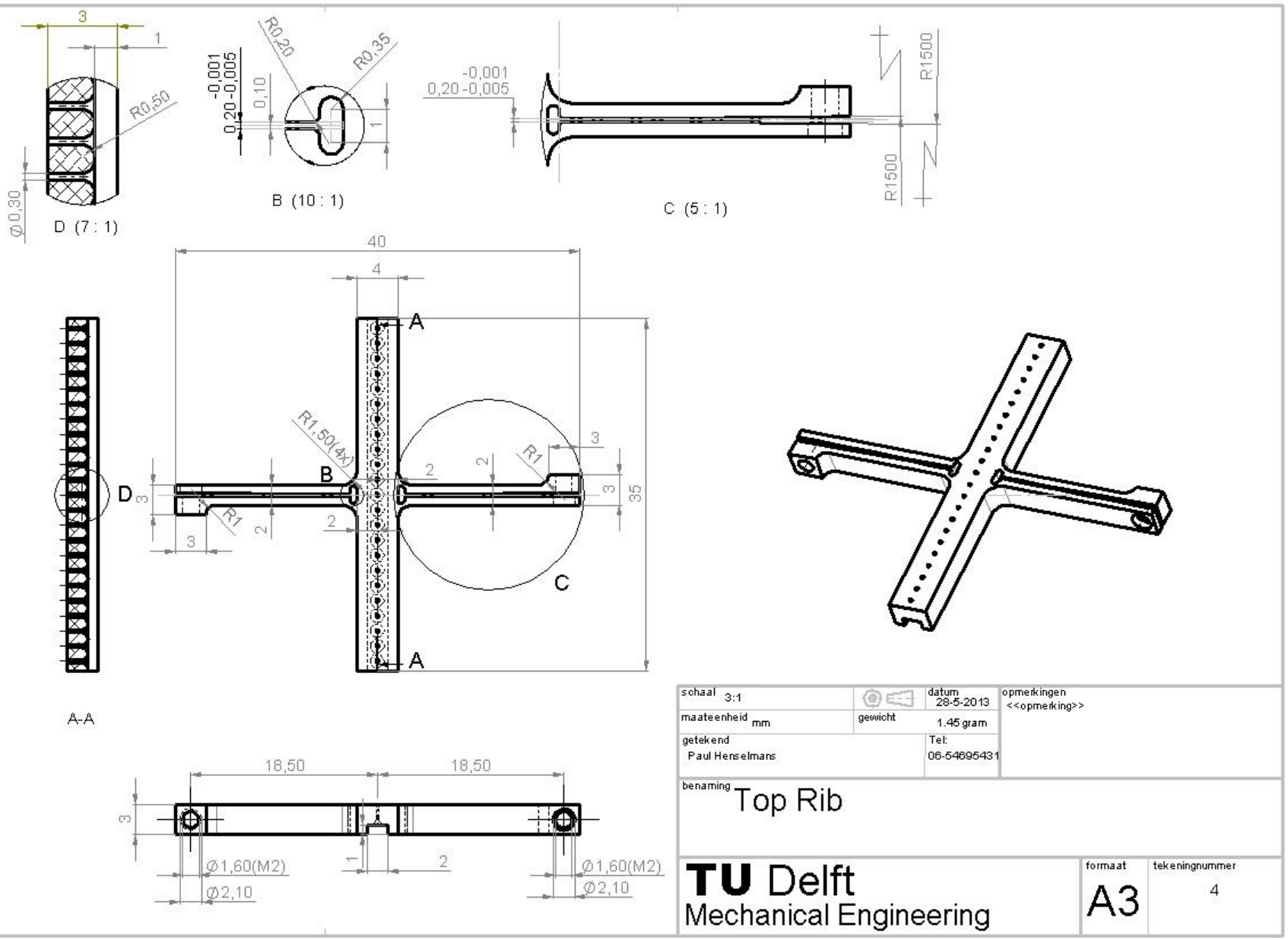
3
1
R0,50
Ø0,30
D (7 : 1)
R0,20
R0,35
-0,001
0,20 -0,005
0,10
1
B (10 : 1)
-0,001
0,20 -0,005
R1500
R1500
C (5 : 1)
40
4
A
R1,50(4x)
B
D
3
R1
2
2
2
2
R1
3
3
35
C
A
A-A
18,50
18,50
3
Ø1,60(M2)
Ø2,10
1
2
Ø1,60(M2)
Ø2,10
schaal 3:1
datum 28-5-2013
opmerkingen
<<opmerking>>
maateenheid mm
gewicht 1.45 gram
getekend
Paul Henselmans
Tel:
06-54695431
benaming
Top Rib
TU Delft
Mechanical Engineering
formaat
A3
tekeningnummer
4

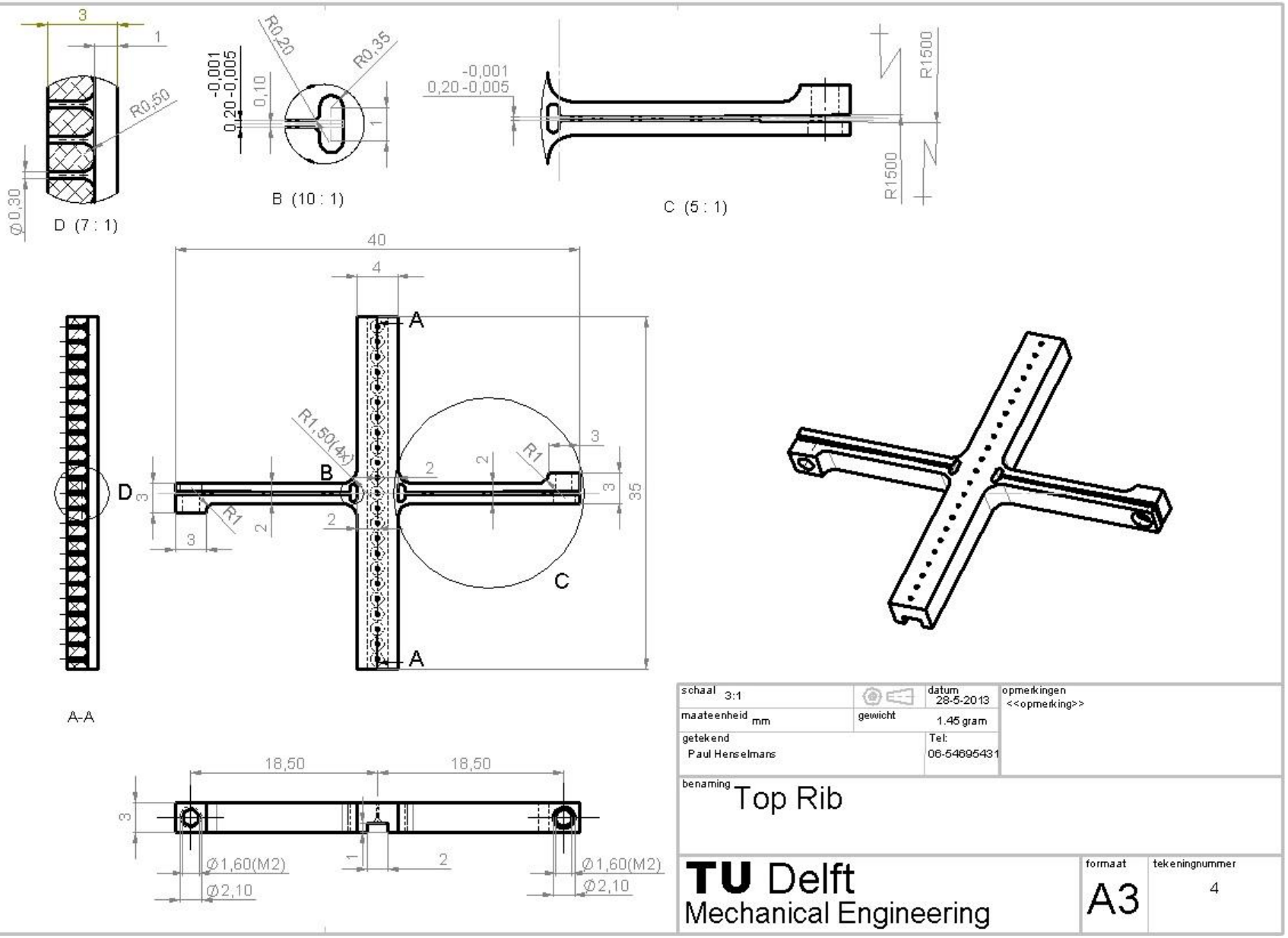
3
1
R0,50
Ø0,30
D (7 : 1)
R0,20
R0,35
-0,001
0,20 -0,005
0,10
1
B (10 : 1)
-0,001
0,20 -0,005
R1500
R1500
C (5 : 1)
40
4
A
R1,50(4x)
B
D
3
R1
2
2
2
2
R1
3
3
35
C
A
A-A
18,50
18,50
3
Ø1,60(M2)
Ø2,10
1
2
Ø1,60(M2)
Ø2,10
schaal 3:1
datum 28-5-2013
opmerkingen
<<opmerking>>
maateenheid mm
gewicht 1.45 gram
getekend
Paul Henselmans
Tel:
06-54695431
benaming
Top Rib
TU Delft
Mechanical Engineering
formaat
A3
tekeningnummer
4

D.2 Demonstration prototype

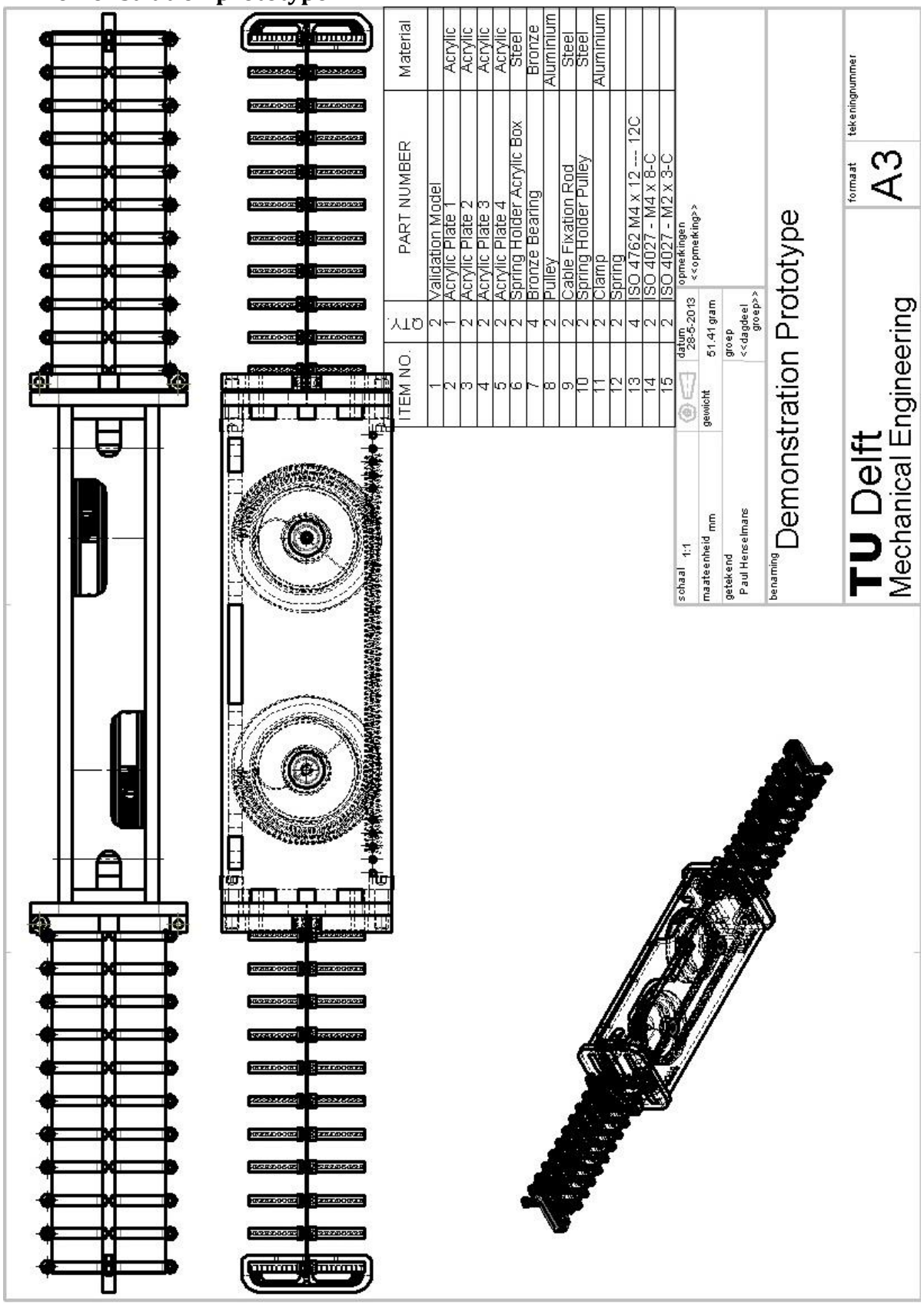

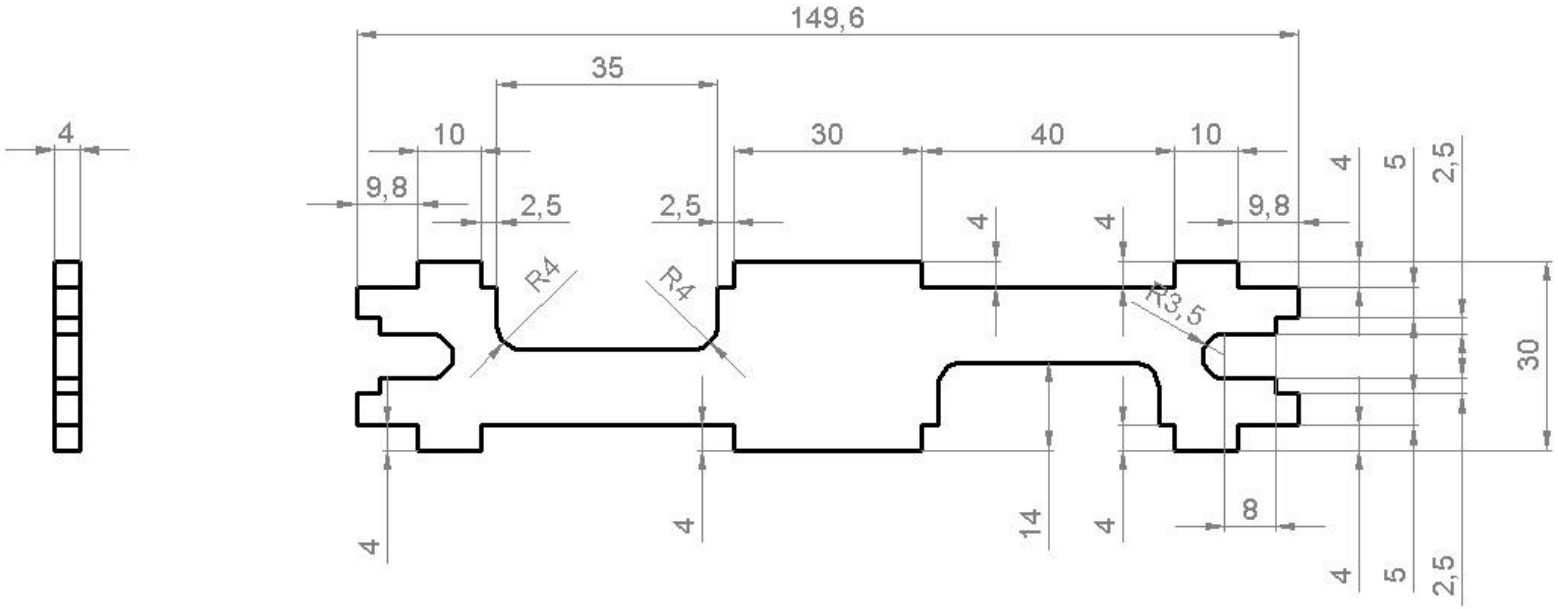

TU Delft Mechanical Engineering	benaming Acrylic Plate 1	datum 28-5-2013		schaal 1:1	maateenheid mm
		getekend Paul Henselmans	groep <<dagdeel>>	formaat A4	gewicht 0.00 gram
					tekening nr. / opmerkingen 2

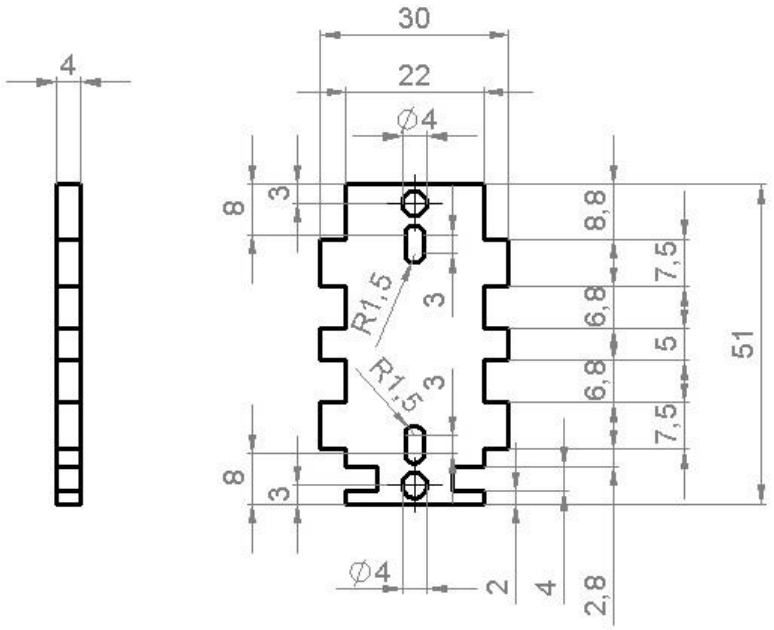

TU Delft Mechanical Engineering	benaming Acrylic Plate 2	datum 28-5-2013		schaal 1:1	maateenheid mm
		getekend Paul Henselmans	groep <<dagdeel>>	formaat A4	gewicht 0.00 gram
					tekening nr. / opmerkingen 3

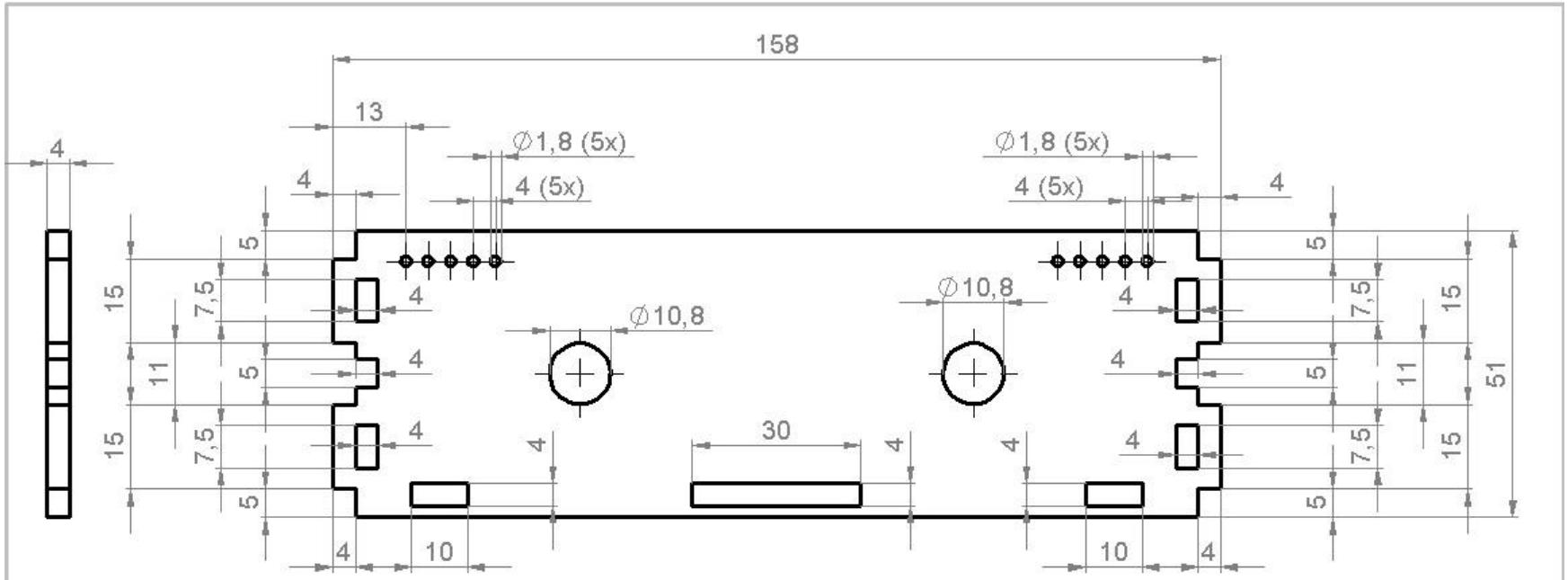

TU Delft Mechancial Engineering	benaming **Acrylic Plate 3**	datum 28-5-2013		schaal 1:1	maateenheid mm
		getekend Paul Henselmans	groep <<dagdeel>>	formaat A4	gewicht 0.00 gram
					tekening nr. / opmerkingen 4

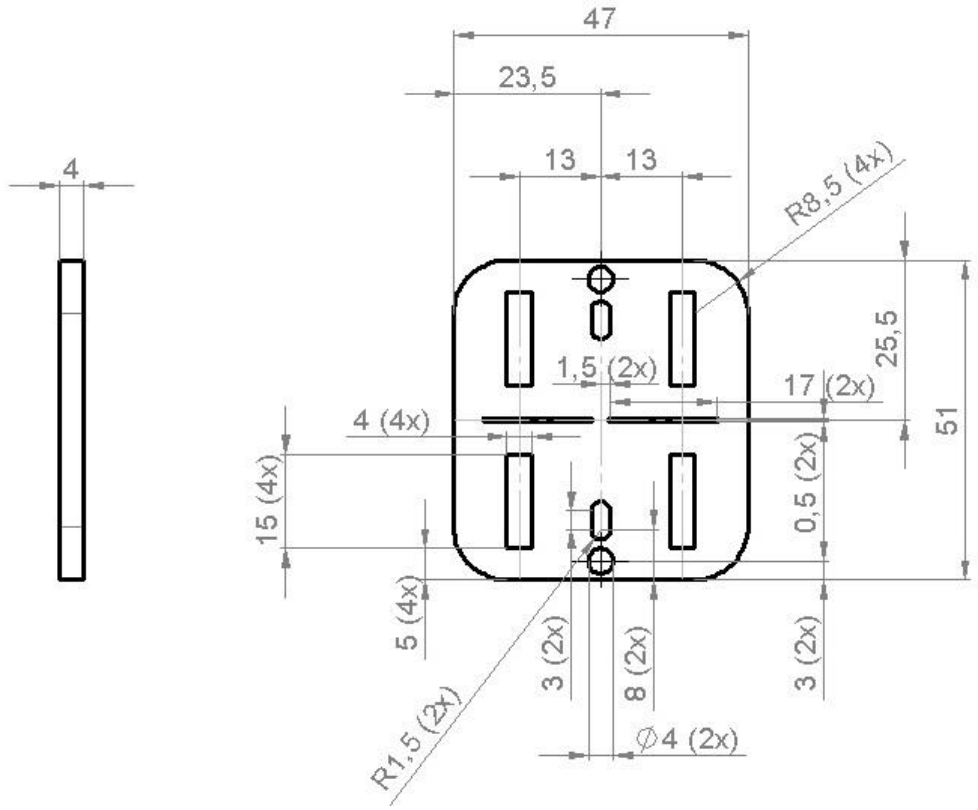

TU Delft Mechanical Engineering	benaming Acrylic Plate 4	datum 28-5-2013		schaal 1:1	maateenheid mm
		getekend Paul Henselmans	groep <<dagdeel>>	formaat A4	gewicht 0.00 gram
					tekening nr. / opmerkingen 5

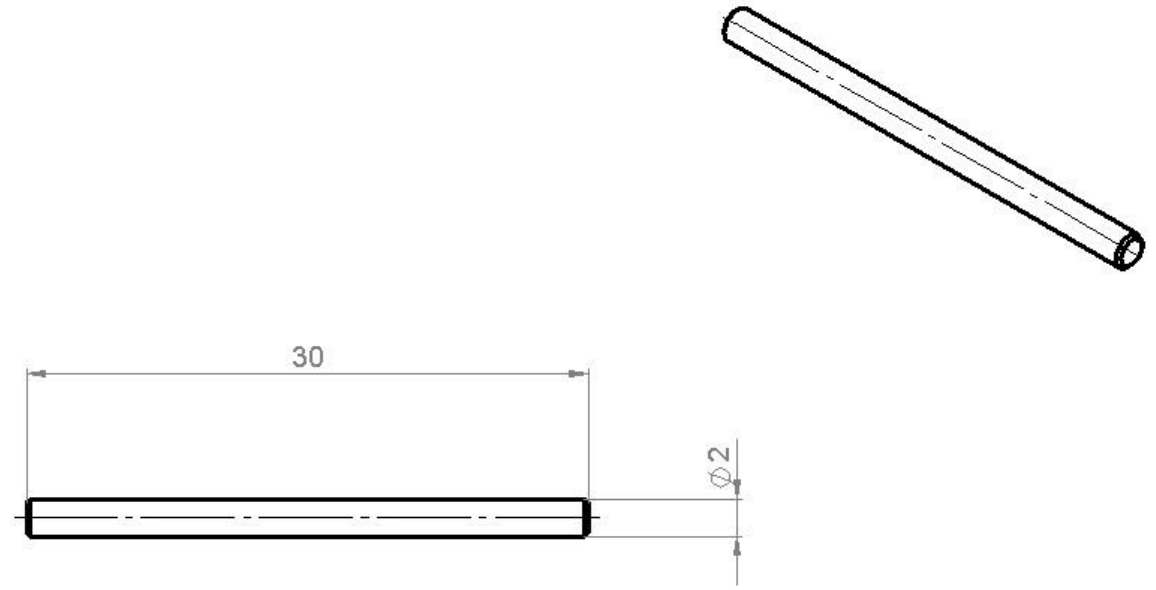

TU Delft Mechanical Engineering	benaming Spring Holder Acrylic Box	datum 28-5-2013		schaal 3:1	maateenheid mm
		getekend Paul Henselmans	groep <<dagdeel>>	formaat A4	gewicht 0.00 gram
					tekening nr. / opmerkingen 6

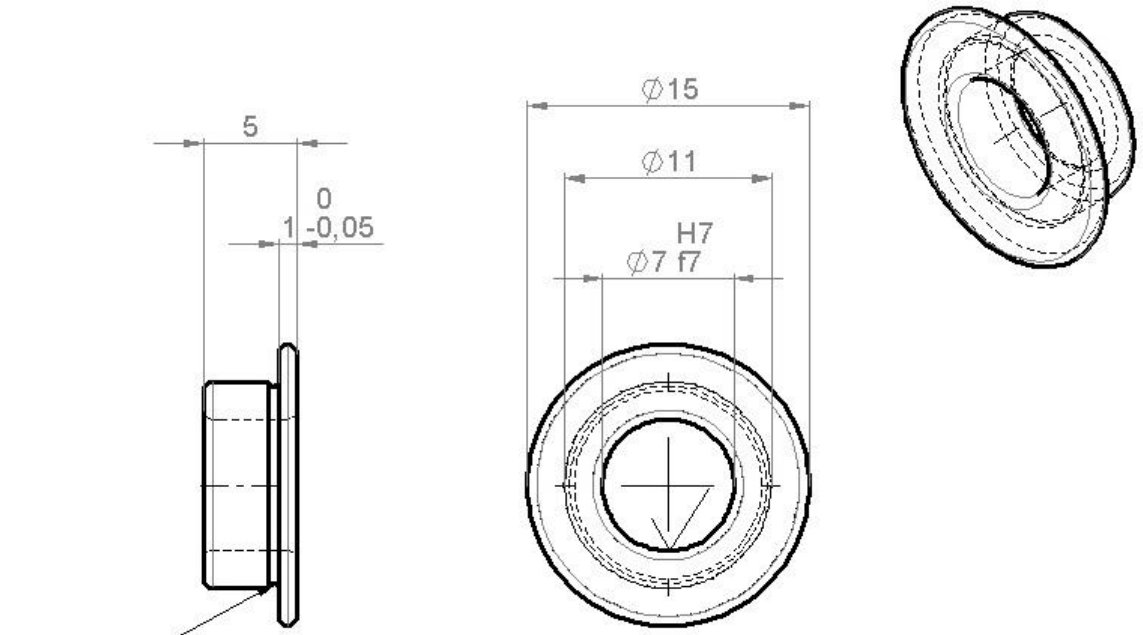

Inkeeping voor goede aansluiting in het huis

TU Delft Mechanical Engineering	benaming Bronze Bearing	datum 28-5-2013		schaal 3:1	maateenheid mm
		getekend Paul Henselmans	groep <<dagdeel>>	formaat A4	gewicht 0.00 gram
					tekening nr. / opmerkingen 7

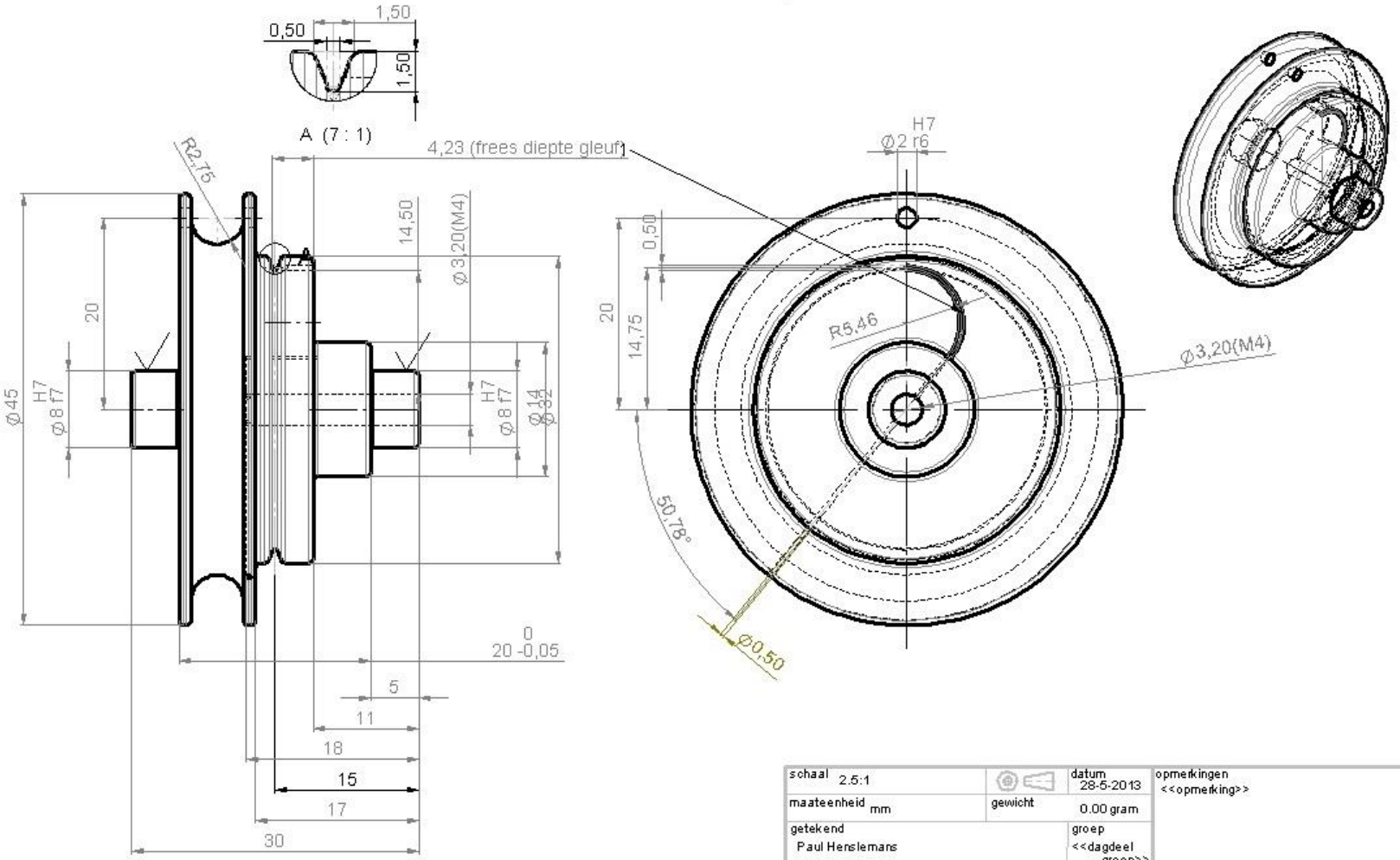

schaal 2.5:1		datum 28-5-2013	opmerkingen <<opmerking>>
maateenheid mm	gewicht	0.00 gram	
getekend Paul Henslemans		groep <<dagdeel groep>>	

benaming **Pulley**

TU Delft
Mechanical Engineering

formaat	tekeningnummer
A3	8

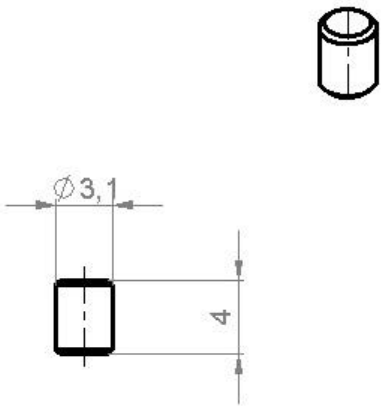

TU Delft Mechnical Engineering	benaming Cable Fixation Rod	datum 28-5-2013		schaal 3:1	maateenheid mm
		getekend Paul Henselmans	groep <<dagdeel>>	formaat A4	gewicht 0.00 gram
					tekening nr. / opmerkingen 9

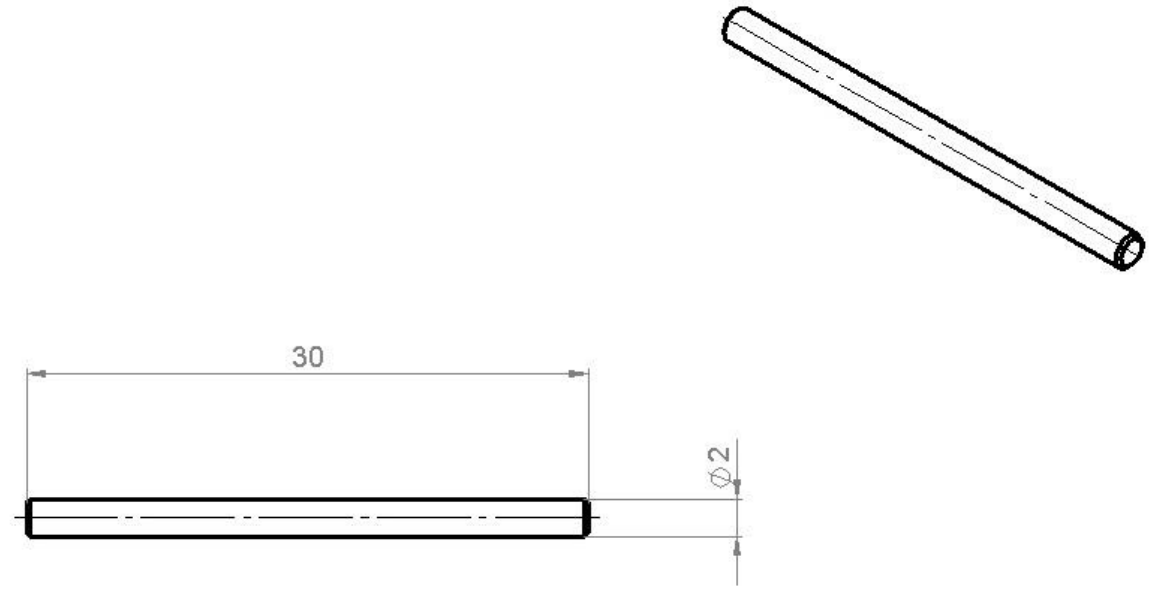

TU Delft Mechanical Engineering	benaming Spring Holder Acrylic Box	datum 28-5-2013		schaal 3:1	maateenheid mm
		getekend Paul Henselmans	groep <<dagdeel>>	formaat A4	gewicht 0.00 gram
					tekening nr. / opmerkingen 6

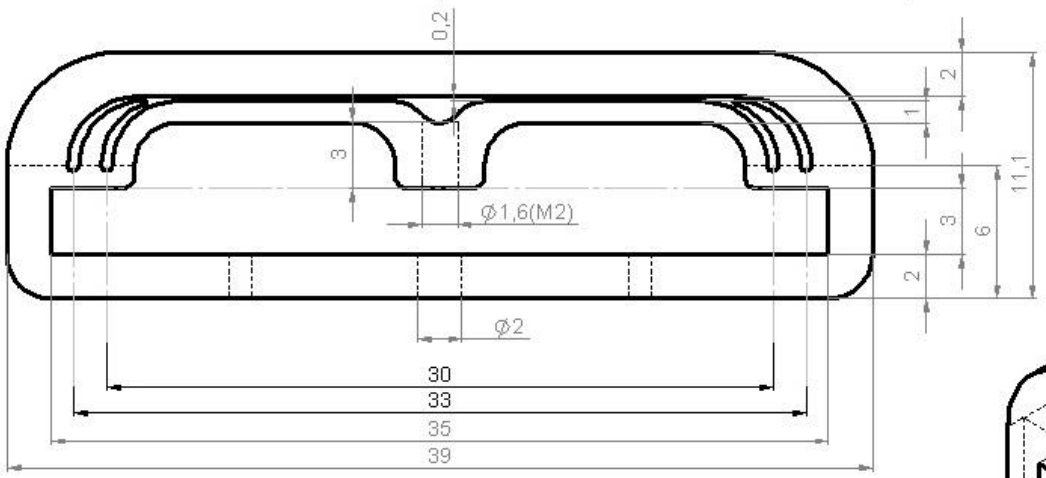

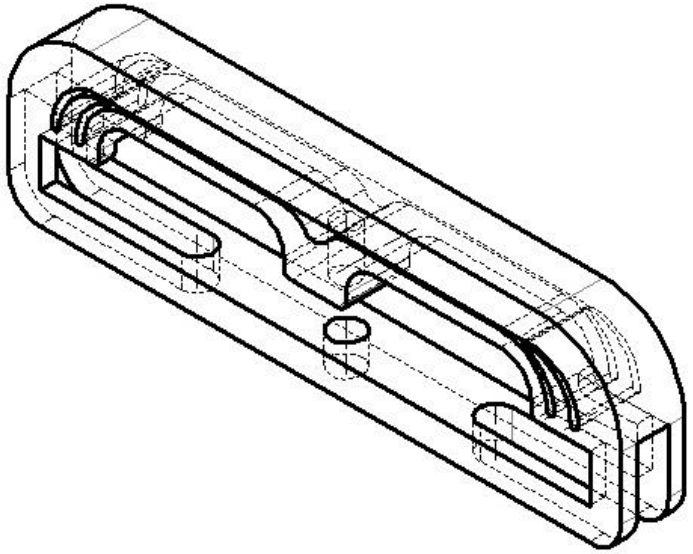

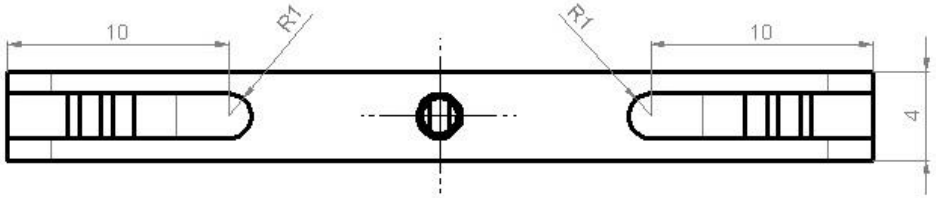

schaal 1:1		datum 28-5-2013	opmerkingen 2 stuks: aluminium
maateenheid mm	gewicht	0.00 gram	
getekend Paul Henselmans		groep <<dagdeel groep>>	

benaming Clamp

TU Delft
Mechanical Engineering

formaat	tekeningnummer
A3	11